Departamento de Biología Molecular
Facultad de Ciencias
Universidad Autónoma de Madrid

DIRECTED EVOLUTION OF UNSPECIFIC PEROXYGENASE:

SYNTHESIS OF HUMAN DRUG METABOLITES AND DESIGN OF FUNCTIONAL FUSION ENZYMES

Instituto de Catálisis y Petroleoquímica (ICP)
Consejo Superior de Investigaciones Científicas (CSIC)

Patricia Gómez de Santos
Licenciada en Biología

Director: Dr. Miguel Alcalde Galeote
Tutor: Dra. Marta Martín Basanta

TESIS DOCTORAL

Madrid, 2020

Miguel Alcalde Galeote, en calidad de Dr. en Ciencias Biológicas, Profesor de Investigación del CSIC

CERTIFICA:

Que el presente trabajo "DIRECTED EVOLUTION OF UNSPECIFIC PEROXYGENASE: SYNTHESIS OF HUMAN DRUG METABOLITES AND DESIGN OF FUNCTIONAL FUSION ENZYMES" constituye la Memoria que presenta Patricia Gómez de Santos, para optar al grado de Doctor, y que ha sido realizado bajo su dirección en el departamento de Biocatálisis del Instituto de Catálisis y Petroleoquímica del CSIC, Campus de Excelencia Internacional UAM + CSIC, Madrid.

Y para que conste, firma el presente certificado en Madrid, a 06 de Noviembre de 2020.

Dr. Miguel Alcalde Galeote

A mi madre y a mi abuela Paulina
A mi familia

"Ah, it is the fault of our science that it wants to explain all;
and if it explains not, then it says there is nothing to explain"

Bram Stoker, Dracula, 1897

AGRADECIMIENTOS/AWKNOWLEDGEMENTS

En primer lugar debo agradecer la financiación que me ha permitido realizar esta Tesis Doctoral. Gracias al contrato para la formación de personal investigador (FPI) del Ministerio de Ciencia e Innovación (BES-2017-080040) englobado en el proyecto del Plan Nacional "Evolución dirigida y computacional de ligninasas (LIGNOLUTION BIO2016-79106-R)". Al proyecto de la Comunidad de Madrid "Química sintética mediante enzimas quiméricas de fusión diseñadas por evolución dirigida y computacional (EVOCHIMERA Y2018/BIO-4738)", al proyecto del CSIC PIE-201580E042 y al proyecto europeo "New enzymatic oxidation/oxyfunctionalization technologies for added value bio-based products (ENZOX2 H2020-BBI-PPP-2015-2-720297) y al proyecto del Plan Nacional "Evolución dirigida de peroxigenasas fúngicas: creando una nueva ola para química de oxifuncionalizaciones selectivas de enlaces C-H (OXIWAVE PID2019-106166RB-I00)".

Gracias a mi director de Tesis, el Prof. Miguel Alcalde por darme la oportunidad de realizar la tesis en su laboratorio. Gracias por haber confiado tanto en mí, por haberme dejado libertad experimental y por haberme hecho sentir tan cómoda tanto a nivel profesional como personal. Te agradezco enormemente haberme ayudado a desarrollarme como científica, haberme proporcionado la oportunidad de hacer dos estancias maravillosas y haberme dado responsabilidades preparándome para el mundo real. Gracias por contar siempre conmigo y por seguir haciéndolo.

Gracias a mi tutora la Dra. Marta Martín Basanta, por haber estado siempre dispuesta a ayudar y a solucionar cualquier problema.

Al Prof. Francisco Plou, por ayudarme con cualquier duda siempre que lo necesitara y por permitirme utilizar los equipos de su laboratorio que tanto ayudaron al desarrollo de esta Tesis Doctoral. Al Prof. Antonio Ballesteros, gracias por haber creado esta gran familia científica y por el asesoramiento. Tu actitud positiva y tus ganas de trabajar son maravillosas.

Gracias a los integrantes del proyecto europeo EnzOx2. Ha sido muy enriquecedor poder aprender de grupos tan diversos. Gracias al Prof. Ángel T. Martínez del Centro de Investigaciones Biológicas Margarita Salas (CIB), coordinador del proyecto. A los Dres. Marta Pérez-Boada y Javier Ruiz-Dueñas por vuestra ayuda y por esos momentos tan divertidos en los viajes. Gracias al grupo de la Prof. Ana Gutiérrez (IRNAS) and special thanks to the german team, Prof. Martin Hofrichter's group (with special thanks to

Christiane Liers) and JenaBios team (with special thanks to Jan Kiebist).

I would like to thank Prof. Frank Hollmann (TUDelft), for allowing me to work with his team (twice!) and for always giving me positive feedback. Thank you for guiding me during my stays and for your good advice concerning Academia. I really appreciate the time you spent hearing any crazy idea that came into our minds. Special thanks for the whole biocatalysis department, this will take some lines. Thank you Florian for welcoming me there the first time to survive to reviewer#3 comments, and for giving me the best food recommendations. Thanks to Caroline, for showing me the best tips to make a nice poster, for your scientific advice, for your tasty and your weird chocolate (the *soil taste* one) and for the great apéritifs. Thanks to Andrada for all your kind help, your way of working in science is the healthiest I've ever seen; and thanks to Nati, I will never forget the tulip field's ride and the muscle pain I had for the rest of the week. Thanks to Sabry and Wuyuan, for trying all the mutants I had with everything you came to your minds and for showing me how to work like a chemist for some weeks. Special thanks to the PhD team: Séb and Marine, thanks for always being there, for showing me the best Italian restaurant out of Italy, for discovering me *Magic Maze* and cheers for a future play-date of our near-future dogs; Georg, Hanna, Morten, Xiaomin, Albert, Julia, Elisabeth, Fabio… thanks for making me feel those three months like if I was at home.

Muchas gracias al Dr. Victor Guallar y a Marina Cañellas del Barcelona Supercomputing Center (BSC) por su gran ayuda con los métodos computacionales.

Thanks to Dr. Sarel Fleishman (Weizmann Institute of Science) and his lab members for helping me with the design of new variants that made me learn a lot of peroxygenases.

Muchas gracias a los Dres. Isabel de la Mata, Miguel Arroyo y Carmen Acebal por haberme dado la oportunidad de trabajar en su laboratorio e iniciarme en la biotecnología enzimática. Muchas gracias a mis compañeros que tanto me enseñaron: Javi, Alba, Iria y los Jesuses, y muy especialmente a Virginia y a Rodrigo por haberme iniciado en el mundo de la investigación y haberme tratado tan bien.

Bueno, qué decir del ICP… Gracias a Eva por el apoyo y a Diana por animarme tanto con los proyectos descabellados. Gracias a David por esos momentos en la cafetería, la confianza, el *patipati* y la imagen del pangolín. Gracias a Patri por haber permitido la creación de las crápulas y apoyarme en los momentos *patriiiiiiiicias*. Muchas gracias al team

Rubis (Javi y Lopa) por habernos sostenido sobre esos paisajes mutacionales y haber sobrevivido (Lopa, sigamos pasándonos patrones como abuelas); a Isa, gracias por tu alegría y por introducirme en el mundo de las agendas Mr. Wondeful® que me aportan ironía a la vida; a Iván por mostrarnos la forma de vida birdo; a Xavi… gracias por haberme aguantado tantas fantasías, historietes, dramas varios, por Agatha, las capibaras, Luna y Valentina y por seguir ayudándome y apoyándome cómo lo haces; a Sofía por haberme ayudado tanto, haber sido tan maja siempre y seguirnos la corriente a Xavi y a mí con las fantasías. Gracias a Isra por ayudar al *perro sudando* y enseñar tan bien las cosas, da gusto aprender de ti. Gracias a todos los que han pasado por el laboratorio y nos han aportado tanto (Dat, Kat, Goça, JiaWei, Leyre…) y a todos los recién llegados que son el futuro del labo (Dani, Alex, Jesús, Merve…). Desde el segundo piso: a Noa por sus furanchos y su pegatina en el HPLC que me salvó la existencia; a Fafa por su ayuda durante toda la tesis y su buena onda; a David por ser tan salao y natural; a Joselu por sus conversaciones y risas en biológicas y a Lucía por su cariño. Gracias al grupo del Dr. Manuel Ferrer, por ayudarnos cada vez que necesitábamos cualquier cosa, a Moni, Rafa, Cosco, David y Laura. Muchas gracias también al resto de compañeros de Biocatálisis: Lara, Chiara, Alejandro y Janaina. También agradezco a todo el personal de administración, limpieza, mantenimiento e informática por ayudarnos siempre.

Muchas gracias a mi grupo de amigos de la uni. A Llamas porque aunque te vemos poco es una alegría enorme; a Tap por sus partidas de rol y sus conocimientos sobre bichitos; a Rafa, que sigas cosechando tantos éxitos científicos; a Irene porque me alegro mucho de habernos reencontrado y por tu apoyo; a Dani por empujarme al mundo friki desde el Bang, al rol, y a cualquier otro juego que se te ocurra ya que sabes que soy débil; a Javi y a Cris (¡y a Marta!), por todo vuestro apoyo y alegría, me encanta aprender de vosotros y es un lujo teneros como amigos; a Marta por todos esos momentos, por haber sido un apoyo vital durante la carrera (bipartición de MarPat), la tesis y después, que no cambie; y especialmente a Diego por haberme aguantado los años de la tesis y haberme puesto mil documentales monotemáticos y mundiales de LoL.

A mis amigos de la uni postizos (frikis), que son el otro grupo de un universo paralelo y eso es genial ya que así tengo 2x1. Muchas gracias a todos por haber pasado tanto tiempo juntos, los juegos de mesa, las anécdotas y las risas, sobre todo las risas que tanto hacen falta.

A mis amigos de Segovia, porque aunque no estaban muy seguros de lo que hacía exactamente, sabían que trabajaba con bichitos, con cosas de ciencia y si hacía falta servía de *patipedia* (☺). Gracias por vuestro apoyo todos estos años, algunos estáis ahí desde que tengo memoria y eso es una gozada.

A Berni, porque lo mejor que me llevo de la tesis eres tú.

A mi familia zamorana, por todo vuestro apoyo y vuestra ayuda. Sois una segunda familia para mí. A Bartolo por la tranquilidad que transmites.

A mi familia, a mi tía Estrella y mis primos por todo su apoyo, a mis abuelos Petra y Anastasio por todos esos preciosos recuerdos. A mis tíos Nico y Rosaura (y mis primos), por haber estado siempre ahí, en los buenos y los malos momentos, no sé qué habría hecho sin vosotros. A mi abuela Paulina, gracias por haber sido una segunda madre, por habernos cuidado tantísimo, por haberlo pasado tan bien contigo y por todo lo que me has enseñado, está siendo muy duro que no puedas estar aquí para acompañarme pero sé que estarías orgullosa de mí.

A mi padre, a Darío y a Carlota, no hubiese podido hacer esto sin vosotros, sin vuestro apoyo, sin vuestros ánimos y sin vuestra confianza en mí.

A mi madre, por todo, siempre, todo lo que soy es gracias a ti.

SUMMARY

Discovery and testing of new bioactive compounds are becoming emergent fields in contemporary chemistry. All metabolites formed above 10% of the parent drug should be tested in terms of safety; therefore it is fundamental to produce high amounts of them. However, the main drawback is that their chemical synthesis is associated to low yields and cumbersome processes, presenting enzymes as feasible options for this aim. Unspecific peroxygenases (UPOs, EC 1.11.2.1) are stable and extracellular heme-thiolate enzymes considered by many as the *generational relief* of P450s, acting on drugs as "extracellular livers". These enzymes have been studied before for the synthesis of human drug metabolites (HDMs) presenting a wide range of substrate conversion. In the present Doctoral Thesis, the engineering of UPO from *Agrocybe aegerita* (*Aae*UPO) has been studied in terms of i) efficient production of HDMs from the β-blocker drug propranolol, ii) exploration of enzyme variants for further HDMs synthesis studies, and iii) creating a self-sufficient system based on fusion protein technology.

To accomplish an efficient production of HDMs from propranolol, structure-guided evolution was carried out assisted by the *Saccharomyces cerevisiae* device along with a reliable high-throughput screening assay. Several UPO mutant libraries were constructed and screened in search for improved peroxygenase activity and diminished peroxidase activity during this given biotransformation. The final mutant, SoLo, carried one single mutation (F191S) and showed a catalytic efficiency for the conversion of propranolol enhanced by two orders of magnitude together with 99% regioselectivity in the synthesis of the true HDM 5´-hydroxypropranolol (5´-OHP). Reaction engineering of the UPO mutant for the production of 5´-OHP was performed by coupling a H_2O_2 *in situ* generation system using methanol as sacrificial electron donor to achieve total turnover numbers of up to 264,000.

This mutant together with other evolved *Aae*UPO variants were further tested with drugs dextromethorphan, tolbutamide and naproxen, unveiling the importance of the amino acids lining the heme channel. Future efforts focusing on this structural region can expand the UPO's substrate scope.

In the light of the successful result obtained by combining enzyme and reaction engineering for the production of HDMs, UPO fusion enzymes were designed by linking the evolved UPO to aryl-alcohol oxidase (AAO, EC 1.1.3.7), a fungal flavoenzyme that

supplies H_2O_2 to the ligninolytic consortium during natural wood decay. After testing several orientations, signal sequences and peptide linkers, five constructions of UPO_AAO were functionally expressed in yeast and characterized biochemically. The H fusion was tested with dextromethorphan and 4-fluorobenzyl alcohol as substrates, achieving 62,145 TTNs for HDM dextrorphan synthesis. This fusion represents a self-sufficient system to produce HDMs in a preparative manner from newly discovered drugs as well as to be applied in cascade reactions where both AAO and UPO partners could interact.

RESUMEN

El descubrimiento y evaluación de nuevos compuestos bioactivos constituye un campo emergente dentro de la química contemporánea. Todos los metabolitos formados a partir de un fármaco en una proporción superior al 10% deben ser evaluados en términos de seguridad, por lo que su producción para tales estudios se considera prioritaria. Sin embargo, su síntesis química se encuentra generalmente asociada con bajos rendimientos y procesos muy complejos, por lo que están surgiendo nuevos procesos enzimáticos como potencial solución. En este sentido, las peroxigenasas inespecíficas (UPOs, EC 1.11.2.1) son enzimas hemotioladas estables y extracelulares que son consideradas por muchos como el relevo generacional de las citocromo P450 monooxigenasas, pudiendo actuar sobre los fármacos como "hígados extracelulares". Estas enzimas han sido estudiadas con anterioridad para la síntesis de metabolitos humanos de fármacos (HDMs), presentando una gran diversidad en cuanto a conversión de sustrato. En la presente Tesis Doctoral, se ha estudiado la ingeniería de la UPO de *Agrocybe aegerita* (*Aae*UPO) i) para la producción eficiente de HDMs del β-bloqueante propranolol, ii) para la exploración de variantes enzimáticas para futuros estudios de síntesis de HDMs, y iii) para la creación de un sistema autosuficiente para este propósito basado en la tecnología de proteínas de fusión.

Para lograr la producción eficiente de HDMs de propranolol, se llevó a cabo evolución dirigida guiada por la estructura de la proteína, conjugando un sistema de expresión en *Saccharomyces cerevisiae* junto con un robusto método de cribado de alto rendimiento. Se construyeron y evaluaron diversas genotecas buscando un incremento en la actividad peroxigenasa y una disminución en la actividad peroxidasa para esta transformación en particular. El mutante final, SoLo, presentó una única mutación (F191S) y mostró una eficiencia catalítica para la conversión del propranolol aumentada en dos órdenes de magnitud junto con una regioselectividad del 99% en la producción del HDM 5´-hidroxipropranolol (5´-OHP). Con el fin de aumentar el rendimiento del sistema, se realizaron experimentos de ingeniería de la reacción acoplando el mutante a un sistema de generación de H_2O_2 *in situ* que hacía uso metanol como donador de electrones, alcanzando unos números de recambio totales (TTN) de 264,000.

Este mutante, junto con otras variantes evolucionadas de *Aae*UPO fueron evaluadas con dextrometorfano, tolbutamida y naproxeno, desvelando la importancia que tienen los aminoácidos que tapizan el interior del canal del hemo. Futuros esfuerzos centrados en esta región podrían permitir expandir la promiscuidad de sustrato de la UPO.

Debido a los buenos resultados obtenidos al combinar la ingeniería de la enzima y el de la reacción para la producción de HDMs, se diseñaron enzimas de fusión uniendo la UPO evolucionada a una aril-alcohol oxidasa (AAO, EC 1.1.3.7), una flavoenzima fúngica que proporciona H_2O_2 al consorcio ligninolítico durante la degradación natural de la madera. Tras probar diferentes orientaciones, péptidos señales y *linkers*, se expresaron funcionalmente en levadura 5 construcciones de UPO_AAO que fueron caracterizadas bioquímicamente. La fusión H fue evaluada con dextrometorfano y alcohol 4-fluorobencílico como sustratos, alcanzando unos TTN de 62,145 para la síntesis de dextrorfano. Esta fusión representa un sistema autosuficiente para la producción preparativa de HDMs de nuevos fármacos, así como para la aplicación en reacciones en cascada en las que tanto la AAO como la UPO puedan interaccionar.

CONTENTS

1. Introduction 1

    1.1. Unspecific peroxygenase (UPO) 1

        1.1.1. Discovery, classification and families 1

        1.1.2. Structure and mechanism 2

        1.1.3. Activity and substrate scope 6

        1.1.4. Industrial applications of UPOs focused on the pharmaceutical sector: human drug metabolites (HDMs) 13

        1.1.5. Challenges for industrial use 17

    1.2. Fusion proteins 19

        1.2.1. Characteristics and applications 19

        1.2.2. Aryl alcohol oxidase (AAO) 21

    1.3. Directed molecular evolution 22

        1.3.1. Overview of the technique and the S. cerevisiae toolbox 22

        1.3.2. Directed evolution of AaeUPO 24

        1.3.3. Functional expression of AAO 26

2. Objectives 31

3. Material and methods 35

    3.1. General material and methods 35

        3.1.1. Reagents and materials 35

        3.1.2. Culture media preparation 38

            - Culture media for bacteria (*E. coli*) growth 38

            - Culture media for yeast (*S. cerevisiae* and *P. pastoris*) growth 39

    3.2. Methods for Chapter 1 42

        3.2.1. Laboratory evolution 42

3.2.2. Production, purification and biochemical characterization 45

3.2.3. Reaction optimization and product identification... 47

3.2.4. Computational analysis 48

3.3. Methods for Chapter 2 49

3.3.1. Expression and purification of UPO variants... 49

3.3.2. Reactions and product characterization.. 50

3.3.3. Semi-preparative production of dextrorphan and NMR analysis 50

3.3.4. Site-directed mutagenesis at position 241 51

3.4. Methods for Chapter 3 52

3.4.1. Fusions engineering.. 52

3.4.2. Activity screening assays 57

3.4.3. Expression and purification of enzyme fusions 58

3.4.4. Kinetic characterization 60

3.4.5. Evaluation of the enzyme fusion system... 61

4. Results and discussion.. 66

4.1. Chapter 1: Selective synthesis of the human drug metabolite 5´-hydroxypropranolol by an evolved self-sufficient peroxygenase. 66

4.1.1 Screening method and benchmarking... 66

4.1.2. Directed evolution studies 68

4.1.3. Computational analysis 74

4.1.4. Reaction engineering.. 78

4.1.5. Conclusions 79

4.2. Chapter 2: Benchmarking of laboratory evolved unspecific peroxygenases for the synthesis of human drug metabolites.. 80

4.2.1. Dextromethorphan, naproxen and tolbutamide conversion 81

4.2.2. Mutational analysis and SoLo-D241G 83

4.2.3. Conclusions 85

4.3. Chapter 3: Evolved peroxygenase-aryl alcohol oxidase fusions for self-sufficient oxyfunctionalization reactions 86

4.3.1. Point of departure to construct the chimeric fusion enzymes: the laboratory evolved AAO and UPO variants 86

4.3.2. Construction of the enzyme fusion libraries 87

4.3.3. Production and biochemical characterization 90

4.3.4. Production of dextrorphan, a human drug metabolite from dextromethorphan 94

4.3.5. Conclusions 98

5. Global discussion 102

5.1. Directed evolution of unspecific peroxygenase for HDMs 102

5.1.1. Propranolol 102

5.1.2. Dextromethorphan, naproxen and tolbutamide 104

5.2. UPO_AAO fusions: a new twist in UPO engineering 105

6. Conclusions 112

7. Conclusiones 113

8. References 116

9. Annex 134

9.1. ^{1}H NMR spectrum for Chapter 1 134

9.2. ^{1}H NMR and ^{13}C spectra for Chapter 2 135

9.3. Publications and patent from the Doctoral Thesis 137

9.4. Other publications from the author 137

ACRONYMS

4´-OHP	4´-hydroxypropranolol
4-AAP	4-aminoantipirine
4-keto-CPA	4-ketocyclophosphamide
5´-OHP	5´-hydroxypropranolol
AA	Ascorbic acid
AAO	Aryl-alcohol oxidase
Abs	Absorbance
ABTS	2,2'-azino-bis(3-ethylbenzothiazoline-6-sulphonic acid)
ACN	Acetonitrile
Amp	Ampicillin
***Ao*FOx**	Formate oxidase from *Aspergillus oryzae*
AOx	Alcohol oxidase from *Pichia pastoris*
APA	Aldophosphamide
***Ath*SO**	Sulfite oxidase from *Arabidopsis thaliana*
bp	Base pairs
BSA	Bovine serum albumin
CPO	Chloroperoxidase
CT1 and CT2	Charge transference bands 1 and 2
CV	Coefficient of variation
$\mathit{dd}\mathrm{H_2O}$	Ultra-pure and sterile water
DFF	2,5-diformylfuran
DIP	desisopropylpropranolol
dNTPs	Deoxyribonucleotides
epPCR	Error-prone PCR
evSp	Evolved signal peptide

$\boldsymbol{\varepsilon}$	Extinction molar coefficient
FAD	Flavin adenine dinucleotide
FDA	US food and drug administration
FDCA	Furan-2,5-dicarboxylic acid
FDM	Formate dismutase from *Pseudomonas putida*
FFCA	5-Formyl-2-furancarboxylic acid
FID	Flame ionization detector
GC	Gas chromatography
HDMs	Human drug metabolites
HMF	5-hydrodymethylfurfural
HPLC	High performance liquid chromatography
HRP	Horseradish peroxidase
HTS	High throughput screening
IVOE	*in vivo* Overlap Extension
$\boldsymbol{k_{cat}}$	Catalytic constant
$\boldsymbol{k_{cat}/K_m}$	Catalytic efficiency
$\boldsymbol{K_m}$	Michaelis-Menten constant
LB	Luria Bertani medium
LC	Liquid chromatography
MIST	Metabolites in safety testing
MORPHING	Mutagenic organized recombination process by homologous *in vivo* grouping
MS	Mass spectrometry
NASH	Nonalcoholic steatohepatitis
NMR	Nuclear magnetic resonance
$\mathbf{OD_{600}}$	Optical density at 600 nm
OleTJE	Fatty acid decarboxylase cytochrome P450

***P*:*p* ratio**	Peroxygenase:peroxidase activity ratio
PDA	Photometric diode array
PDB	Protein data bank
P_{DF}	Orthologous CAT1 promoter
PEF	poly(ethylene-2,5-furandicarboxylate)
PELE	Protein energy landscape exploration
PNGaseF	Peptide-*N*-Glycosidase F
PSK	Potassium persulfate
QM/MM	Quantum mechanics/Molecular mechanics
Rz	Reinheitszahl value
SDS-PAGE	Sodium dodecyl sulfate-polyacrylamide gel electrophoresis
SEM	Selective expression medium
SRP	Signal recognition particle
T_{50}	Kinetic thermostability
***tert*-BuOOH**	*tert*-butyl hydroperoxide
TTN	Total turnover number
UPO	Unspecific peroxygenase
UPO_AAO	Enzyme fusion of UPO and AAO
UPO+AAO	Enzyme cocktail with UPO and AAO non-fused
VP	Versatile peroxidase
YNB	Yeast nitrogen base
YPD	Yeast peptone dextrose medium
Zeo	Zeocine

INTRODUCTION

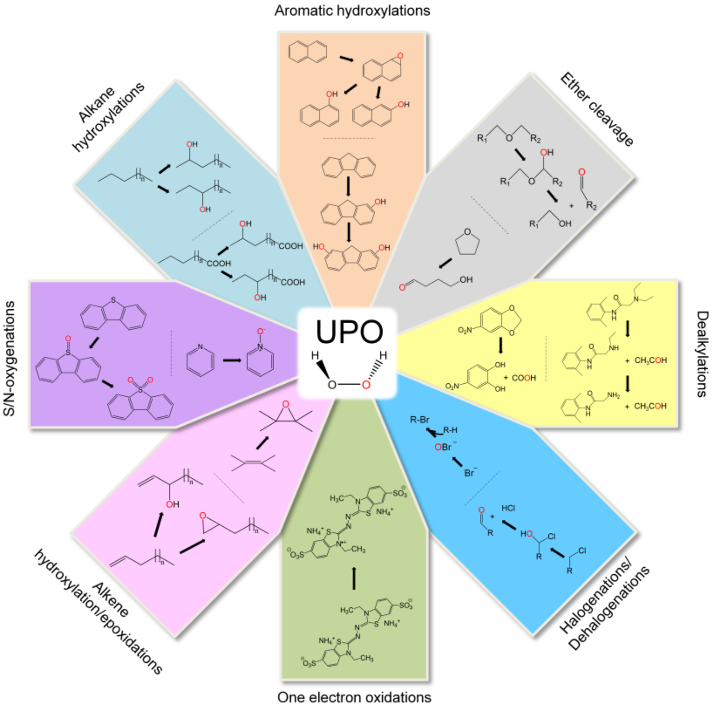
Aromatic hydroxylations
Ether cleavage
Dealkylations
Halogenations/
Dehalogenations
One electron oxidations
Alkene
hydroxylation/epoxidations
S/N-oxygenations
Alkane
hydroxylations
UPO
H
H
O
O
COOH
OH
R-Br
R-H
OBr⁻
Br⁻
HCl
+ CH₃COH
+ COOH
O₂N

1. Introduction

1.1. Unspecific peroxygenase (UPO)

1.1.1. Discovery, classification and families

The first reported true heme-thiolate peroxygenase isolated from an edible mushroom that produces white rot, the peroxygenase from *Agrocybe aegerita* (*Aae*UPO) (Ullrich et al., 2004), represents to date the main model enzyme for all peroxygenase chemistry (Hofrichter et al., 2015). After its initial misclassification as an unusual alkaline lignin peroxidase, and later as a haloperoxidase, it was referred to as an aromatic peroxygenase (APO), and finally recognized as unspecific peroxygenase (UPO), constituting the first member of a new sub-subclass of oxidoreductases (EC 1.11.2.1). Four other enzymes are part of this subclass: myeloperoxidase (EC 1.11.2.2; $Cl^- + H_2O_2 + H + \rightarrow HClO + H_2O$) (Klebanoff, 2005), plant seed peroxygenase (EC 1.11.2.3; $R_1H + R_2OOH \rightarrow R_1OH + R_2OH$) (Hanano et al., 2006), fatty acid peroxygenase (EC 1.11.2.4; fatty acid + H_2O_2 → 3- or 2-hydroxy fatty acid + H_2O) (Lee et al., 2003) and 3-methyl-L-tyrosine peroxygenase (EC 1.11.2.5; 3-methyl-L-tyrosine + H_2O_2 → 3-hydroxy-5-methyl-L-tyrosine + H_2O) (Tang et al., 2012).

UPO is able to insert oxygen into unactivated carbon atoms (both in aliphatic and aromatic compounds), being more enantio- than regioselective and it can be considered a *Swiss Army knife* for oxyfunctionalization chemistry whose promiscuity is reflected by its extensive portfolio of transformations (see **Section 1.1.3**). Despite its broad substrate specificity (over 400 compounds already described), the peroxygenase sole catalytic requirement is hydrogen peroxide, which acts as both the final electron acceptor and the main oxygen donor (Hofrichter et al., 2020). While showing a similar chemistry as P450 monooxygenases (P450s), UPOs have much less requirements to perform complex oxyfunctionalization reactions with high efficiency, in the absence of expensive redox cofactors or auxiliary flavoproteins, being highly active and extracellular secreted enzymes. More significantly, UPOs escapes from the O_2 uncoupling which for P450s represents a recurrent problem as up to 90% of all the reducing equivalents provided by the sacrificial substrate can be wasted in the futile uncoupling reaction (the so called "oxygen dilemma") (Holtmann and Hollmann, 2016). Given that UPOs can carry out one-electron oxidations (as generic peroxidases) and two-electron oxidations (the base for oxyfunctionalization chemistry), they are considered from a catalytic point of view as the "missing link" between common peroxidases -with a His residue as axial ligand- and heme-thiolate containing enzymes -with a Cys as axial ligand-. This latter group includes UPOs, P450s and the classical chloroperoxidase from *Caldariomyces fumago* (*Cfu*CPO, EC 1.11.1.10). When comparing *Cfu*CPO and UPO, they both share a similar reaction mechanism triggered by H_2O_2, yet *Cfu*CPO cannot perform oxygenations of alicyclic/aromatic rings or n-alkanes like UPO. The role of UPO in nature remains uncertain, with several activities proposed, including the synthesis of metabolites, detoxification processes and the lignin degradation by its *O*-demethylation -etherase- activity (Hofrichter et al., 2015; Kinne et al., 2011).

In terms of natural diversity, over 4,000 putative peroxygenase sequences from different fungi have been deposited in the genomic databases, with the characterization of the following wild type UPOs (*i.e.* produced from the natural fungus): the original *Agrocybe aegerita* -*Aae*UPO- (Ullrich et al., 2004), *Coprinellus radians* -*Cra*UPO-, *Coprinopsis verticillata* -*Cve*UPO- (Anh, 2008; Anh et al., 2007), *Marasmius rotula* -*Mro*UPO- (Gröbe et al., 2011), *Agrocybe parasitica* -*Apa*UPO- (Hofrichter et al., 2015), *Chaetomium globosum* –*Cgl*UPO- (Kiebist et al., 2017), *Marasmius wettsteinii* -*Mwe*UPO- (Ullrich et al., 2018) and *Psathyrella aberdarensis* -*Pab*UPO- (Hofrichter et al., 2020). In the light of their widespread distribution in fungi, UPOs have been phylogenetically sorted into family I (short peroxygenases) and family II (long peroxygenases).

1.1.2. Structure and mechanism

Short UPOs (like *Mro*UPO or *Cgl*UPO), are broadly found throughout the fungal kingdom and they are generally homodimeric proteins (with molecular weights of ~26 kDa per monomer) with a histidine residue as a charge stabilizer at the active site. While lacking intramolecular disulfide bridges, they do establish an intermolecular disulfide bridge to connect both monomers. By contrast, long UPOs with molecular weights of ~44 kDa (like *Aae*UPO or *Pab*UPOs) are found in basidiomycetes and ascomycetes, and they are monomeric enzymes with an internal disulfide bridge and an arginine residue as a charge stabilizer (Hofrichter et al., 2015). Both families have highly conserved sequences at the active site (*i.e.* -EHD-S-E- and -EGD-S-R-E for short and long UPOs, respectively) as observed from their available crystal structures -for *Aae*UPO and *Mro*UPO-, solved at a high resolution (Piontek et al., 2013, Ramirez-Escudero et al., 2018, and unpublished material). The composition, dimensions and shape of the heme access channel between the short and long clades are reflected in their distinct substrate profiles and functions, **Table 1.1** (Hofrichter et al., 2020). Short UPOs heme access channel is upholstered by flexible aliphatic amino acids and it is shorter, yet wider compared with that of long UPOs, which is translated to the former towards a strong preference for bulky substrates like steroids (Kiebist et al., 2019). Conversely, long UPO's channel is formed by rigid aromatic amino acids, which determine a substrate preference towards smaller aromatic substrates (**Figure 1.1**).

Table 1.1. General comparison between *M. rotula* (short) and *A. aegerita* (long) UPOs.

UPO family/Representative	Short/*Mro*UPO	Long/*Aae*UPO
Molecular weight	29 kDa	44.4 kDa
pI	6.4	5.8
Conformation	Dimeric	Monomeric
Disulfide bridges	Intermolecular to connect monomers	C-terminal
Hydrophobic amino acids lining the channel	Aliphatic amino acids	Aromatic amino acids
Charge stabilizer	His86	Arg189
Other examples	*Mwe*UPO, *Cgl*UPO	*Pab*UPOs, *Cra*UPO, r*Cci*UPO

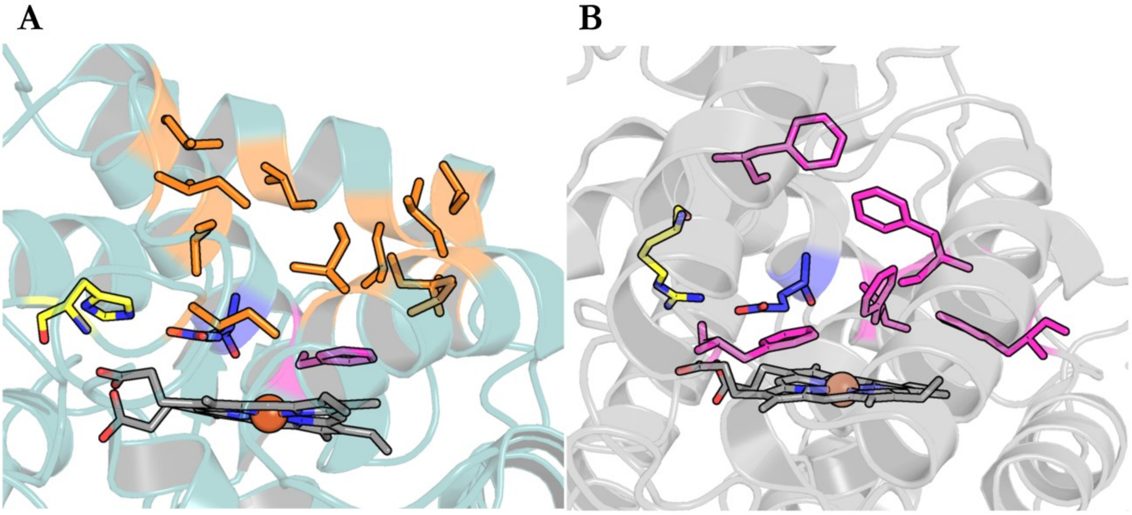

Figure 1.1. Heme access channel of (**A**) *Mro*UPO (short UPO family) and (**B**) *Aae*UPO (long UPO family). Glutamic acid from the acid base pair is depicted in blue (Glu157 in *Mro*UPO and Glu196 in *Aae*UPO) and charge stabilizer amino acid is colored in yellow (His86 in *Mro*UPO and Arg189 in *Aae*UPO). Heme access channel coating amino acids are represented in orange (hydrophobic aliphatic in *Mro*UPO) and in pink (hydrophobic aromatic in *Aae*UPO). The models were visualized with PyMOL (http://pymol.org) using the crystal structure of *Mro*UPO at a resolution of 1.83 Å (PDB ID: 5FUJ) and *Aae*UPO at a resolution of 2.19 Å (PDB ID: 2YOR).

While both UPOs present a glutamic acid residue (Glu196/157 in *Aae*UPO/*Mro*UPO) which acts as an acid-base catalyst in the cleavage of H_2O_2, the charge stabilizer is an histidine (His86 in *Mro*UPO) or an arginine (Arg189 in *Aae*UPO) (Hofrichter et al., 2020). The active site contains a heme (iron protoporphyrin IX) as prosthetic group which is coordinated through a cysteine as proximal (5th) ligand (heme-thiolate protein). This cysteine along with two proline residues represent the PCP motif (Pro35/16-Cys36/17-Pro37/18 in *Aae*UPO/*Mro*UPO), which places the thiolate (Cys-SH) towards the heme iron (Hofrichter et al., 2015). The distal heme position in UPOs is occupied by a water molecule (6th ligand) in the resting state that is replaced by a hydrogen peroxide molecule (electron accepting co-substrate) when the catalytic cycle begins. *Aae*UPO and *Mro*UPO present a structural magnesium ion (Mg^{2+}) coordinated by three carboxylates and one alcohol group from heme propionate -glutamate (Glu122/85), aspartate (Asp124/87) and serine (Ser126/89)-, and it seems to be involved in stabilizing the porphyrin system, **Figure 1.2**.

UPOs have a typical UV-Vis spectra of heme containing proteins with a Soret band between 415 and 420 nm in the resting state [heme-$Fe^{3+} \leftarrow H_2O$] with two maximum of absorption at 572 and 540 nm (CT1 and CT2 charge transfer bands, respectively) and between 445 and 450 nm in the reduced carbon monoxide complex [heme-Fe^{2+}-CO] (Ullrich et al., 2004). The absorption maximum of the latter complex is within the same range as the one for P450s or *Cfu*CPO (Omura, 2005).

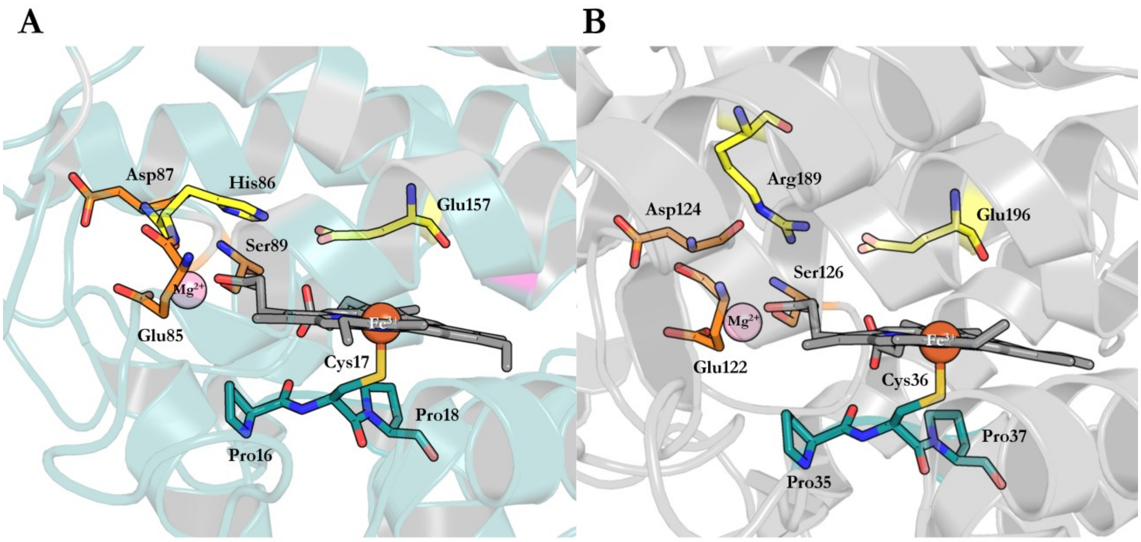

Figure 1.2. Conserved amino acid residues in the active site of (A) *Mro*UPO and (B) *Aae*UPO. Acid base pairs are depicted in yellow, PCP motif in teal and amino acids coordinating Mg^{2+} in orange. The models were visualized with PyMOL (http://pymol.org) using the crystal structure of *Mro*UPO at a resolution of 1.83 Å (PDB ID: 5FUJ) and *Aae*UPO at a resolution of 2.19 Å (PDB ID: 2YOR).

The dual catalytic cycle of unspecific peroxygenase (**Figure 1.3**) combines the classic heme peroxidase cycle with the "peroxide shunt" pathway of P450s (Hofrichter et al., 2015). Starting from UPO at its resting heme ferric state (Heme-$Fe^{3+} \leftarrow H_2O$), H_2O_2 enters the heme and replaces the molecule of H_2O that was acting as distal ligand leading to the formation of a pre-Compound 0 (Heme-$Fe^{3+} \leftarrow H_2O_2$). This intermediate is deprotonated *via* a conserved glutamic acid (Glu196 in *Aae*UPO) to form Compound 0, which decays under electron re-arrangement into Compound I, a reactive oxo ferryl cation radical complex ($^{+\bullet}$Heme-$Fe^{4+}=O$). Compound I can then undergo into two different routes: peroxygenase (mono(per)oxygenase) or peroxidase.

During the peroxygenase route (*i.e.* two electron oxidation), a hydrogen (H^+ and e^-) is abstracted from the substrate (R-H) resulting in the protonated ferryl hydroxide complex (Compound II, Heme-Fe^{4+}-OH) and the substrate radical ($R^\bullet$ that stays near the oxygen). Substrate radical and Compound II react immediately with each other to form the hydroxylated product while water binds again as distal heme ligand so the catalytic cycle starts again (route a, **Figure 1.3**). In the case of epoxidation reactions, the cycle is slightly modified (route b, **Figure 1.3**) according to previous findings of P450s alkene epoxidation (de Visser et al., 2001). In such a case, Compound II transitionally binds the substrate as a radical via the ferryl oxygen, forming an alkoxy radical complex so there is no H abstraction (Peter, 2013; Peter et al., 2013).

In the peroxidase cycle, both Compound I and deprotonated Compound II (in equilibrium with its protonated counterpart) may abstract single electrons (and the corresponding protons) from two substrate molecules (A-HO), which are then released as radicals and may undergo spontaneous coupling or disproportionation reactions (Hofrichter et al., 2015; Hofrichter and Ullrich, 2014).

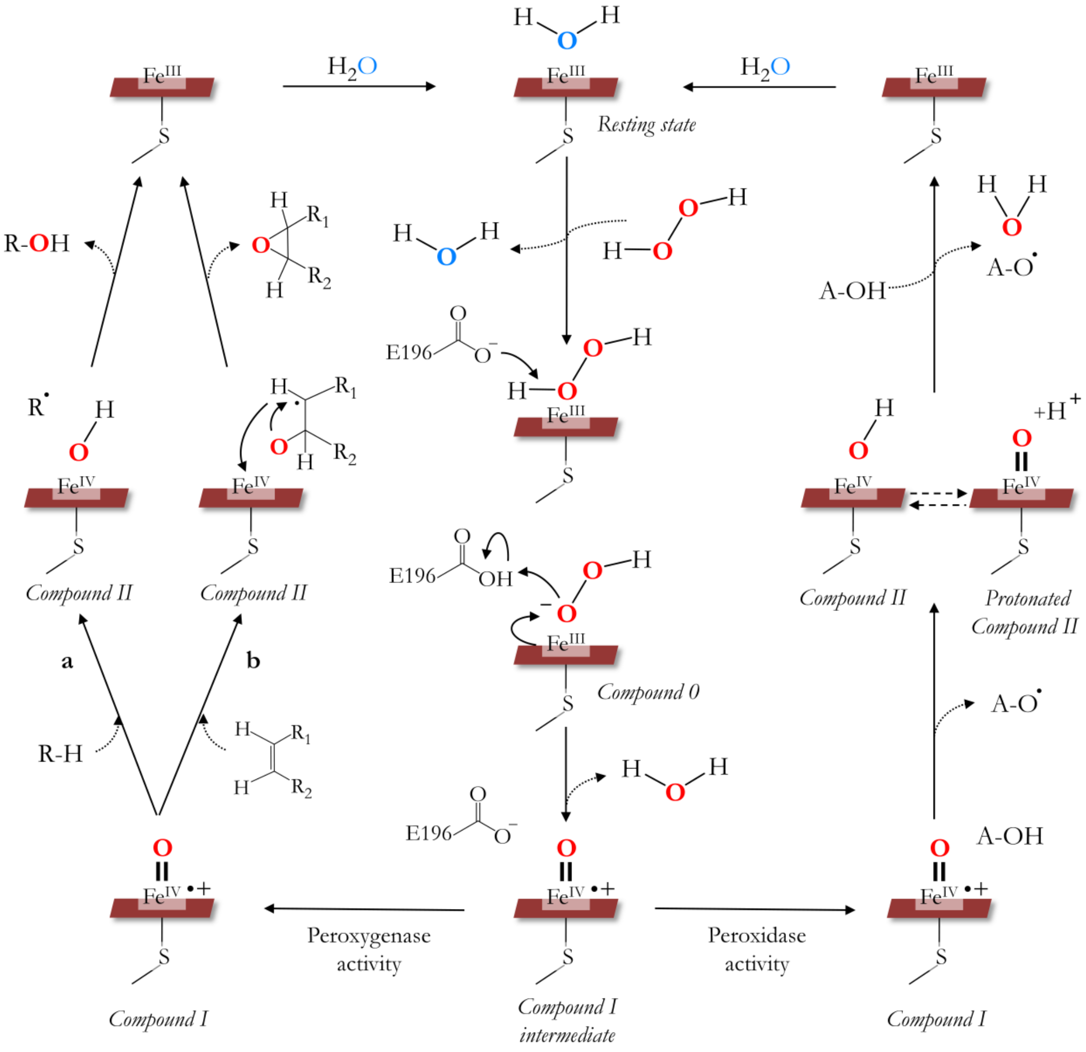
H$_2$O
H$_2$O
Fe^{III}
S
Resting state
R-OH
R$^•$
R$_1$
R$_2$
H
O
E196
H$_2$O
A-OH
A-O$^•$
+H$^+$
Fe^{IV}
Compound II
Compound II
Compound II
Protonated Compound II
Compound 0
a
b
R-H
Fe^{IV} •+
Compound I
Peroxygenase activity
Compound I intermediate
Peroxidase activity
Compound I

Figure 1.3. Catalytic cycle of UPO. Right: peroxidase activity. Left: peroxygenase activity with two different routes, (a) for classic hydroxylation and (b) for epoxide formation.

1.1.3. Activity and substrate scope

The vast majority of UPOs characterized to date have an acidic pH optimum (ranging from pH 2.0 to 5.0) for one-electron oxidations (peroxidase activity) or halid oxidation and a neutral pH optimum (pH 6.0-7.0) for two-electron oxidation reactions (peroxygenase activity) (Hofrichter and Ullrich, 2014). In general terms, stability is higher at neutral or slightly alkaline conditions rather than at acidic pH. However, three UPOs recently described from *Psathyrella aberdarensis* (an East African ink-cap; (Melzer et al., 2018)) are active with veratryl alcohol (peroxygenase substrate) in a broad pH range (pH 2.0-9.0). Besides, these three UPOs (*Pab*UPOI-III) possess different pH stabilities. While *Pab*UPOII is rather stable at alkaline pH, *Pab*UPOI loses its activity at this pH, but it is still active at pH 3.0, where the other isoform losses activity rapidly. As described in Hofrichter et al., 2020, these different physicochemical properties of UPOs could point to adaptations of the fungi for growing in the voluble fungal microenvironment.

UPOs are fairly unstable at high temperatures, yet they remain stable at room temperature for hours. Below 20 °C UPOs are stable, being stored at 4 ºC for months without significant drops of activity (*Cgl*UPO represents an exception as it loses activity rapidly at temperatures above 4 °C). UPO stability in organic solvents is considered high, and indeed, they maintain some activity at high concentrations of cosolvents or even under neat conditions (Fernández-Fueyo et al., 2016a; Molina-Espeja et al., 2014; Rauch et al., 2019). Among the solvents tested, acetonitrile and acetone are often the solvents of choice, as they are not UPO substrates like ethanol, methanol or hexane, and only affect partially UPO activity (Molina-Espeja et al., 2014; Peter et al., 2013, 2011). Nevertheless, it should be considered the risk of using acetone together with co-substrate H_2O_2 because highly explosive acetone peroxide crystals (APEX) can be formed under certain conditions.

Regarding the substrate scope, more than 400 compounds have shown to be UPO substrates. Most of the studies have been performed with *Aae*UPO as it was the first peroxygenase discovered, and more significantly because it is the most successful recombinant systems developed to date (see **Section 1.3.2**), but newly characterized UPOs are broadening the substrate palette. As seen in **Figure 1.4**, UPOs can perform several different reactions as hydroxylation of unactivated C-H bonds of *n*-alkanes and fatty acids, the epoxidation of alkenes and aromatics (with further re-aromatization), *O*-dealkylation (ether/ester cleavage), *N*-dealkylation, halogenation and dehalogenation, oxygenation of heteroatoms (N, S) and one-electron oxidation of phenolic compounds.

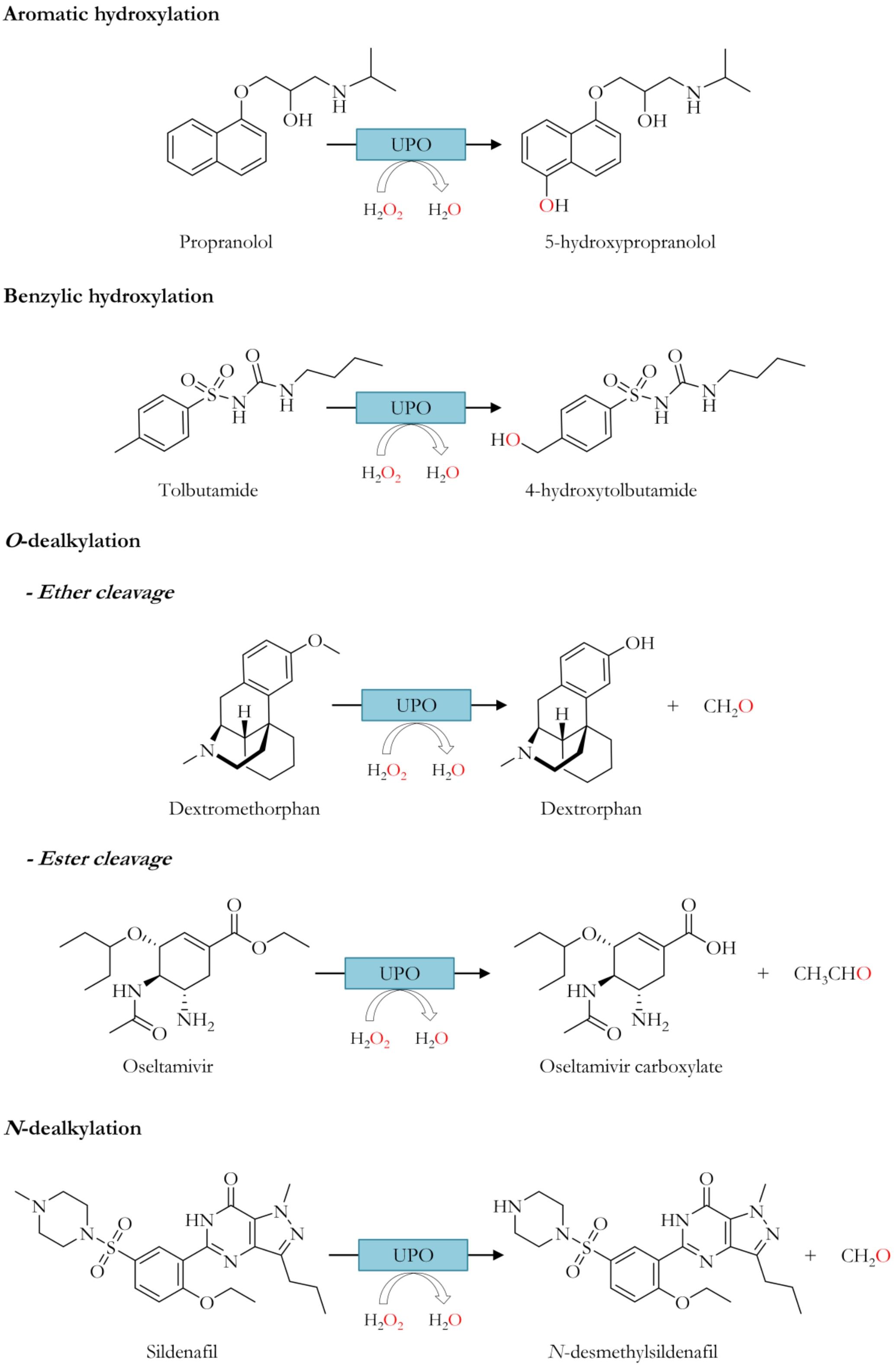
Aromatic hydroxylation
O
OH
N
H
UPO
H_2O_2
H_2O
OH
Propranolol
5-hydroxypropranolol
Benzylic hydroxylation
O
O
S
N
H
HO
Tolbutamide
4-hydroxytolbutamide
O-dealkylation
- *Ether cleavage*
H
N
OH
+
CH_2O
Dextromethorphan
Dextrorphan
- *Ester cleavage*
HN
NH_2
CH_3CHO
Oseltamivir
Oseltamivir carboxylate
N-dealkylation
Sildenafil
N-desmethylsildenafil

Figure 1.4. Substrate scope of UPOs (mostly focused on the transformation of pharma compounds into the corresponding human drug metabolites). Continues on next page.

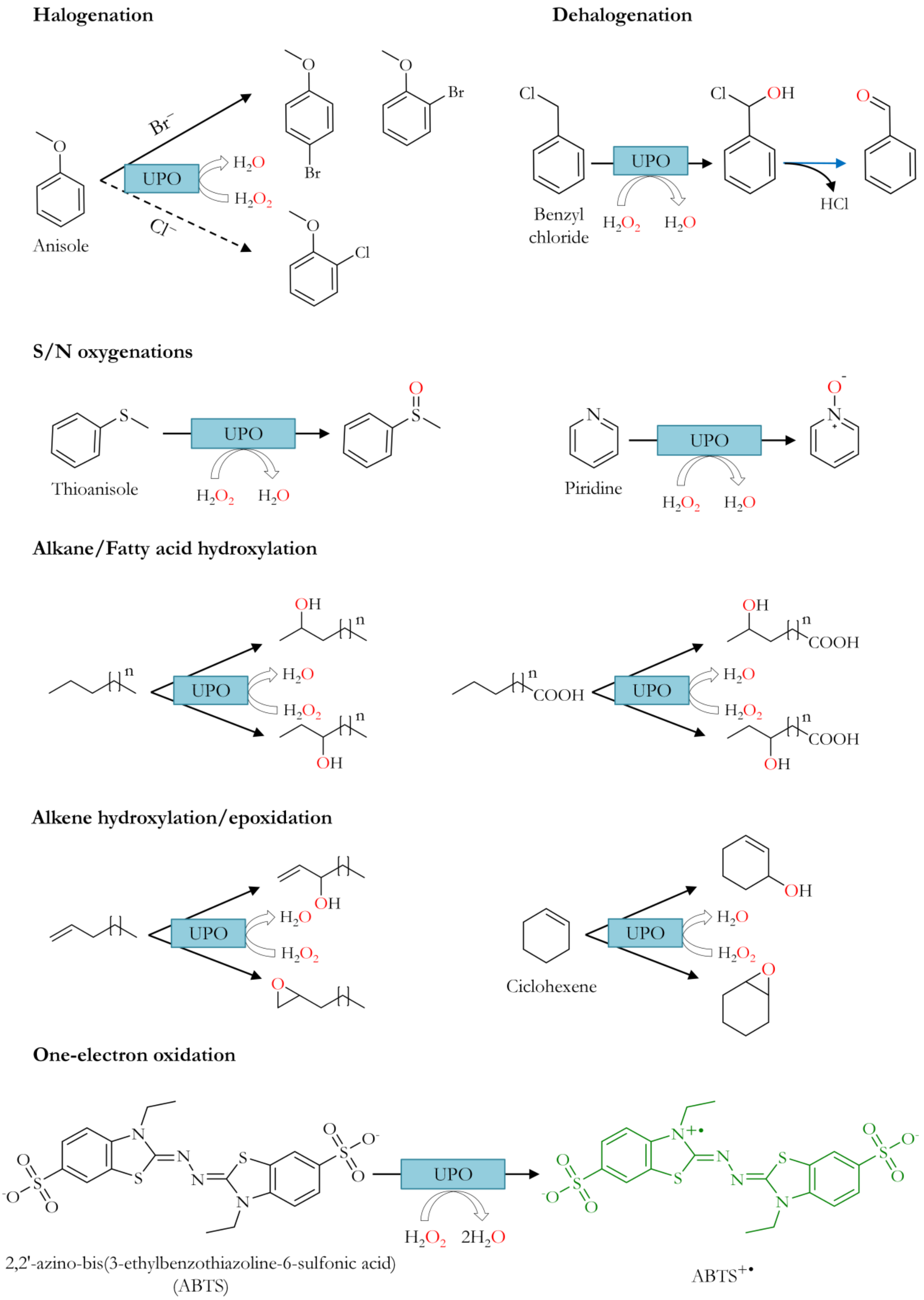
Halogenation
Anisole
UPO
Br⁻
Cl⁻
H_2O
H_2O_2
O
Br
Cl
Dehalogenation
Benzyl chloride
UPO
H_2O_2
H_2O
Cl
OH
HCl
O
S/N oxygenations
Thioanisole
UPO
H_2O_2
H_2O
S
O
Piridine
UPO
H_2O_2
H_2O
N
O⁻
Alkane/Fatty acid hydroxylation
UPO
H_2O
H_2O_2
OH
n
COOH
Alkene hydroxylation/epoxidation
UPO
H_2O
H_2O_2
OH
O
Ciclohexene
One-electron oxidation
UPO
H_2O_2
$2H_2O$
2,2'-azino-bis(3-ethylbenzothiazoline-6-sulfonic acid)
(ABTS)
ABTS$^{+\bullet}$
N
S
O
⁻O
N+•

Figure 1.4. Substrate scope of UPOs. Dashed arrow: less common reaction. Blue arrow: spontaneous rearrangement.

UPOs catalyze the hydroxylation of linear, branched and cyclic alkanes and alkyls including propane, ciclohexane, fatty acids and long chain alcohols (Peter et al., 2011). *n*-Alkanes are mainly hydroxylated to 2- and 3-alkanols or diols with differences in efficiency and selectivity depending of the UPO and substrate used. In the case of fatty acids (*e.g.* from C12 to C20) *Aae*UPO produces ω-1 and ω-2 hydroxy and keto derivatives (over-oxidation via *gem*-diol intermediates) (Gutiérrez et al., 2011). Ratios of the products can vary depending on the chain length. It is worth mentioning the behavior of *Mro*UPO with alkanes and fatty acids, in both cases hydroxylation occurs preferably at the terminal position (ω-OH) with further production of carboxylic acids by stepwise over-oxidation (Olmedo et al., 2016). Besides, *Mro*UPO was found to hydroxylate fatty acids to the corresponding α-hydroxy acids, which are further oxidized to α-keto intermediates whose decarboxylation produces one-carbon shorter fatty acids (Olmedo et al., 2017).

UPOs also oxidize linear, branched or cyclic alkenes (olefins) and unsaturated fatty acids via epoxidation and allylic hydroxylation; the ratio of both activities is dependent on the chemical structure of the substrate and the UPO used (Aranda et al., 2018; Peter et al., 2013). Small alkenes such as propene or 2-butene are exclusively epoxidized, while linear 1-alkenes from 1-butene to 1-octene as well as cyclohexene are both epoxidized and hydroxylated in the allylic position (with preference for epoxidation reaction). An interesting epoxidation reaction is the catalysis of the bulky molecule of testosterone by *Cgl*UPO, it produces the 4,5β-epoxide which is a useful precursor of 4-hydroxytestosterone, currently being studied due to its aromatase inhibitor properties and its potential cytostatic effect for the treatment of breast cancer (Zweifel et al., 2017). In addition to the epoxide, small amounts of hydroxylation product at C16 (16α-hydroxytestosterone) can be formed depending on the amount of co-solvent used (Kiebist et al., 2019, 2017).

Peroxygenation of aromatics was one of the first reactions studied, with the potential for oxygen transfer demonstrated for the first time during the oxygenation of toluene and naphthalene by *Aae*UPO (Ullrich and Hofrichter, 2005). These reactions proceed via the formation of semi-stable epoxide intermediates, which rearrange at pH<7 (the so called NIH-shift) to the corresponding phenolic products and later can be transformed into quinones due to peroxidase activity. As an example, naphthalene is epoxidized by UPO at double bond between positions 1-2, this epoxide will rearrange by NIH-shift into 1-naphthol (97%) and in a lower proportion to 2-naphthol (2%). 1-naphthol is an important agrochemical, and its production with UPO has been enhanced through directed evolution in previous studies in our group (see **Section 1.3.2**) (Molina-Espeja et al., 2016a). During these studies, noticeable amounts of 1-4 naphthoquinone were produced, pointing to a possible second epoxidation reaction at positions 3-4, turning spontaneously into naphthalene-1,4-diol. The latter is substrate for the UPO's peroxidase activity whereby quinones are produced and further polymerized (**Figure 1.5**). This double hydroxylation event has also been studied in depth for the preparation of diepoxides of naphthalene at high pHs (manuscript in preparation).

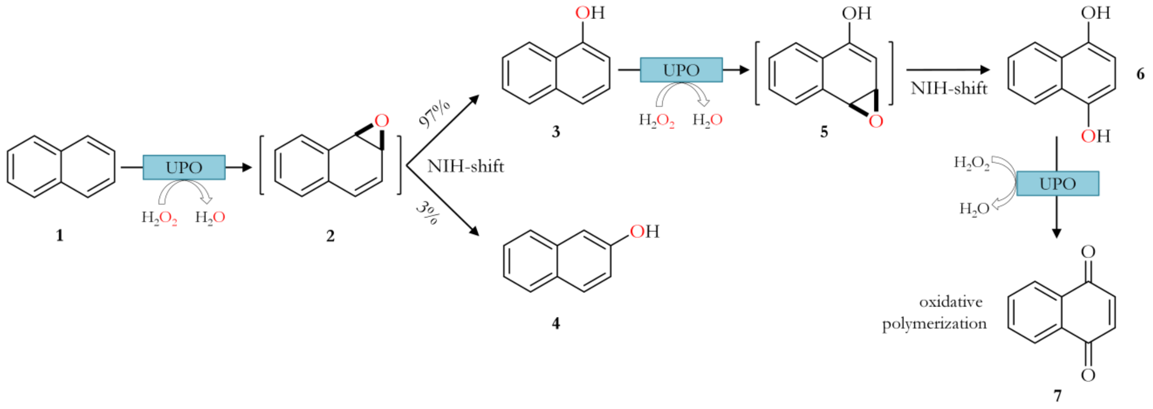

Figure 1.5. Conversion of naphthalene by *Aae*UPO. Naphthalene (1) is substrate of peroxygenase activity of UPO, giving rise to 1-2 naphthalene oxide (2), which rearranges by NIH-shift into 1-naphthol (3) and in a lower proportion to 2-naphthol (4). 1-naphtol can be substrate again of peroxygenase activity producing an epoxide at positions 3-4 (5) which eventually rearranges into naphthalene-1,4-diol (6), the latter can be substrate of the peroxidase activity via one-electron oxidation and produce 1,4 naphthoquinone (7).

In the case of toluene, *Aae*UPO converted one third of the substrate via aromatic ring hydroxylation and two thirds by benzylic hydroxylation (stepwise oxidation of the methyl group). On the contrary, *Mro*UPO formed less than 5% ring hydroxylation products but >90% benzylic hydroxylation products by a stepwise oxygenation reactions (*i.e.* from benzyl alcohol to benzaldehyde and finally to benzoic acid) (Gröbe et al., 2011). The fact that *Aae*UPO is particularly efficient in the oxidation of aromatic rings gave rise to one of the first names for UPO, aromatic peroxygenase (APO).

UPO dealkylations (the cleavage of ethers and secondary/tertiary amines), can be regarded as special cases of alkyl hydroxylation because the catalysis proceeds via hydroxylation of adjacent methylene or methine groups. The resulting unstable hemiacetals and hemiaminals spontaneously decay, releasing water and forming alcohols/phenols, primary (or secondary) amines and aldehydes (Kinne, 2010; Kinne et al., 2009). Dealkylation reactions by UPO have been widely studied in the context of pharmaceuticals.

Drugs like naproxen (NSAID), dextromethorphan (antitussive) and sildenafil (PDE5 inhibitor) are converted to their *O*- and *N*-demethylated analogues. Ester cleavage is a specific case of *O*-dealkylation as *Cra*UPO selectively cleaved oseltamivir (antiviral) to oseltamivir carboxylate and acetaldehyde in high yield. Interestingly, oseltamivir is not converted by *Aae*UPO (Kinne, 2010; Poraj-Kobielska et al., 2011).

Concerning the halogenating activity, *Aae*UPO and *Cra*UPO can perform bromination of phenol in the presence of bromide producing 2-bromo- and 4-bromophenol at a ratio 1:4. The chlorinating activity of both enzymes is much lower, in the presence of chloride and with much more quantity of enzyme, *p*-benzoquinone is the major product with only traces of 2-chlorophenol (1%) and without 4-chlorophenol detected (Anh et al., 2007; Ullrich and Hofrichter, 2005). However, neither *Mro*UPO nor *Cgl*UPO are capable of brominating or chlorinating phenol in the presence of bromide/chloride. It seems that short UPOs lack of halogenation activity (Gröbe et al., 2011; Kiebist et al., 2017). Dehalogenation activity proceeds via initial oxygenation with posterior spontaneous reaction, as seen with benzyl chloride and the geminal halohydrin formation (Hofrichter and Ullrich, 2014).

UPOs incorporate oxygen also into heterocyclic ring systems as those of pyridine or dibenzothiophene, which result in the formation of *N*-oxides and sulfoxides, respectively (Aranda et al., 2009; Ullrich et al., 2008). *Aae*UPO also oxidizes enantioselectively the side chain of aryl alkyl sulfides such as thioanisole into the corresponding (*R*)-sulfoxide with high efficiency (Bassanini et al., 2017).

One-electron oxidations catalyzed by UPOs are assayed with classical peroxidase substrates such as ABTS (2,2'-azino-bis(3-ethylbenzothiazoline-6-sulfonic acid)), or 2,6-dimethoxyphenol (Anh et al., 2007; Gröbe et al., 2011; Ullrich et al., 2004). These oxidations represent a synthetic hurdle as they can cause the formation of phenoxy radicals (from phenolic structures that may appear due to hydroxylation activity of the enzyme), which can undergo spontaneous coupling reactions (oxidative polymerization) and/or disproportionations (1,4 naphthoquinone formation, **Figure 1.5**). To circumvent this problem, radical scavengers such as ascorbic acid can be added to the reaction mixture to facilitate the reduction of the resulting phenoxy radicals back to phenols (**Figure 1.6**) (Hofrichter et al., 2015), however more efficient methods are highly demanded, specially paying attention to UPO engineering methods as those approached in this Doctoral Thesis.

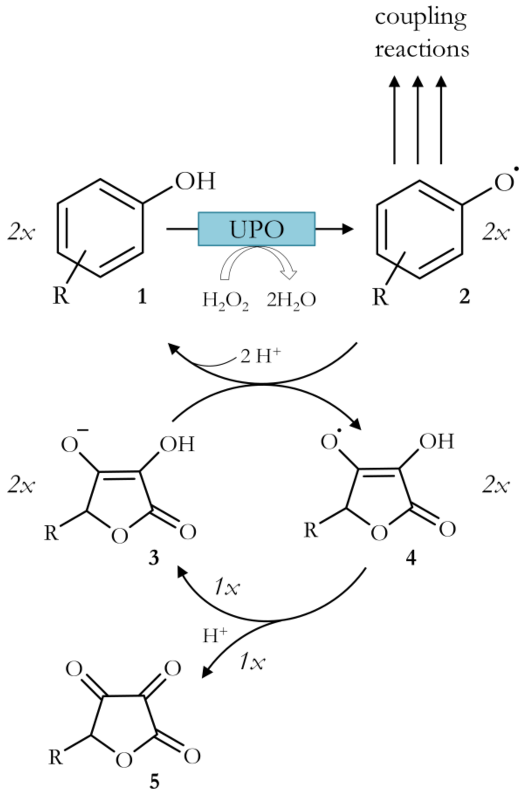

Figure 1.6. Re-reduction of phenoxyl radicals by ascorbic acid derived from unwanted peroxidase activity of UPOs. Two molecules of a phenolic substrate (1) produce two phenoxyl radicals due to peroxidase activity which can undergo polymerization (2), while two molecules of ascorbic acid at pH 7 (3) can render two molecules of ascorbyl radical (4) that disproportionate to dehydroascorbic acid (5) and ascorbic acid again. Adapted from (Hofrichter et al., 2015).

1.1.4. Industrial applications of UPOs focused on the pharmaceutical sector: human drug metabolites (HDMs)

New drugs are currently being designed thanks to a better understanding of the biological targets associated with different diseases. Thus, modern organic chemistry is becoming more and more involved in the discovery and testing of new bioactive compounds (National Research Council, 2015). Human liver is in charge of the metabolism of most drugs, principally through the catalytic action of cytochrome P450s. Their activities are responsible for the release of human drug metabolites (HDMs), which may be biologically active through different pharmacological, toxicological or physiological interactions or they can be converted into more polar and hence more excretable species. As such, it is important to be capable of synthesizing significant amounts of HDMs in order to perform adequate drug bioavailability, pharmacodynamics and pharmacokinetics studies (Atrakchi, 2009; Baillie et al., 2002). Indeed, the US Food and Drug Administration (FDA) guidelines for metabolites in safety testing (MIST) declare that all metabolites generated at >10% of the total parent drug-related exposure must be subjected to safety testing (Atrakchi, 2009, updated in 2020). The amount of metabolite required varies from sub-milligram for structure determination/*in vitro* activity assay, to grams for bioanalytical assay or *in vivo* studies; that means that the method for metabolite preparation (chemical or biosynthetic methods) should be selected based on metabolite structure and assay to be performed (Li et al., 2009). Chemical synthesis is the preferred method for larger scale metabolite preparation, but it is often a resource-intensive exercise and certain metabolites have particularly difficult synthetic challenges and they are often accompanied by low yields or lack in scalability. Microbial transformation is also an alternative (Zöllner et al., 2010) but it typically requires specific fermentation know-how and equipment, as well as downstream processes for the isolation of products from complex media. Taken together, enzymes are presented as feasible options for this aim (Kiebist et al., 2019).

For instance, the use of enzymes to hydroxylate propranolol (a β-blocker widely used to treat high blood pressure, to control heart rhythm or to prevent migraines (Al-Majed et al., 2017)) has been previously studied. Human P450s isolated from hepatic microsomes or produced in heterologous hosts have been tried, yet the constraints on expression, instability and the low reaction rates are still serious obstacles that must be circumvented (Eiben et al., 2006). Human P450s are membrane bound and cofactor dependent biocatalysts, such that a simpler and more autonomous system would be desirable. Accordingly, soluble bacterial P450-BM3 was engineered to work *via* the "peroxide shunt" pathway, *i.e.* fueled by catalytic amounts of H_2O_2 in the absence of redox cofactors (NADPH) and auxiliary flavoproteins, just like an "artificial" peroxygenase. In addition, an ensemble of P450-peroxygenase variants was tailored to transform propranolol into a complex mixture of compounds enriched in the dealkylation product desisopropylpropranolol (DIP), along with low amounts of 4´-hydroxypropranolol (4´-OHP) and 5´- hydroxypropranolol (5´-OHP) (Otey et al., 2006); being the last two the main HDMs of propranolol which have equipotent β-receptor antagonist activity compared to that of propranolol (Greenslade and Newquist, 1978). The production of HDMs from propranolol has been studied in the present Doctoral Thesis by means of directed *Aae*UPO evolution.

As mentioned before, UPO-catalyzed reactions generally resemble those of P450s, which is the reason for using this synthesis tool for metabolite preparation. This application was firstly studied with long UPOs (*Aae*UPO and *Cra*UPO) in 2011 (Poraj-Kobielska et al., 2011), using 23 different drugs such as anti-inflammatories (diclofenac, acetanilide, ibuprofen…), β-blockers (propranolol and metoprolol), a Na^+-channel blocker (tolbutamide), a neuraminidase inhibitor (sildenafil), an antiviral (oseltamivir) or antitussive drugs (dextromethorphan) among others (see **Figure 1.4**). Ideally, a handful of UPO mutants may cover the catalytic diversity of as much as 60 human P450s in terms of oxyfunctionalizing pharmaceuticals to form the corresponding HDMs.

Another relevant example of application of UPO for HDMs is in vitamins biotransformations. Vitamins D_{1-5} (calciferols) are a group of liposoluble secosteroids essential for calcium and phosphate homeostasis in animal metabolism, which causes rickets in children and osteomalacia in adults when deficient (Bikle, 2014). Vitamin D_3 (cholecalciferol) and vitamin D_2 (ergocalciferol) were hydroxylated regioselectively at the C25-position by r*Cci*UPO, see **Figure 1.7** (Babot et al., 2015b, 2015a). 25-Hydroxyvitamin D_3 (25-OH-D_3, 25-hydroxycholecalciferol) is the first metabolically relevant form of circulating vitamin D (catalyzed by human P450 CYP2R1) whereas 1α25-dihydroxyvitamin D_3 (calcitriol) represents the major active form (formed by CYP27B1). Positive effects of supplementation with 25-OH-D_3 were shown for hyperglycemia or chronic kidney disease (Jones, 2013). In addition to the physiological focus of 25-OH-D_3 for human health, this metabolite is also useful for feeding poultry and other animals (Fritts and Waldroup, 2003).

Regarding short UPOs, *Mro*UPO is capable of synthetizing HDMs from the bile acid reabsorption inhibitor volixibat, a drug candidate developed by Sanofi under the name of SAR548304 and now under clinic investigation in phase I by Shire (SHP626) for the treatment of nonalcoholic steatohepatitis (NASH) (Siebers et al., 2018). Stepwise *N*-demethylation was the main metabolic pathway observed in Sanofi *in vitro* studies with human and hamster microsomes (P450 activity), which were the same products obtained when incubating volixibat with *Mro*UPO (Kiebist et al., 2015). In contrast, the chemical synthesis required five steps starting from a volixibat precursor to obtain an overall yield of the bis-*N*-demethylated of 27% compared to the 66% generated by the direct biotransformation with *Mro*UPO (**Figure 1.7**). Very recently, HDMs of cyclophosphamide (CPA, a widely used anti-cancer prodrug) have been synthetized using this enzyme (4-hydroxycyclophosphamide (4-OH-CPA), its tautomer aldophosphamide (APA) and the overoxidized product 4-ketocyclophosphamide (4-keto-CPA)). 4-OH-CPA was isolated and tested with two human cancer cell lines, demonstrating that peroxygenase-produced 4-OH-CPA can be used for direct cyto- and genotoxicity evaluation in human cancer cells (Steinbrecht et al., 2020).

Moreover, an interesting cleavage reaction was reported for corticosteroids when using *Mro*UPO and *Mwe*UPO. Three model steroids, cortisone (**Figure 1.7**), Reichstein's substance S and prednisone were stepwise oxygenated at the C17 side chain and finally C–C cleaved to obtain adrenosterone, androstendione and 1,4-androstadien-3,11,17-trione respectively. As an example, cortisone oxidation starts with the hydroxylation of the terminal carbon (C21) (cortisone 21-*gem*-diol) and later with a second hydroxylation resulting in the corresponding α-ketocarboxylic acid (cortisone 21-oic acid). The latter decomposes forming adrenosterone as well as formic and carbonic acid (Ullrich et al., 2018).

The regio- and stereoselective oxyfunctionalization into complex pharmaceuticals represents a great challenge for organic chemistry. As described in this introduction, the versatility of UPOs (sometimes regarded as an "extracellular fungal liver"), offers a broad spectrum of oxyfunctionalization reactions of great utility in both the pharmaceutical and chemical industry.

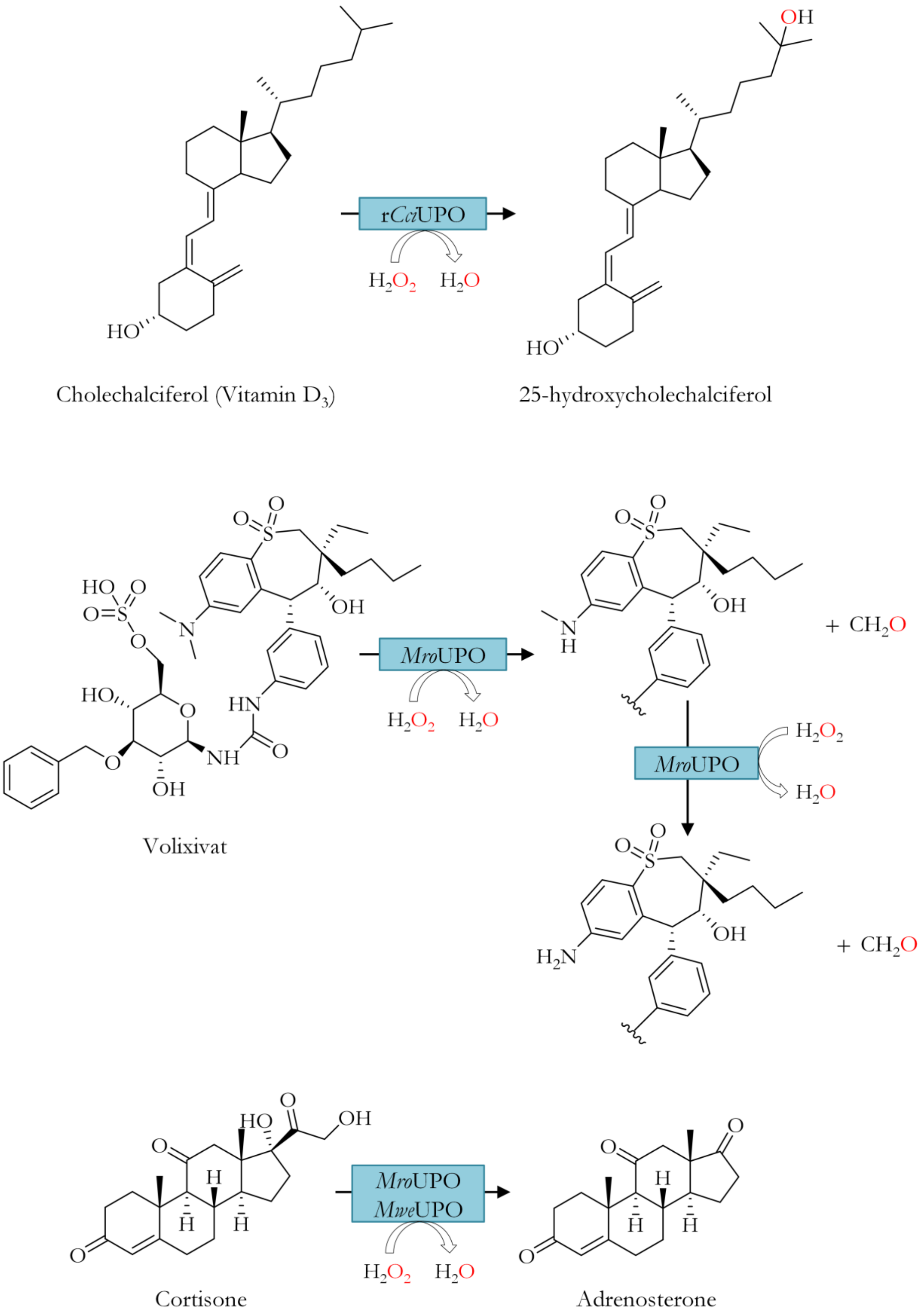
OH
rCciUPO
H2O2
H2O
HO
Cholechalciferol (Vitamin D3)
25-hydroxycholechalciferol
MroUPO
Volixivat
+ CH2O
H2N
MweUPO
Cortisone
Adrenosterone

Figure 1.7. Examples of other HDMs and hormone synthesis with different UPOs.

1.1.5. Challenges for industrial use

The main hurdle for a new peroxygenase-based chemistry is the production and engineering of UPO in efficient and robust recombinant expression systems. Only a few examples have been hitherto described in the literature: the evolved *Aae*UPO secretion mutant (called PaDa-I variant, see **Section 1.3.2**) and its offspring of variants for multiple applications (Martin-Diaz et al., 2018; Mate et al., 2017; Molina-Espeja et al., 2014, 2015, 2016a, 2016b; Ramirez-Escudero et al., 2018), as well as the UPOs developed by Novozymes A/S (Denmark) heterologously expressed in *Aspergillus oryzae*: UPO from *Coprinopsis cinerea* (r*Cci*UPO) (Babot et al., 2013) and UPO from an undetermined mold (rNOVO) (Peter et al., 2014). Besides, very recently *Mro*UPO (Carro et al., 2019), *Collariella virescens* UPO (r*Cvir*UPO) (González-Benjumea et al., 2020) and *Daldinia caldariorum* UPO (r*Dca*UPO) (Linde et al., 2020) have been reported to be expressed in *Escherichia coli*. Even with all of these expression examples, only if cost-effective and reliable heterologous production of recombinant UPO proteins at adequate level is implemented, their application in the pharmaceutical, cosmetic or fine chemical sectors will be a realistic option. Depending on the product of interest, the production of "g to Kg-per-Liter" can be found successful as fine chemicals and active pharmaceutical ingredients (APIs) do not require a ton level amount of products. Successful attempts in this direction have been made by Novozymes for the expression r*Cci*UPO, reaching the "g-per-Liter" level (data not published) and lately by the newly created startup EvoEnzyme S.L., with variants of UPO from *Aae*UPO obtained by directed evolution techniques and expressed in the methylotrophic yeast *Pichia pastoris* (*Komagataella phaffii*).

Another issue to be taken into account is the peroxygenase-peroxidase activity duality of UPOs (*P:p* ratio), which represents a potential problem depending on the desired product sought. As described before, phenolic compounds can be further oxidized by UPO, reducing the amount of product of interest. Several efforts have been made in this direction not only by reaction engineering (*i.e.* use of ascorbic acid) but also by protein engineering, trying to find variants with a weaker peroxidase activity while protecting the desired peroxygenase activity within a given biotransformation (Mate et al., 2017; Molina-Espeja et al., 2016a). This concern has also been studied in the present Doctoral Thesis.

It is also worth mentioning that many of the UPO substrates are rather hydrophobic and exhibit low water solubility. As aforementioned, UPOs stability in organic solvents can be considered high as they have been used even under neat conditions (Fernández-Fueyo et al., 2016a; Kinne et al., 2009). However, although stable, UPO is hardly active at high cosolvent concentrations. Immobilization has been a successful approach, with two recent examples of *Aae*UPO; in a covalently epoxide-modified polyacrylic matrix (Immobead IB-COV-1, Chiralvision, Netherlands) for the production of styrene derivatives (Rauch et al., 2019) and in alginate beads where UPO was active for up to seven days under neat reaction conditions (Hobisch et al., 2020). Our laboratory is also making an important effort in this regard by directed UPO evolution: we have recently applied a *palette* of different laboratory evolution methods (neutral genetic drift, adaptive evolution, site directed recombination) to tailor *Aae*UPO variants active and stable in organic solvents of different chemical nature and polarity (Martin-Diaz, 2019).

Last but not least, the low oxidative stability of UPO (the fast and irreversible inactivation caused by catalytic concentrations of H_2O_2) has always been a matter of concern. Departing from Compound II, in the presence of a large excess of hydrogen peroxide it can turn into Compound III [Heme-Fe^{3+}-$^{\bullet}OOH$] which may be involved in irreversible heme-bleaching (verdoheme and biliverdin formation) by hydroxyl radicals ($^{\bullet}OH$) (Karich et al., 2016). A strategy to limit Compound III formation is to use high substrate-UPO and UPO-H_2O_2 concentration ratios. Other strategies to prevent UPO damage by excess of peroxide and derived radicals include gentle *in situ* H_2O_2 supply. This strategy is being actively studied by combining UPOs with photo-, electro- and chemo-catalysis, as well as by using enzyme cascade reactions, all of them aimed at controlling the gradual supply of H_2O_2 *in situ* (Burek et al., 2019; Fernández-Fueyo et al., 2016a; Freakley et al., 2019; Hobisch et al., 2020; Li et al., 2020; Tieves et al., 2019; van Schie et al., 2019, 2020; Willot et al., 2020, 2019; Yayci et al., 2020; Yoon et al., 2020; Zhang et al., 2017, 2018). The protein engineering of UPO for H_2O_2 stability could be an interesting option, however it has to be noted that other efforts in this direction were already done with the versatile peroxidase from *Pleorotus eryngii* (VP): while the resistance against peroxide was strongly increased, it was at the cost of jeopardizing some of the catalytic sites of the enzyme (Gonzalez-Perez et al., 2014a). Given this experience with VP engineering and bearing in mind the broad UPO promiscuity, we don't consider the engineering of UPO variants for H_2O_2 tolerance as the most suited option to face this problem; instead, the engineering of UPO enzyme fusions to control the *in situ* the supply of H_2O_2 is an attractive alternative that is studied in this Doctoral Thesis.

1.2. Fusion proteins

1.2.1. Characteristics and applications

Due to the H_2O_2 damage described before and the good results obtained when using H_2O_2 supplying enzymes, the use of a fusion protein as a whole system catalyst may result in an appealing approach. Fusions are a cheap option as only one polypeptide -

containing the two enzyme partners- has to be expressed and purified; and the proximity of the catalytic sites avoids the diffusion of the intermediate product (co-substrate, H_2O_2), increasing the combined reaction rate (substrate channeling) (Aalbers and Fraaije, 2019a) which can also be determinant in cascade reactions. Since the first bifunctional fusion enzyme was published in 1970 (a histidinol dehydrogenase/aminotransferase) (Yourno et al., 1970), several fusion enzymes have been created. Some of them are designed for cofactor regeneration (Aalbers and Fraaije, 2019b; Beyer et al., 2017), for enzymatic cascade (Deng et al., 2016; Huang et al., 2019) with only a couple of examples of enzyme fusions for *in situ* peroxide generation systems *(i.e.* with bacterial peroxidases and fatty acid decarboxylase cytochrome P450 (OleTJE) (Colpa et al., 2017; Matthews et al., 2017).

A successful construction of an enzyme fusion is typically arranged around three key elements: the connection between the enzyme partners, their order within the fusion and the enzymes involved. Rather than directly connecting UPO to the other enzyme, *i.e.* placing the genes together without a stop codon, inserting a peptide linker to connect one to the other can avoid misfolding and/or lack of expression (Amet et al., 2008; Zhao et al., 2008). Given that not only the type of the amino acids of the linker but its length can be crucial, flexible and rigid linkers of different sizes and composition are usually tried. Flexible linkers allow certain degree of movement to take place between the enzyme partners (mainly composed of repetitions of small or hydrophilic amino acids such as Gly), whereas rigid linkers with stiff structures (*e.g.* α-helical structures or multiple Pro residues) may separate functional domains more efficiently, albeit at the cost of flexibility. By adjusting the copy number "n", the length of this GS linker can be optimized to achieve appropriate separation of the functional domains, or to maintain necessary interdomain interactions. Cleavable linkers are generally used when releasing the free functional domain *in vivo* is needed (Chen et al., 2013) **Table 1.2**. Enzyme partners are chosen in terms of their cooperative function; in our case UPO plays the lead role (oxyfunctionalization partner) and another enzyme the supporting role (H_2O_2 generation partner). Accordingly, choosing the correct enzyme ally for UPO can be crucial for designing a functional enzyme fusion.

Table 1.2. Summary of empirical linkers. Adapted from (Chen et al., 2013).

Linker	Advantages	Characteristics	Examples
Flexible 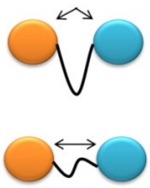	Allows interaction between domains and gives distance between them	Small or hydrophilic aminoacids	$(GGGGS)_n$ $(G)_n$
Rigid 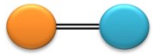	Mantains the distance between domains	α-helix or proline rich	$(EAAAK)_n$ $(XP)_n$
Cleavable	Allows *in vivo* separation of domains	Reductive or enzymatic cleavage	Disulfide, or protease sensitive sequences

1.2.2. Aryl alcohol oxidase (AAO)

In order to design a self-sufficient peroxygenase fusion, the aryl-alcohol oxidase (AAO; EC 1.1.3.7) can be presented as a natural UPO partner. It is a monomeric extracellular flavoprotein, which oxidizes a wide range of aromatic alcohols to their corresponding carbonyl compounds, producing H_2O_2 as the only byproduct while acting as a supplier of H_2O_2 in the fungal ligninolytic secretome (Hernández-Ortega et al., 2012) (**Figure 1.8**). With common natural occurrences and complementary functions, both AAO and UPO belong to the group of fungal ligninolytic oxidoreductases (also referred to as ligninases), along with high-redox potential laccases and peroxidases, which are the main enzymes responsible for the degradation of recalcitrant lignin in plants (Alcalde, 2015; Ruiz-Dueñas and Martínez, 2009). Generally speaking, ligninases are precious biocatalysts with a range of applications in environmental biocatalysis, from bioremediation to novel green processes, yet they are extremely difficult to be engineered for practical purposes due to the lack of functional expression in heterologous hosts, and AAO and UPO are not an exception (Martínez et al., 2017). Missing chaperones along with different post-translational modifications (glycosylation, disulfide bridge, N- and C- terminal processing) among natural and heterologous hosts are large hurdles that must be circumvented (Ruiz-Dueñas et al., 2006). As such, the directed evolution of ligninases towards heterologous functional expression becomes a crucial step.

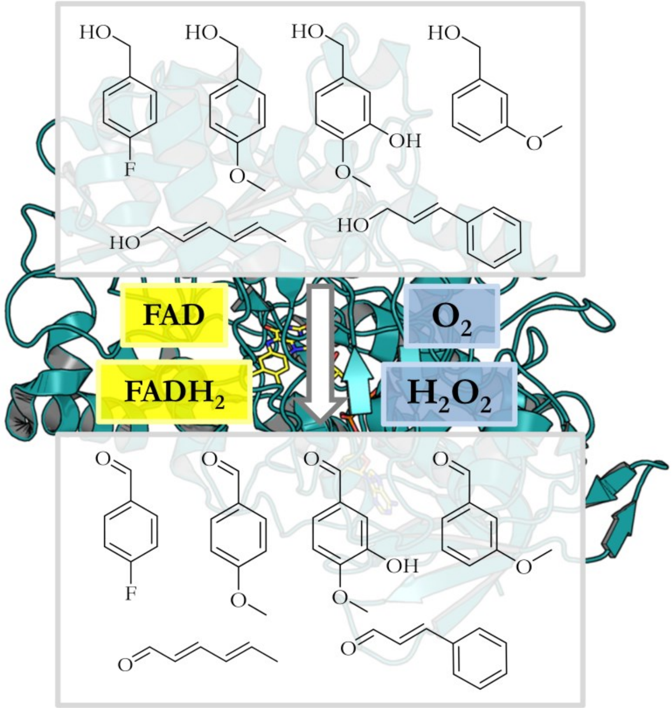

Figure 1.8. AAO creates an aromatic alcohol/aldehyde redox system to generate a constant supply of H_2O_2 to peroxidases and peroxygenases during lignin degradation.

1.3. Directed molecular evolution

1.3.1. Overview of the technique and the S. cerevisiae toolbox

Native enzymes usually require *ad hoc* modifications to turn them into industrial catalysts. This need gave rise to protein engineering approaches such as directed evolution, a revolutionary technique invented by Prof. Frances H. Arnold from the California Institute of Technology (CALTECH, USA) and for which she was awarded with the Nobel Prize in Chemistry 2018. The relevance of this technique is such that modern protein engineering is spinning around laboratory evolution methods aimed at creating enzymes for a more environmentally friendly manufacture of chemical substances (such as pharmaceuticals) or the production of renewable fuels for a greener transport sector, to name just a few. Departing from the natural evolution paradigm established by Charles Darwin (*i.e.* the survival of the fittest by inherited genetic changes and selection) the directed enzyme evolution cycle is based on three essential steps: 1) generation of DNA diversity by random mutagenesis and/or DNA recombination; 2) heterologous functional expression of the gene library in a proper host organism; and 3) screening/selection of the enzyme variants depending on the features of interest. This process can be repeated until the desired enzyme attribute is obtained, **Figure 1.9** (Bloom and Arnold, 2009; Bornscheuer et al., 2012; Molina-Espeja et al., 2016c; Turner, 2009).

S. cerevisiae represents a magnificent heterologous host for directed evolution campaigns of eukaryotic enzymes. With its high frequency of homologous DNA recombination, it represents a molecular toolbox for the development of innovative and easily implantable library creation methods. Rad51 recombinase (orthologue of the bacterial recA) is the main character of the recombination machinery of *S. cerevisiae,* as it allows the assembly of DNA fragments with 40 homologous nucleotides with high fidelity (Gonzalez-Perez et al., 2012; Mate et al., 2017; Zaitseva et al., 1999). This feature contributes to generate genetic diversity, empowering the *in vivo* cloning of libraries into linearized expression vectors in just one single transformation step. Together with the well-developed random mutagenesis methods (*e.g.* by error prone PCR (*ep*PCR)), DNA recombination methods based on the *in vivo* gap repair mechanism help to enrich mutant libraries in function and diversity. Among the main library creation methods supported by the *S. cerevisiae* device; IVOE, DNA shuffling and MORPHING where the ones predominantly used in this Doctoral Thesis.

IVOE (*In Vivo* Overlap Extension) protocol was developed as a fast and reliable way to perform site directed mutagenesis, site-saturation combinatorial libraries and gene assembly, as mutations are located in the primer used for extension of the gene (Alcalde, 2010). DNA shuffling is a common DNA recombination method used for sequences with identities above 50% and with mutations separated 20 residues from each other. It can be also used to evaluate beneficial combinatorial effects between mutations from the offspring of variants (Oldenburg et al., 1997). MORPHING (mutagenic organized recombination process by homologous *in vivo* grouping) combines the methods previously described as it allows the introduction of mutations in certain segments of the gene (using *ep*PCR fragments, as short as 90 base pairs) while protecting the rest of the gene from mutagenesis (amplified with high fidelity polymerases). The resulting DNA fragments possess flanking homologous overhangs to be *in vivo* spliced together with linearized plasmid in a one-pot transformation step (Gonzalez-Perez et al., 2014b). This technique has been used for the directed evolution of signal peptides in order to obtain functional expression variants (Gonzalez-Perez and Alcalde, 2014; Molina-Espeja et al., 2014; Viña-Gonzalez et al., 2015) and to explore different enzyme segments to unveil structural determinants (Gonzalez-Perez et al., 2014a; Mate et al., 2017).

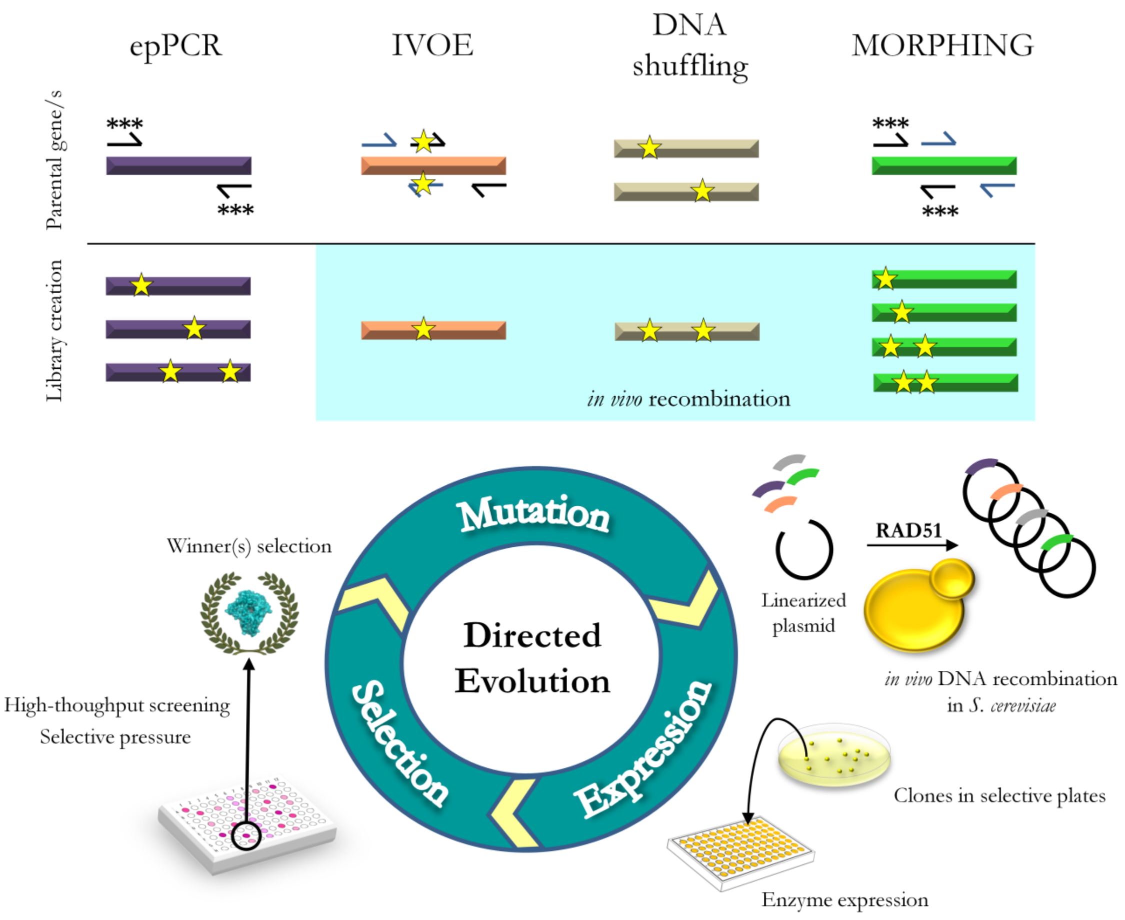
epPCR
IVOE
DNA shuffling
MORPHING
Parental gene/s
Library creation
***
***
***
***
in vivo recombination
Mutation
Directed Evolution
Selection
Expression
Winner(s) selection
High-thoughput screening
Selective pressure
Linearized plasmid
RAD51
in vivo DNA recombination in S. cerevisiae
Clones in selective plates
Enzyme expression

Figure 1.9. Main directed evolution strategies and library creation methods used in this Doctoral Thesis.

1.3.2. Directed evolution of AaeUPO

Six years ago, the first UPO functionally expressed in a heterologous host was published. After 5 rounds of directed evolution combining *in vivo* shuffling and *ep*PCR (with different mutational loads), as well as DNA polymerases with different mutational bias, a final secretion variant called PaDa-I emerged. This mutant accumulated four mutations in the signal peptide plus five in the mature protein. MORPHING at the *Aae*UPO signal peptide yielded three mutations (discovered in single mutants) that significantly enhanced secretion (Gonzalez-Perez et al., 2014b). Those changes (F[12]Y, A[14]V and R[15]G) lie in the hydrophobic core of the signal peptide; together with the previously identified A[21]D mutation, these changes diminished the hydrophobicity of the region, and they may favor potential interactions between the signal peptide and the signal recognition particle (SRP) in the endoplasmic reticulum pathway for co-translational translocation (Molina-Espeja et al., 2014). The role of mutations in the mature protein (V57A-L67F-V75I-I248V-F311L, **Figure 1.10**), were analyzed deeply thanks to the crystal structure of the mutant, which was solved at a resolution of 1.5 Å. Several differences were detected between the evolved and native *Aae*UPO, including the presence of a full N-terminus and a broader heme access channel due to some of the mutations that accumulated through directed evolution (I248V-F311L). The most significant change comes from mutation at Phe311, which lies at 3.6 Å from Phe76, establishing a hydrophobic contact. As seen in **Figure 1.1b**, both Phe76 and Phe191 form a pair of protruding aromatic residues at the entrance of the heme channel that help in the access of the substrate to the active site. The change of a bulky Phe to a smaller Leu at position 311 shifts the Phe76 side chain, weakening the contact with Phe191 and possibly leaving Phe191 more exposed to the solvent. This change was accompanied by a dual conformation of Phe191 whose consequence was the broadening of the heme access channel, with distances between Phe191 and Phe76 of 4.1 and 7.8 Å in native *Aae*UPO and PaDa-I, respectively (Ramirez-Escudero et al., 2018).

PaDa-I had similar biochemical properties to the wild type *Aae*UPO in terms of N-terminal processing, degree of glycosylation, isoelectric point, pH activity profiles, stability and spectroscopic features. Regarding the catalytic constants, both enzymes exhibited similar values, although the overall secretion of PaDa-I by *S. cerevisiae* increased by 1,114-fold (to ~8 mg L^{-1}). When the mutant was cloned in *P. pastoris* for overproduction in bioreactor, these values were enhanced to 217 mg L^{-1} (and to the g-per-Liter level after optimization by ADM Biopolis, Spain, data not published), with the variant conserving all the evolved properties (Molina-Espeja et al., 2015).

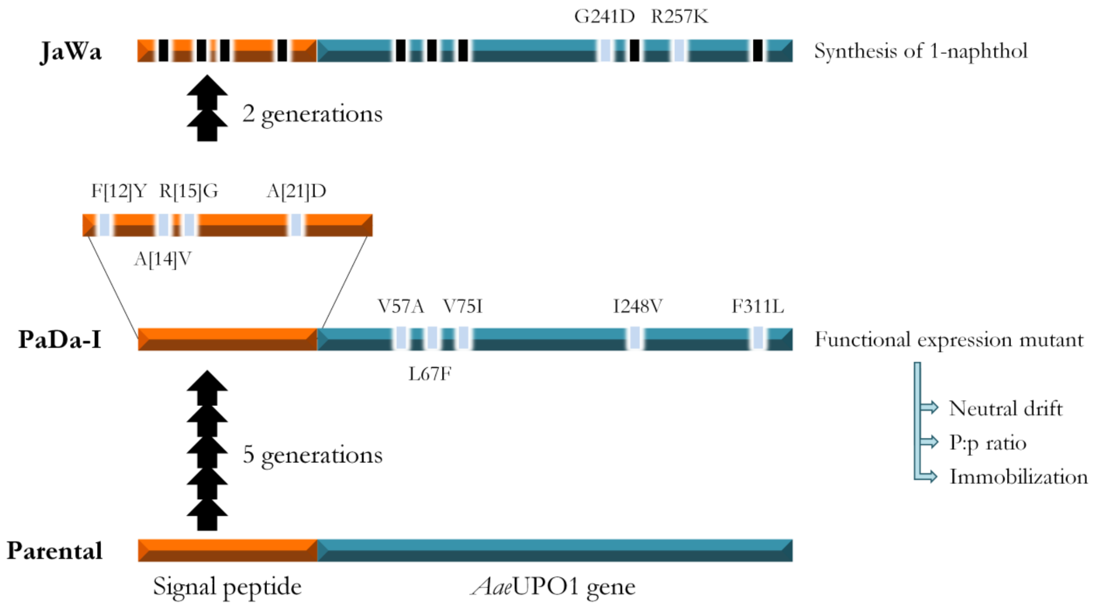
G241D
R257K
JaWa
Synthesis of 1-naphthol
2 generations
F[12]Y
R[15]G
A[21]D
A[14]V
V57A
V75I
I248V
F311L
PaDa-I
Functional expression mutant
L67F
Neutral drift
P:p ratio
Immobilization
5 generations
Parental
Signal peptide
*Aae*UPO1 gene

Figure 1.10. Directed evolution campaigns for *Aae*UPO. Final mutant names are written in bold on the left side of the figure. Blue arrows on the right indicate other engineering works carried out from the PaDa-I variant.

This evolution platform enabled further rounds of random mutation and screening to tailor an efficient UPO for the synthesis of 1-naphthol, (disclosing the JaWa variant with the G241D-R257K mutations) (Molina-Espeja et al., 2016a) (**Figure 1.10**). Leaving aside further directed evolution experiments based on MORPHING and neutral genetic drift (Mate et al., 2017; Martin-Diaz et al., 2018), the JaWa variant is the starting point used in this Doctoral Thesis.

1.3.3. Functional expression of AAO

AAO from white rot fungus *Pleurotus eryngii* was heterologously functionally expressed in *S. cerevisiae* by fusing a chimeric signal peptide (preαproK) and applying structure-guided evolution (Viña-Gonzalez et al., 2015). The chimeric signal peptide fused the pre- and pro- region of the α-factor and the K_1 killer toxin prepro-leaders from *S.cerevisiae* whereas for the evolution of mature protein a combination of MORPHING and *in vivo* shuffling was carried out. The panel of AAO secretion variants was leaded by the FX7 mutant, in which the consensus/ancestral substitution (H91N) was responsible for a ~100-fold improvement in total activity, as well as enhanced stability in terms of temperature and pH. Additionally, FX7 was *in vivo* shuffled with other variant winners giving rise to FX8, where the T[50]A mutation in the proK segment, the L170M mutation at the surface of the protein and the ancestral H91N were combined, producing a 2.5-fold improvement in total activity. Secretion was further improved by MORPHING at the signal peptide. The ultimate secretion variant, the FX9 mutant, included substitutions both in the preα segment and in the proK segment. These mutations increased secretion to up to 4.5 mg/L, giving a 350-fold improvement over the departure point. Afterwards, FX9 was transferred to *P. pastoris* yielding 25.5 mg L^{-1} in fed-batch bioreactor without any optimization (Viña-Gonzalez et al., 2018). **Figure 1.11**. FX9 variant is one of the points of departure to construct a functional UPO fusion in this Doctoral Thesis.

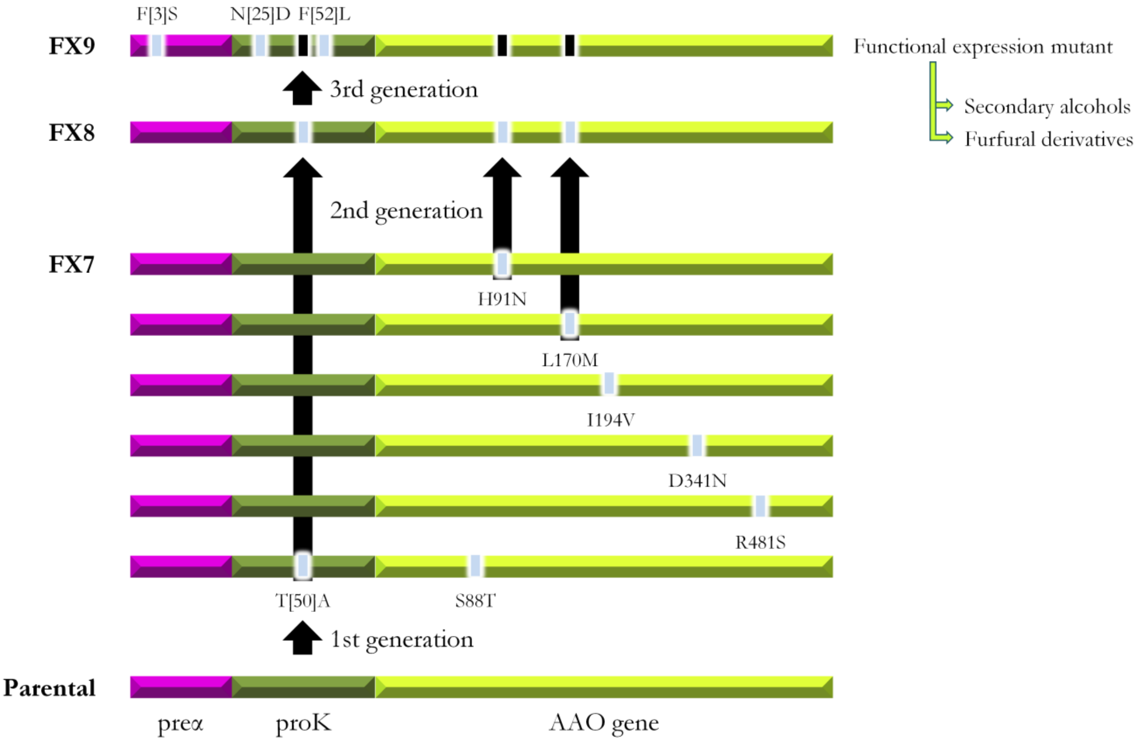
F[3]S
N[25]D
F[52]L
FX9
Functional expression mutant
3rd generation
Secondary alcohols
Furfural derivatives
FX8
2nd generation
FX7
H91N
L170M
I194V
D341N
R481S
T[50]A
S88T
1st generation
Parental
preα
proK
AAO gene

Figure 1.11. Directed evolution campaigns for AAO. Final mutant names are written in bold on the left side of the figure. Green arrows on the right indicate other engineering works carried out from the FX9 variant.

As it happened with UPO before, this evolution platform enabled further rounds of directed evolution to obtain efficient evolved AAO variants for the resolution of racemic mixtures of benzyl alcohols or for the synthesis of furan-2,5-dicarboxylic acid (FDCA) from 5-hydroxymethylfurfural (HMF), a promising building block that can be used in the polymer industry for the production of poly(ethylene-2,5-furandicarboxylate) (PEF) (Serrano et al., 2019; Viña-Gonzalez et al., 2020, 2019).

OBJECTIVES

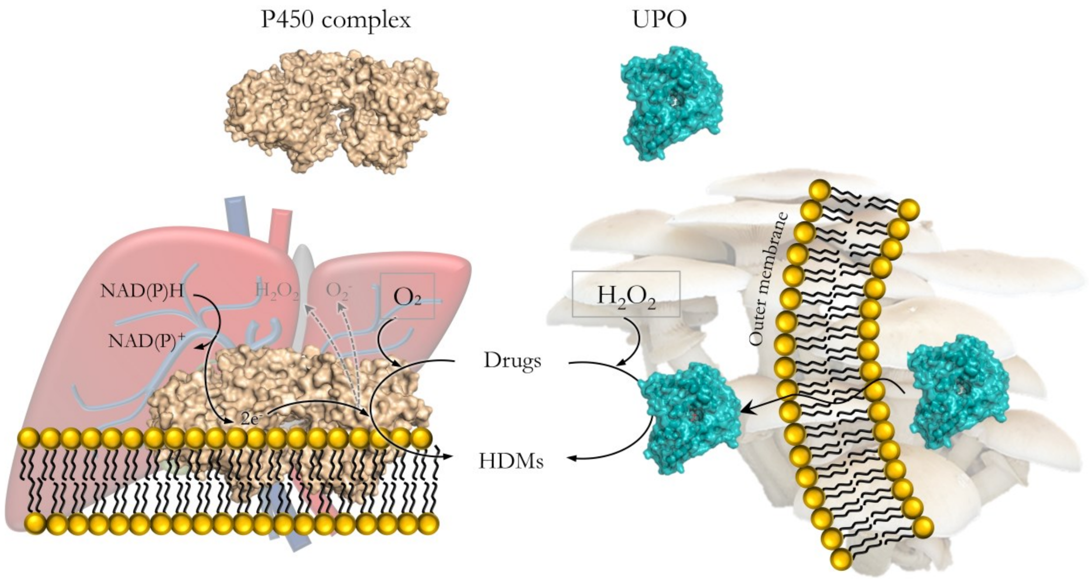
P450 complex
UPO
NAD(P)H
NAD(P)+
H2O2
O2-
O2
2e-
Drugs
HDMs
H2O2
Outer membrane

2. Objectives

The preparation of HDMs using UPOs is a process of great interest that has to be improved for a future use in the pharmaceutical industry. For this purpose, the main objectives of this Doctoral Thesis were:

- To design an efficient *Aae*UPO mutant with improved activity and selectivity in the transformation of the β-blocker drug propranolol into its true HDM 5´-hydroxypropranolol (5´-OHP). This objective included i) the development of a sensitive high-throughput screening assay for detecting mutants with a high peroxygenase activity on propranolol and a weak peroxidase activity over 5´-OHP and ii) the construction of mutant libraries by focused evolution through MORPHING.
- To perform reaction engineering studies by coupling the *Aae*UPO mutant to new H_2O_2 feeding systems in order to reach high total turnover numbers (TTNs).
- To evaluate/benchmark different *Aae*UPO variants in the production of other HDMs of industrial relevance (from dextromethorphan, naproxen and tolbutamide) with the goal of unveiling the main structural determinants involved in such biotransformations.
- To design UPO_AAO fusions as self-sufficient systems whereby producing HDMs in an efficient and straight manner. This objective included the construction of fusions libraries and their screening with a colorimetric assay to dissect both UPO_AAO activities, the biochemical characterization of the best fusions along with the proof-of-concept of their use in the synthesis of dextrorphan, the HDM from dextromethorphan.

MATERIAL AND METHODS

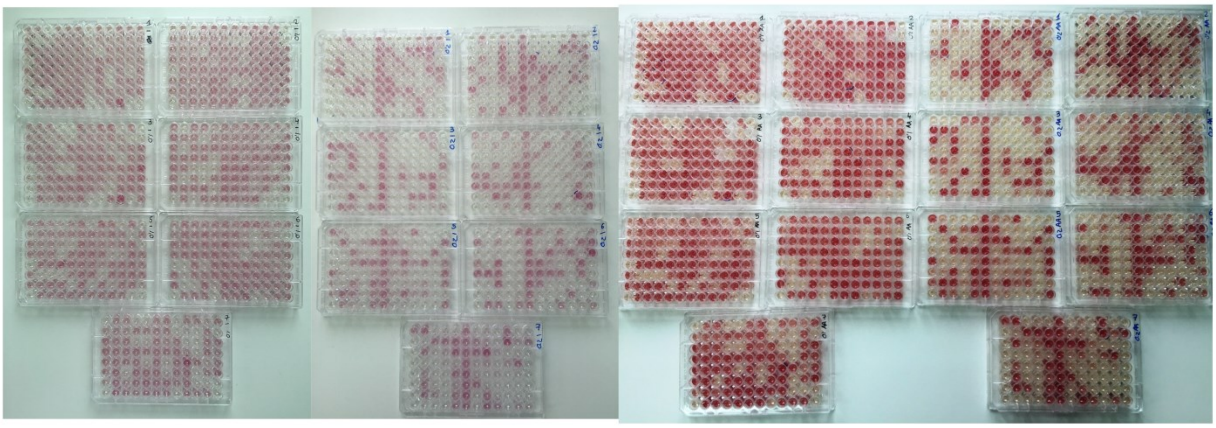

3. Material and methods

3.1. General material and methods

3.1.1. Reagents and materials

Table 3.1. Reagents.

Reagents	Company
2,2'-azino-bis(3-ethylbenzothiazoline-6-sulfonic acid) (ABTS)	Panreac
3-chlorobenzyl alcohol	Sigma-Aldrich
3-hydroxy-4-methoxybenzyl alcohol	Sigma-Aldrich
3-methoxybenzyl alcohol	Sigma-Aldrich
4-chlorobenzyl alcohol	Sigma-Aldrich
4-fluorobenzyl alcohol	Sigma-Aldrich
4-methoxybenzyl alcohol	Sigma-Aldrich
5'-hydroxypropranolol	Santa Cruz Biotechnology
Agarose	BioRad
Ascorbic acid	Sigma-Aldrich
Benzyl alcohol	Sigma-Aldrich
Biotin	Sigma-Aldrich
Bovine serum albumin (BSA)	Sigma-Aldrich
Dextromethorphan hydrobromyde	Santa Cruz Biotechnology
Dextrorphan tartrate	Sigma-Aldrich
DL-propranolol hydrochloride	Acros
Ethanol	Panreac
Glycerol	Panreac
Hydrogen peroxide	Sigma-Aldrich
Imidazole	Sigma-Aldrich
Magnesium chloride	Sigma-Aldrich
Magnesium sulfate heptahydrate	Sigma-Aldrich

Methanol	Panreac
Naproxen	Santa Cruz Biotechnology
Potassium hydroxide	Sigma-Aldrich
Potassium phosphate monobasic	Sigma-Aldrich
Purpald®	Sigma-Aldrich
SeeBandProtein Staining solution	Gene Bio-Application Ltd
Sodium hydroxide	Sigma-Aldrich
Tolbutamide	Sigma-Aldrich
β-Mercaptoethanol	Sigma-Aldrich

Table 3.2. Medium components.

Medium components	Company
Ampicillin	Sigma-Aldrich
Bacto Agar	Difco (BD)
Bacto peptone	Difco (BD)
Chloramphenicol	Sigma-Aldrich
D-(+)-Galactose	Sigma-Aldrich
D-(+)-Glucose	Sigma-Aldrich
D-(+)-Raffinose pentahydrate	Sigma-Aldrich
Yeast extract	Difco (BD)
Yeast Nitrogen Base Without Amino Acids	Sigma-Aldrich
Yeast Synthetic Drop-out Medium Supplements without uracil	Sigma-Aldrich
Zeocin	Ibian

Table 3.3. Molecular biology kits.

Molecular biology kits	Company
4–20% Mini-PROTEAN® TGX™	BioRad
Deoxyribonucleotide triphosphate (dNTP)	Sigma-Aldrich

Gel Loading Solution	Sigma-Aldrich
GelRed® Nucleic Acid Gel Stain	Biotium
GeneRuler 100pb Plus DNA Ladder	Thermo Scientific
GeneRuler 1Kb DNA Ladder	Thermo Scientific
Gibson Asssembly™ Master Mix	New England Biolabs
NucleoSpin plasmid® Kit	Macherey Nagel
NucleoSpin Gel and PCR Clean-up Kit	Macherey Nagel
Protein assay dye reagent Kit II (Bradford)	BioRad
Spectra™ Multicolor high range protein ladder	Thermo Scientific
Yeast Transformation Kit	Sigma-Aldrich
Zymoprep™ Yeast Plasmid Miniprep I	Zymo Research

Table 3.4. Strains and plasmids.

Strains and plasmids	Company
Escherichia coli XL2-Blue competent cells	Agilent
Expression shuttle vector pJRoC30	Caltech
Pichia pastoris expression vector (pBSY5Z)	Bisy
Pichia pastoris strain BSYBG11	Bisy
Saccharomyces cerevisiae strain BJ5465	LGC Promochem

Table 3.5. Commercial enzymes.

Commercial enzymes	Company
Antarctic phosphatase	New England Biolabs
DNA ligase	New England Biolabs
iProof high fidelity DNA polymerase	BioRad
PfuUltra high fidelity DNA polymerase	Agilent
Taq DNA polymerase	Sigma-Aldrich
BamHI restriction enzyme	New England Biolabs

BglII restriction enzyme	New England Biolabs
NotI restriction enzyme	New England Biolabs
SwaI restriction enzyme	New England Biolabs
XhoI restriction enzyme	New England Biolabs

3.1.2. Culture media preparation

Composition of all media described is referred to a final volume of one liter of distilled water. All media and solutions, if not specified otherwise, were autoclaved 30 min at 121 °C.

- **Culture media for bacteria (*E. coli*) growth**

Table 3.6. Luria-Bertani medium with ampicillin (LB/Amp).

Ingredient	Amount
Bacto Peptone	10 g
Yeast Extract	5 g
NaCl	10 g
Ampicillin (100 mg/mL)	1 mL

LB/Amp medium was used for the selective growth of *E. coli* cells transformed with pJRoC30 vector which contains ampicillin resistance gene (Green and Sambrook, 2012). First, yeast extract, bacto peptone and NaCl were dissolved in distilled water and pH was adjusted to 7.0. After the sterilization by autoclaving it was necessary to wait until temperature decreased to 50 °C and thereafter, filtered ampicillin was added. In order to prepare solid medium, 20 g of agar were added before sterilization.

Table 3.7. Luria-Bertani low salts medium with zeocin (LB/Zeo).

Ingredient	Amount
Bacto Peptone	10 g
Yeast Extract	5 g
NaCl	5 g
Zeocin (25 mg/mL)	1 mL

LB/Zeo medium was used for the selective growth of *E. coli* cells transformed with pBSY5Z vector which contains zeocin resistance gene. First, yeast extract, bacto peptone and NaCl were dissolved in distilled water and pH was adjusted to 7.5. After the sterilization by autoclaving it was necessary to wait until temperature decreased to 50 °C and thereafter, filtered ampicillin was added. In order to prepare solid medium, 15 g of agar were added before sterilization.

Table 3.8. Super optimal broth medium (SOB).

Ingredient	Amount
Bacto Peptone	20 g
Yeast Extract	5 g
NaCl	0.5 g
KCl	0.186 g

Ingredients were dissolved in distilled water, pH was adjusted to 7.0 and sterilized.

Table 3.9. Super optimal broth medium with catabolite repression (SOC). 100 mL final volume.

Ingredient	Amount
SOB medium	97.5 mL
$MgCl_2$ (2M)	0.5 mL
Glucose (20% w/v)	2 mL

SOC medium is used for *E. coli* transformation (Green and Sambrook, 2012). $MgCl_2$ and glucose were previously filter-sterilized and thereafter mixed with SOB medium. For each transformation it was necessary to prepare fresh SOC solution.

- **Culture media for yeast (*S. cerevisiae* and *P. pastoris*) growth**

Table 3.10. YP medium (2X).

Ingredient	Amount
Bacto Peptone	40 g
Yeast Extract	20 g
ddH_2O	1000 mL

YP medium is used for UPO and UPO_AAO expression medium.

Table 3.11. YPD medium.

Ingredient	Amount
Bacto Peptone	20 g
Yeast Extract	10 g
ddH_2O	900 mL

YPD medium is used for yeast growth before DNA extraction. After the sterilization by autoclaving it was necessary to wait until temperature decrease to 50 °C and thereafter, filtered glucose (20% w/v) (100 mL) and chloramphenicol (25 mg/mL) (1 mL) were added. In order to prepare solid medium, 20 g of agar were added before sterilization.

Table 3.12. Minimal liquid medium (Synthetic Complete -SC- drop-out medium).

Ingredient	Amount
YNB medium (67 g/L)	100 mL
Amino acids supplements (10 x)	100 mL
Raffinose (20% w/v)	100 mL
Chloramphenicol (25 mg/mL)	1 mL

Selective medium without uracil for the growth of *S. cerevisiae* cells transformed with pJRoC30 (containing the gene coding the enzyme interest), which contains gene *ura3* that complements for uracil auxotrophy. Water is previously autoclaved (700 mL) and after the temperature decrease to 50 °C, the remaining components (previously sterilized by filtration) were added.

Table 3.13. Minimal solid medium (SC drop-out plates).

Ingredient	Amount
YNB medium (67 g/L)	100 mL
Amino acids supplements (10 x)	100 mL
Glucose (20% w/v)	100 mL
Bacto Agar	20 g
Chloramphenicol (25 mg/mL)	1 mL

Selective medium without uracil for the growth of *S. cerevisiae* cells transformed with pJRoC30 (containing the gene coding the enzyme interest), which contains gene *ura3* that complements for uracil auxotrophy. Water is previously autoclaved (700 mL) together with agar and after the temperature decrease to 50 °C, the remaining components (previously sterilized by filtration) were added.

Table 3.14. UPO and UPO_AAO expression medium.

Ingredient	Amount
YP medium (2X)	555 mL
KH_2PO_4 (1 M, pH 6.0)	67 mL
Galactose (20% w/v)	111 mL
Ethanol absolute	31.6 mL
$MgSO_4$ (100 mM)	20 mL
Chloramphenicol (25 mg/mL)	1 mL
ddH_2O	214.4 mL

KH_2PO_4, $MgSO_4$, galactose and chloramphenicol were sterilized by filtration. Ethanol was not added for UPO_AAO expression. This medium was also used for UPO_AAO expression in microplate format (96-well) during high-throughput screenings (HTS).

Table 3.15. Selective expression medium for UPO (SEM).

Ingredient	Amount
YNB medium (67 g/L)	100 mL
Amino acids supplements (10 x)	100 mL
KH_2PO_4 (1 M, pH 6.0)	67 mL
Galactose (20% w/v)	100 mL
Ethanol absolute	31.6 mL
$MgSO_4$ (100 mM)	20 mL
Chloramphenicol (25 mg/mL)	1 mL
ddH_2O	580.4 mL

SEM was used for UPO expression in microplate format (96-well) during high-throughput screenings (HTS) in Chapter 1. KH_2PO_4, $MgSO_4$, galactose, YNB, amino acids supplements and chloramphenicol were sterilized by filtration.

3.2. Methods for Chapter 1

3.2.1. Laboratory evolution

Focused evolution at D187-V248 segment: The region between Asp187-Val248 selected from docking experiments was subjected to MORPHING (Gonzalez-Perez et al., 2014b). Two Mutagenic PCR were prepared in a final volume of 50 µL containing 3% DMSO, 90 nM MJaWa Fw (5’-gcgcattcaagactccattg-3’), 90 nM MJaWa Rev (5’-gatcttgccgacatttttcc-3’), 0.3 mM dNTPs (0.075 mM each), $MnCl_2$ (mutational loads of 0.1 mM and 0.2 mM), 1.5 mM $MgCl_2$, 0.05 U/µL Taq DNA polymerase, and 1 ng/µl template. The amplification parameters were 94 °C for 2 min (1 cycle); 94 °C for 45 s, 48 °C for 30 s, and 72 °C for 90 s (28 cycles); and 72 °C for 10 min (1 cycle). The remaining portions of the whole JaWa gene were amplified by high-fidelity PCR in a final volume of 50 µL containing 3% DMSO, 0.5 µM HFJaWa Fw (5’-caggctcatcctatgcagccc-3’) and 0.5 µM RMLC (5’-gggagggcgtgaatgtaagc-3’) or 0.5 µM HFJaWa Rev (5’-caaaggagaaattggggttggtcg-3’) and 0.5 µM RMLN (5’-cctctatactttaacgtcaagg-3’) for the other high fidelity fragment, 1 mM dNTPs (0.25 mM each), 0.05 U/µL PfuUltra DNA polymerase, and 2 ng/µL template. High-fidelity PCR was carried out on a gradient thermocycler using the following parameters: 95 °C for 2 min (1 cycle); 95 °C for 45 s, 48 °C for 30 s, and 72 °C for 90 s (28 cycles); and 72 °C for 10 min (1 cycle). The whole gene was *in vivo* reassembled and recombined by transforming the different PCR products into *S. cerevisiae* competent cells, a process facilitated by ~40 bp overhangs flanking each recombination area (Alcalde, 2010). The DNA transformation mixture was composed of linearized plasmid (100 ng) mixed with the mutagenized fragment (200 ng) and both non-mutagenized fragments (200 ng). 1220 individual clones were screened (610 clones per mutant library).

Combinatorial saturation mutagenesis (F76 and S191): three PCR reactions were carried out in a final volume of 50 µL containing 3% DMSO, 0.3 mM dNTPs (0.075 mM each), 0.05 U/µL PfuUltra DNA polimerase, and 2 ng/µL template but each of them with different primers. PCR 1 with 0.25 µM of RMLN, 0.25 µM of F76 VHG R (5’-gcaagtccgtaatgagattgccgtccacaaggtgggccgcatatgtggc*cdb*gattgcggc-3’), 0.25 µM of F76 NDT R (5’-gcaagtccgtaatgagattgccgtccacaaggtgggccgcatatgtggc*ahn*gattgcggc-3’) and 0.25 µM of F76 TGG R (5’-gcaagtccgtaatgagattgccgtccacaaggtgggccgcatatgtggc*cca*gattgcggc-3’). PCR 2 with

0.25 μM of HF F (5’-gcggcccaccttgtggacggcaatctcattacggacttgc-3’), 0.25 μM of S191 VHG R (5’-cccatccacaaaaagattcgcggggaaggtggtctcgccgtaagcagt*cdb*gaacctaaag-3’), 0.25 μM of S191 NDT R (5’-cccatccacaaaaagattcgcggggaaggtggtctcgccgtaagcagt*ahn*gaacctaaag-3’) and 0.25 μM of S191 TGG R (5’-cccatccacaaaaagattcgcggggaaggtggtctcgccgtaagcagt*cca*gaacctaaag-3’). PCR 3 with 0.25 μM of HF F-RMLC (5’-cggcgagaccaccttccccgcgaatctttttgtggatggg-3’) and 0.25 μM of RMLC. Codon substitutions are shown in italics (where N = A/T/C/G; D = no C; V = no T, H = no G; y B = no A)(Kille et al., 2013). PCR reactions were carried out on a gradient thermocycler using the following parameters: 95 °C for 2 min (1 cycle); 95 °C for 45 s, 48 °C for 45 s, and 72 °C for 60 s (28 cycles); and 72 °C for 10 min (1 cycle). Combinatorial saturation mutagenesis library was transformed into *S. cerevisiae* and the whole genes were *in vivo* reassembled and recombined by transforming the different PCR products into *S. cerevisiae* competent cells, a process facilitated by ~40 bp overhangs (underlined in each primer) flanking each recombination area (Alcalde, 2010). The DNA transformation mixtures were composed of linearized plasmid (100 ng) mixed with the rest of the appropriate fragments (200 ng). 1480 clones were screened according to 22-trick method guidelines (Kille et al., 2013).

Saturation mutagenesis at F69, F121, F199: saturation mutagenesis was carried out using degenerated NNK codons (N = A/T/C/G; K = T/G, M = A/C), creating three different libraries. Library F69: two PCR reactions were carried out in a final volume of 50 μL containing 3% DMSO, 0.2 mM dNTPs (0.05 mM each), 0.02 U/μL iProof DNA polymerase, 2 ng/μL template (SoLo) with 0.5 μM RMLN and 0.5 μM F69 R (5’-gaagattgcggcttgattgtcmnnattgaatc-3’), or 0.5 μM RMLC and 0.5 μM F69 F (5’-cgcggttcaggaaggattcaatnnkgacaatc-3’). Library F121: two PCR reactions were carried out in a final volume of 50 μL containing 3% DMSO, 0.2 mM dNTPs (0.05 mM each), 0.02 U/μL iProof DNA polymerase, 2 ng/μL template (SoLo) with 0.5 μM RMLN and 0.5 μM F121 R (5’-catactggcgtcgccttcmnnggtgccatgc-3’), or 0.5 μM RMLC and 0.5 μM F121 F (5’-ggactcaatgagcatggcaccnnkgaaggcg-3’). Library F199: two PCR reactions were carried out in a final volume of 50 μL containing 3% DMSO, 0.2 mM dNTPs (0.05 mM each), 0.02 U/μL iProof DNA polymerase, 2 ng/μL template (SoLo) with 0.5 μM RMLN and 0.5 μM F199 R (5’-ccacaaaaagattcgcgggmnnggtggtctcg-3’), or 0.5 μM RMLC and 0.5 μM F199 F (5’-ctactgcttacggcgagaccaccnnkcccgcg-3’). PCR reactions were carried out on a gradient thermocycler using the following parameters: 98 °C for 30 s (1 cycle); 98 °C for 10 s, 48 °C for 30 s, and 72 °C for 30 s (28 cycles); and 72 °C for 10 min (1 cycle). Each library was transformed independently and the whole genes were *in vivo* reassembled and recombined by transforming the different PCR products into *S. cerevisiae* competent cells, a process facilitated by ~40 bp overhangs flanking each recombination area (Alcalde, 2010). The DNA transformation mixtures were composed of linearized plasmid (100 ng) mixed with the rest of the appropriate fragments (200 ng). Each library contained 170 clones.

All PCR products were loaded onto a preparative agarose gel and purified by use of the NucleoSpin Gel and PCR Clean-up kit. The recovered DNA fragments were cloned under the control of the GAL1 promoter of the pJRoC30 expression shuttle vector, with use of *Bam*HI and *Xho*I to linearize the plasmid and to remove the parent gene. The linearized vector was loaded onto a preparative agarose gel and purified with the NucleoSpin Gel and PCR Clean-up kit.

High Throughput Dual screening: Individual clones were picked and inoculated in sterile 96-well plates (Greiner Bio-One, GmbH, Germany), referred to as master plates, containing 200 mL of SEM per well. In each plate, column number 6 was inoculated with the parent type, and one well (H1-control) was inoculated with *S. cerevisiae* transformed with pJRoC30-MtL plasmid (laccase without activity). Plates were sealed with parafilm to prevent evaporation and incubated at 30 °C, 220 rpm and 80% relative humidity in a humidity shaker (Minitron, Infors, Switzerland) for five days. The master plates were centrifuged (Eppendorf 5810R centrifuge, Germany) for 10 min at 2,500*g* and 4°C. Aliquots of the supernatants (20 μL) were transferred from the master plates to two replica plates with the aid of a liquid handler robotic station Freedom EVO (Tecan, Switzerland). 50 μL of the reaction mixture (with or without ascorbic acid) were added to the two replica plates with the help of a pipetting robot (Multidrop Combi Reagent Dispenser, Thermo Scientific, MA, USA). Reaction mixture for replica plate 1 contained 50 mM potassium phosphate buffer (pH 7.0), 5 mM propranolol and 2 mM H_2O_2. Reaction mixture for replica plate 2 contained 50 mM potassium phosphate buffer (pH 7.0), 5 mM propranolol, 2 mM H_2O_2 and 4 mM ascorbic acid. Replica plates 1 and 2 were incubated at room temperature for 30 and 60 min, respectively. Afterwards, the amount of 5'-OHP formed in each well was determined by the 4 aminoantipyrine (4-AAP) assay (Otey and Joern, 2003) (**Figure 3.1**). Plates were stirred briefly and absorption at 530 nm was recorded in a plate reader (SPECTRAMax Plus 384, Molecular Devices, USA). The values were normalized against the parent type of the corresponding plate and selected variants came from the ratio between the values obtained in the absence (peroxygenase+peroxidase activities) and in the presence (peroxygenase activity) of ascorbic acid. To rule out the selection of false positives, two re-screenings were carried out as described elsewhere (Molina-Espeja et al., 2014).

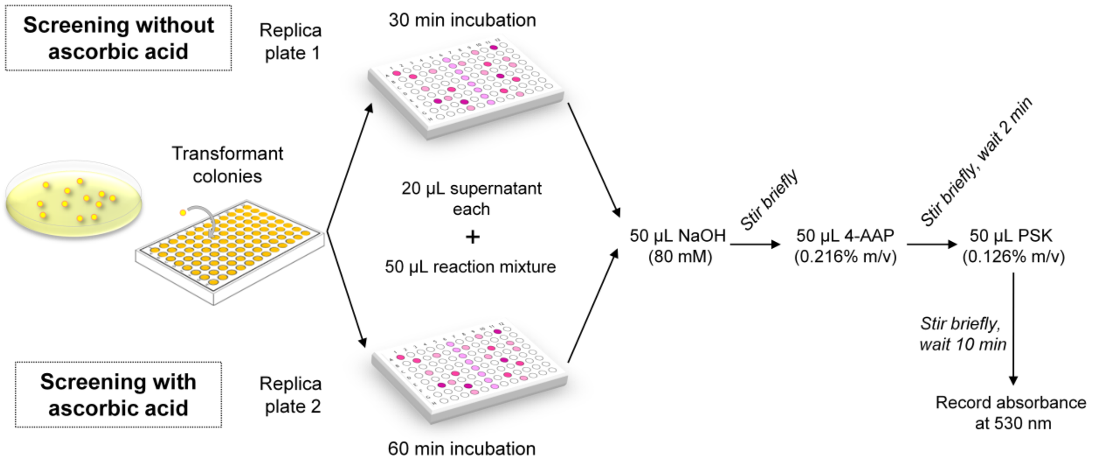
Screening without ascorbic acid
Replica plate 1
30 min incubation
Transformant colonies
20 µL supernatant each
+
50 µL reaction mixture
Screening with ascorbic acid
Replica plate 2
60 min incubation
50 µL NaOH (80 mM)
Stir briefly
50 µL 4-AAP (0.216% m/v)
Stir briefly, wait 2 min
50 µL PSK (0.126% m/v)
Stir briefly, wait 10 min
Record absorbance at 530 nm

Figure 3.1. Step-by-step screening protocol with and without AA.

3.2.2. Production, purification and biochemical characterization

*Aae*UPO wildtype and recombinant UPO PaDa-I were produced and purified by Prof. Martin Hofrichter's group and Prof. Roland Ludwig's group (Molina-Espeja et al., 2015; Ullrich et al., 2004). Recombinant UPO purification (JaWa and SoLo) was achieved by cationic exchange chromatography and anion exchange chromatography (ÄKTA purifier, GE Healthcare, WI, US). The crude extract was concentrated and dialyzed in sodium phosphate/citrate 20 mM at pH 3.3 (buffer A) by tangential ultrafiltration (Pellicon; Millipore, Temecula, CA, US) through a 10-kDa-pore-size membrane (Millipore) by means of a peristaltic pump (Masterflex Easy Load; Cole-Parmer, Vernon Hills, IL). The sample was filtered and loaded onto a strong cation-exchange column (HiTrap SP FF GE Healthcare) pre-equilibrated with buffer A. The proteins were eluted with a linear gradient from 0 to 40% of buffer A within 60 mL of NaCl and from 40 to 100% within 5 mL at a flow rate of 1 mL/min. Fractions with UPO activity *vs.* ABTS were harvested, concentrated, dialyzed against buffer Tris HCl 20 mM at pH 7.8 (buffer B) and loaded onto a 10 µm high resolution anion-exchange Biosuite Q column (Waters) pre-equilibrated with buffer B. The proteins were eluted with a linear gradient from 0 to 20% within 40 mL of NaCl and from 20 to 100% within 5 mL at a flow rate of 1 mL/min. The fractions with UPO activity *vs.* ABTS were pooled, dialyzed against buffer potassium phosphate 10 mM at pH 7.0 and stored at 4 °C.

Steady-state kinetic constants: ABTS kinetics were measured in sodium phosphate/citrate buffer (pH 4.0, 100 mM), containing H_2O_2 (2 mM), and for propranolol in potassium phosphate buffer (pH 7.0, 50 mM) containing H_2O_2 (2 mM). For H_2O_2, benzyl alcohol was used as a reducing substrate under the corresponding saturated conditions. Reactions were performed in triplicate, and substrate oxidations were followed through spectrophotometric changes (ε_{418}ABTS$^{\bullet+}$=36,000 M^{-1} cm^{-1}; ε_{325} 5´-OHP=1,996 M^{-1} cm^{-1} and ε_{280} benzaldehyde=1,400 M^{-1} cm^{-1}).

HPLC analysis: The reaction mixtures were analyzed by reversed-phase chromatography (HPLC) with equipment consisting of a tertiary pump (Varian/Agilent Technologies) coupled to an autosampler (Merck Millipore) and an Zorbax Eclipse plus C18 (15 cm x 4,6 cm) column at 40 °C. Detection was performed with a PDA (Varian/Agilent Technologies). The mobile phase was a gradient from 10% methanol and 90% *dd*H_2O (both with 0.1% acetic acid) to 90% methanol and 10% *dd*H_2O at a flow rate of 0.8 mL/min. The reaction was quantified at 280 nm (from HPLC standards). Reaction mixtures containing 0.03 μM purified enzyme, 5 mM propranolol, and 2 mM H_2O_2 in 50 mM potassium phosphate pH 7.0 (0.5 mL final volume). After 60 minutes at room temperature, reaction was stopped by heating 10 min at 70 °C and cooling 5 min at 4 °C (see **Figure 4.7.C**). Total turnover numbers were calculated from reaction that contained 0.03 μM purified enzyme, 5 mM propranolol, and pulses of 2 mM H_2O_2 every 10 min in 50 mM potassium phosphate buffer pH 7.0 (0.5 mL final volume). Reactions were stopped at different times (10 to 120 min) as described before (see **Figure 4.7.A, B**). In the determination of 5´-hydroxypropranolol (5´-OHP) consumption by UPO, the mixture contained 0.03 μM purified enzyme, 0.5 mM 5´-OHP, 20% methanol 20% and 2 mM H_2O_2 in 50 mM potassium phosphate buffer pH 7.0 (0.5 mL final volume). The reaction was started by the addition of the H_2O_2 and stopped at different times (2 to 10 min) as described before (see **Figure 4.7.D**). Samples of each experiment (20 μL) were injected and analyzed. Standard deviations were lower than 5% in all experiments. Products were identified and quantified against authentic standards by the HPLC method abovementioned.

Kinetic thermostability: The thermostability of the different UPO samples was estimated by assessing their T_{50} values using 96/384 well gradient thermocyclers. Appropriate UPO dilutions were prepared with the help of the robot in such a way that 20 μL aliquots gave rise to a linear response in the kinetic mode. Then, 50 μL were used for each point in the gradient scale and a temperature gradient profile ranging from 30 to 80 ºC was established as follows (in ºC): 30.0, 31.7, 34.8, 39.3, 45.3, 49.9, 53.0, 55.0, 56.8, 59.9, 64.3, 70.3, 75.0, 78.1 and 80.0. After a 10 min incubation, samples were chilled out on ice for 10 min and further incubated at room temperature for 5 min. Afterwards, 20 µL of samples were assayed in sodium phosphate/citrate buffer (pH 4.0, 100 mM), containing H_2O_2 (2 mM) and ABTS (5 mM). Reactions were performed in triplicate, and substrate oxidations were followed through spectrophotometric changes ($\varepsilon_{418}ABTS^{\bullet+}=36{,}000\ M^{-1}\ cm^{-1}$). The thermostability values were deduced from the ratio between the residual activities incubated at different temperature points and the initial activity at room temperature.

3.2.3. Reaction optimization and product identification

Production of 5´-OHP by SoLo coupled to an *in situ* H_2O_2 generation system: For *in situ* H_2O_2 generation, 10 nM of SoLo mutant, 10 nM alcohol oxidase from *Pichia pastoris* (AOx) and 600 nM formate dismutase from *Pseudomonasputida* (FDM) in combination with 200 mM methanol were used (Fernández-Fueyo et al., 2016b). Reactions were performed at 30 °C and 600 rpm in 100 mM potassium phosphate buffer pH 7.0 with 10 mM of propranolol in a total volume of 375 µL using a thermo shaker device (Eppendorf, Germany). After 3 h, reactions were stopped by heat inactivation for 10 min at 70°C, followed by cooling down the sample and separation of precipitate by centrifugation at 5°C. Quantification of 5´-OHP was carried out by HPLC analytics. HPLC measurements were performed at 40 °C on a Shimadzu LC-20 system with a Shimadzu SPD-M20A Photo Diode Array detector using Waters Xterra RP18 column (4.6 × 150 mm, 3.5 µm). For the mobile phase acetonitrile (ACN) and water containing 5% ACN and 0.1% trifluoroacetic acid (TFA) was used. The separation was performed in an isocratic mode at a flow rate of 1.0 mL/min while increasing the ACN concentration in 3 steps to finally 100%: 25%, 4 min hold, 50% 4 min hold and 100%, 3 min hold. The reaction was quantified at 280 nm based on a calibration using 5´-OHP standard.

Semi-preparative production of 5´-OHP: For the semi-preparative production 5´-OHP, 50 mM propranolol was dissolved in 100 mM potassium phosphate buffer pH 7.0 (10 mL total volume). Reactions were performed at 30°C while gently mixing (neoLab rotator, mode C2, 20 rpm, Germany) in presence or absence of 40 mM of AA using 0.5 µM of SoLo. The reaction was started by the addition of 5 mM *tert*-butyl hydroperoxide (*tert*-BuOOH). Every hour, 5 mM *tert*-BuOOH was added and 200 µL of each reaction time were taken for 5´-OHP quantification by HPLC. After 9 h, 5 mL of the reaction mixture were used for 5´-OHP isolation. The solution was acidified (200 μL, 37% HCl), extracted with ethyl acetate (3x 5 mL), dried with $MgSO_4$, and the solvent was removed under reduced pressure. The crude product was purified by column chromatography using silica gel (60 Å, 230-400 mesh) with a dichloromethane (DCM):methanol eluent (8:2). Separation was followed using thin layer chromatography (TLC) on silica gel-coated plates (Macherey-Nagel, Polygram SIL G/UV254) with a DCM:methanol solvent mixture (9:1).

NMR analytics: NMR spectra were recorded on an Agilent 400 (400 MHz) spectrometer in methanol-*d4*. Chemical shifts are given in ppm with respect to tetramethylsilane. Coupling constants are reported as J-values. 5´-OHP NMR (400 MHz, methanol-*d*4) δ 7.79 (d, 1H, *J* = 8.5 Hz), 7.72 (d, 1H, *J* = 8.5 Hz), 7.31 (dd, 1H, *J* = 8.5, 7.7 Hz), 7.24 (dd, 1H, *J* = 8.5, 7.7 Hz), 6.91 (dd, 1H, *J* = 7.7, 0.9 Hz), 6.83 (dd, 1H, *J* = 7.7, 0.9 Hz), 4.36 (ddt, 1H, *J* = 12.6, 5.4, 3.1 Hz), 4.22 (dd, 1H, *J* = 9.9, 5.0 Hz), 4.15 (dd, 1H, *J* = 9.9, 5.8 Hz), 3.46 (p, 1H, *J* = 6.6 Hz), 3.36 (dd, 1H, *J* = 12.7, 3.1 Hz), 3.23 (dd, 1H, *J* = 12.7, 9.6 Hz), 1.37 (d, 3H, *J* = 3.8 Hz), 1.36 (d, 3H, *J* = 3.8 Hz). Annex **Figure 9.1**.

3.2.4. Computational analysis

System preparation for molecular modeling: The starting structure for PELE (Protein Energy Landscape Exploration) simulations with *Aae*UPO was the *Agrocybe aegerita* peroxygenase crystal structure (PDB ID: 2YOR). For the different UPO mutants, the crystal structure of PaDa-I (Ramirez-Escudero et al., 2018) was used for modeling. Since the optimal pH for propranolol peroxygenation and subsequent 5´-OHP peroxidation is 7.0, all the structures were prepared accordingly with the aid of the Schrödinger Protein Preparation Wizard (Madhavi Sastry et al., 2013) and the H++ web server (Anandakrishnan et al., 2012). All acidic residues were deprotonated. Histidines were δ-protonated, with the exception of His82 (ε-protonated) and His118 and His251 (double-protonated). To relax the systems after mutations insertion, and to investigate their possible effect on the protein structure, 5 ns of Molecular Dynamics simulation (MD) were performed with Desmond (D.E. Shaw Research, 2009) on JaWa and SoLo structures. Finally, the heme site was modeled as compound I after being fully optimized in the protein environment with quantum mechanics/molecular mechanics (QM/MM) using QSite (Schrödinger, 2011). Propranolol and 5´-OHP molecules were also optimized with Jaguar (Bochevarov et al., 2013) at the DFT/M06 level with the 6-31G** basis and PBF implicit solvent in order to obtain their electrostatic potential atomic charges.

Protein energy landscape exploration (PELE) computational analysis: Once all protein and ligand structures were prepared, heme binding site explorations were performed with PELE (Madadkar-Sobhani and Guallar, 2013). Substrates were manually placed in identical positions at the entrance of the heme-access channel, and PELE simulations were carried out in two different stages. First, ligands were driven from the solvent to the UPO heme binding site. Then, once the center of mass of the ligand was within 6 Å of the heme catalytic oxygen, it was free to explore the active site. The results presented here are based on 160 independent 48 h PELE simulations. Moreover, in an attempt to increase the sampling for 5´-OHP diffusion, additional PELE simulations were performed for this substrate. Representative structures at distances lower than 10 Å (considering the distance between the reactive O-heme atom and the H_5 substrate atom) were selected using binning widths of 1 Å from previous PELE simulations and used as starting structures for the new ones. New simulations were setup to freely explore the active site and a total of 196 independent 48 h simulations were run.

Molecular Dynamics and MDpocket*:* To study the changes caused by F191S mutation, 100 ns MD simulations were performed with JaWa and SoLo using Desmond (D.E. Shaw Research, 2009). To prepare the system for MD, previously mentioned prepared JaWa and SoLo systems were placed inside an orthorhombic box containing SPC explicit waters and ions to neutralize the system at a concentration of 0.15 M NaCl. From the solvated system, MD simulations were run with the following parameters: the OPLS-2005 force field, the temperature was regulated with a Nose-Hoover chain thermostat with a relaxation time of 1.0 ps, the pressure with the Martyna-Tobias-Klein barostat with isotropic coupling and a relaxation time of 2.0 ps, and finally, the production phase was run over the course of 100 ns using the NPT canonical ensemble at 300K. From MD simulations, structures at every 0.1 ns were extracted and used for volume pocket calculation with MDpocket (Schmidtke et al., 2011), a fast and open-source tool for protein pocket (cavity) detection on molecular dynamic trajectories or other conformational ensembles.

3.3. Methods for Chapter 2

3.3.1. Expression and purification of UPO variants

UPO variants were produced and purified as described in **Section 3.2.2**.

3.3.2. Reactions and product characterization

Reaction mixtures (1 mL) contained purified peroxygenases (PaDa-I, JaWa, SoLo and SoLo-D241G mutants, 0.1 µM), substrate (1 mM, dissolved in 10% acetonitrile), potassium phosphate buffer (100 mM, pH 7.0), ascorbic acid (4 mM) and a single dosage of H_2O_2 (1 mM). All reactions were stirred at 30 °C for one hour until reaction stopped. The reaction mixtures were analyzed by reversed-phase chromatography (HPLC) using a quaternary pump (Agilent Technologies, model 1100) coupled to a Phenomenex Zorbax Eclipse plus C18 column (4.6 mm diameter by 100 mm length, 3.5 µm particle size), with an autosampler (Hitachi, model L-2200) and a photodiode array detector (PDA, Varian Prostar). Column temperature was kept at 30 °C and flow rate at 1 mL/min. Each injection had a volume of 10 µL and the analytes were eluted with a gradient from 100% of CH_3CN to 100% of H_2O in 5 minutes (with 0.1% vol/vol of formic acid in both solvents), followed by 10 minutes linear gradient from 100% of H_2O to 100% of CH_3CN. UV detection wavelengths were 238 nm for tolbutamide, 280 nm for dextromethorphan and 235 nm for naproxen. Integration of peaks was carried out using the Varian Star LC workstation 6.41.

Identification of reaction products was determined by liquid chromatography-mass spectrometry (HPLC/MS) with a Waters Instrument equipped with a chromatographic module Alliance 2695, diode array detector (PDA 2996) and a quadrupole mass spectrometer (Micromass ZQ). Reversed phase chromatography was performed on a SunFire C18 (2.1 mm diameter, 50 mm length, 3.5 µm particle size, Waters); which was eluted at 1 mL/min with aqueous/acetonitrile (0.1% vol/vol formic acid in both solvents), with 20 minutes linear gradient from 95% of acetonitrile to 95% of H_2O. Samples were ionized by electrospray ionization (ESI, with nitrogen to desolvate the mobile phase) and analyzed in positive reflector mode. Naproxen and *O*-desmethylnaproxen were analyzed employing a mass spectrometer coupled to a hybrid QTOF analyzer (model QSTAR, Pulsari, AB Sciex). The compounds were analyzed by direct infusion and ionized by ESI in negative reflector mode. The ionizing phase was methanol basified with 1% NH_4OH.

3.3.3. Semi-preparative production of dextrorphan and NMR analysis

Dextromethorphan (135.6 mg, 0.5 mmol) was dissolved in acetonitrile (10 mL). The solution was added to potassium phosphate buffer (90 mL, 100 mM pH 7.0) containing ascorbic acid (4 mmol) and SoLo mutant (0.05 µmol). Reactions (2 × 50 mL) were performed at 30 °C and 600 rpm using a thermo shaker device (Eppendorf). H_2O_2 was added with a syringe pump (0.06 mmol/h) over 16.5 h. Afterwards, the solution was heated to 70 °C for 3 min and the precipitated enzyme removed. The conversion (76.2%) was determined by HPLC (water with 0.1% TFA/ acetonitrile, 5/95 to 95/5) on Waters Xterra RP18 column (4.6 × 150 mm, 5 μm). For purification, solvents were removed under reduced pressure and freeze drying from the cleared solution. The crude product was washed with methanol, filtered and purified by flash chromatography (water with 0.1% TFA/ acetonitrile, 5/95 to 95/5) on REVELERIS® C18 column (12 g, 40 μm). Dextrorphan containing fractions were pooled and the solvents removed under reduced pressure and freeze drying obtaining dextrorphan (102.1 mg, 75.2% yield) as white powder. Dextrorphan: ^{1}H NMR (400 MHz, methanol-d_4) δ 7.08 (d, *J* = 8.3 Hz, 1H), 6.80 (d, *J* = 2.5 Hz, 1H), 6.71 (dd, *J* = 8.3, 2.5 Hz, 1H), 3.65 – 3.59 (m, 1H), 3.22 – 3.08 (m, 3H), 2.92 (s, 3H), 2.73 (td, *J* = 13.2, 3.6 Hz, 1H), 2.52 – 2.39 (m, 1H), 1.97 (dt, *J* = 12.4, 3.1 Hz, 1H), 1.87 (td, *J* = 13.8, 4.6 Hz, 1H), 1.79 – 1.27 (m, 7H), 1.26 – 1.11 (m, 1H). ^{13}C NMR (101 MHz, methanol-d_4) δ 128.97, 114.04, 60.57, 43.09, 39.84, 39.37, 35.44, 35.02, 25.54, 22.66, 21.41. (Annex **Figure 9.2** and **9.3**).

3.3.4. Site-directed mutagenesis at position 241

PCR reactions for reversion of Asp241 were carried out with the primers D241G F (5’-gatttcttccgcgcacccagcccgagaagtggtacaggagtcgaggtagttgtacagg-3’) and D241G R (5’-cctgtacaactacctcgactcctgtaccacttctcgggctgggtgcgcggaagaaatc-3’); mutated bases are underlined. The PCR reaction mixtures contained: 1) 50 μL final volume, DMSO (3%), RMLN (0.5 μM), D241G F (0.5 μM), dNTPs (1 mM, 0.25 mM each), high-fidelity DNA polymerase iProof (0.02 U/mL), and the template SoLo (10 ng), and 2) 50 μL final volume, DMSO (3%), RMLN (0.5 μM), D241G R (0.5 μM), dNTPs (1 mM, 0.25 mM each), high-fidelity DNA polymerase iProof (0.02 U/mL), and the template SoLo (10 ng). PCR reactions were carried out on a gradient thermocycler using the following parameters: 98 °C for 30 s (1 cycle); 98 °C for 10 s, 48 °C for 30 s, and 72 °C for 30 s (28 cycles); and 72 °C for 10 min (1 cycle). PCR products were loaded onto a preparative agarose gel and purified with the NucleoSpin Gel and PCR Clean-up kit. The recovered DNA fragments were cloned under the control of the GAL1 promoter of the pJRoC30 expression shuttle vector, with use of *Bam*HI and *Xho*I to linearize the plasmid and to remove the parent gene. The linearized vector was loaded onto a preparative agarose gel and purified with the NucleoSpin Gel and PCR Clean-up kit. The PCR products (200 ng each) were mixed with the linearized plasmid (100 ng) and transformed into *S. cerevisiae* for *in vivo* gene reassembly and cloning by IVOE (Alcalde, 2010).

3.4. Methods for Chapter 3

3.4.1. Fusions engineering

PCR reactions for creation of the linkers and fusions were carried out with the primers listed in **Table 3.16**. The PCRs reaction mixtures contained: PCR 1: 50 μL final volume, DMSO (3%), primer XR (where X is the construction name) (0.5 μM), RMLN (0.5 μM), dNTPs (1 mM, 0.25 mM each), high-fidelity DNA polymerase iProof (0.02 U mL^{-1}), and the template SoLo (construction A, B, B', E, F, G, H, I, J, K and L) or FX9 (constructions C and D) (10 ng). PCR 2.1: For the case of constructions A, B, B', C, and D, due to the length of the linker an additional PCR had to be carried out: 50 μL final volume, DMSO (3%), primer XF1 (0.5 μM), RMLC (0.5 μM), dNTPs (1 mM, 0.25 mM each), high-fidelity DNA polymerase iProof (0.02 U mL^{-1}), and the template SoLo (constructions C and D) or FX9 (constructions A, B, B') (10 ng). PCR 2.2: PCR reaction mixtures contained: 50 μL final volume, DMSO (3%), primer XF1 (0.5 μM), RMLN (0.5 μM), dNTPs (1 mM, 0.25 mM each), high-fidelity DNA polymerase iProof (0.02 U mL^{-1}), and the template (fragment from PCR 2.1) (10 ng). PCR 3: Constructions E, F, G, H, I, J, K and L. PCR reaction mixtures contained: 50 μL final volume, DMSO (3%), primer XF1 (0.5 μM), RMLC (0.5 μM), dNTPs (1 mM, 0.25 mM each), high-fidelity DNA polymerase iProof (0.02 U mL^{-1}), and the template FX9 (10 ng). PCR linker: H linker was synthetized and extracted from commercial pUC18 with a PCR of 50 μL final volume, DMSO (3%), primer HF2 (0.5 μM), primer HR2 (0.5 μM), dNTPs (1 mM, 0.25 mM each), high-fidelity DNA polymerase iProof (0.02 U mL^{-1}), and the template (pUC18-Hlinker) (10 ng). All PCR reactions were carried out in a gradient thermocycler using the following parameters: 98 °C for 30 s (1 cycle); 98 °C for 10 s, 45 °C for 30 s, and 72 °C for 120 s (28 cycles); and 72 °C for 10 min (1 cycle). PCR products were loaded onto a preparative agarose gel and purified with the NucleoSpin Gel and PCR Clean-up kit.

Table 3.16. Sequences of primers and amino acids of the linkers

Construction		**Primers sequences (5'→3')**	**Linker (amino acids)**	**Source**
A	*PCR 1*	RMLN: CCTCTATACTTTAACGTCAAGG AR: CTTCTTTAGCAGCAGCTTCTTTAGCAGCAGCTTCAGCCAAATCTCGCCCGTATGGGAAGA	LA(EAAAK)$_4$ AAA	(Chen et al., 2013)
	PCR 2.1	AF1: AGAAGCTGCTGCTAAAGAAGCTGCTGCTAAAGCTGCTGCTGCCGATTTTGACTACGTTGT RMLC: GGGAGGGCGTGAATGTAAGC		
	PCR 2.2	AF2: TTGGCTGAAGCTGCTGCTAAAGAAGCTGCTGCTAAAGAAGCTGCTGCTAAAGAAGCTGCT RMLC		
B	*PCR 1*	RMLN BR: AGCAGCTTCTTTAGCAGCAGCTTCTTTAGCAGCAGCTTCAGCCAAATCTCGCCCGTATGGGAAGA	LA(EAAAK)$_5$ AAA	(Chen et al., 2013)
	PCR 2.1	BF1: GCTAAAGAAGCTGCTGCTAAAGAAGCTGCTGCTAAAGCTGCTGCTGCCGATTTTGACTACGTTGT RMLC		
	PCR 2.2	BF2: TGAAGCTGCTGCTAAAGAAGCTGCTGCTAAAGAAGCTGCTGCTAAAGAAGCTGCTGCTAA RMLC		
B'	*PCR 1*	RMLN B'R: AGCAGCTTCTTTAGCAGCAGCTTCTTTAGCAGCAGCTTCAGCCAAATCTCGCCCGTATGGGAAGA	LA(EAAAK)$_5$ AAA(GGGGR)$_1$	(Chen et al., 2013)
	PCR 2.1	B'F1:GCTAAAGAAGCTGCTGCTAAAGAAGCTGCTGCTAAAGCTGCTGCTGGTGGTGGTGGTAGAGCCGATTTTGACTACGTTG RMLC		
	PCR 2.2	B'F2: TGAAGCTGCTGCTAAAGAAGCTGCTGCTAAAGAAGCTGCTGCTAAAGAAGCTGCTGCTAA RMLC		
C	*PCR 1*	RMLN CR: CTTCTTTAGCAGCAGCTTCTTTAGCAGCAGCTTCAGCCAATCTACCACCACCACCCTGATCAGCCTTGATAAGAT	(GGGGR)$_1$ LA(EAAAK)$_4$ AAA	(Chen et al., 2013)
	PCR 2.1	CF1: AGAAGCTGCTGCTAAAGAAGCTGCTGCTAAAGCTGCTGCTGAGCCAGGATTACCTCCTGG RMLC		
	PCR 2.2	CF2: TTGGCTGAAGCTGCTGCTAAAGAAGCTGCTGCTAAAGAAGCTGCTGCTAAAGAAG RMLC		
D	*PCR 1*	RMLN DR: CTTCTTTAGCAGCAGCTTCTTTAGCAGCAGCTTCAGCCAATCTACCACCACCACCCTGATCAGCCTTGATAAGAT	(GGGGR)$_1$ LA(EAAAK)$_5$ AAA	(Chen et al., 2013)
	PCR 2.1	DF1: AGAAGCTGCTGCTAAAGAAGCTGCTGCTAAAGCTGCTGCTGAGCCAGGATTACCTCCTGG RMLC		
	PCR 2.2	DF2: TTGGCTGAAGCTGCTGCTAAAGAAGCTGCTGCTAAAGAAGCTGCTGCTAAAGAAGCTGCTGCTAAAGAAG RMLC		

E	*PCR 1*	RMLN ER: ACAACGTAGTCAAAATCGGCACCACCACCACCACCACCACCATCTCGCCCGTATGGAAGA	GGGGGGGG	(Chen et al., 2013)
	PCR 2	EF: TCTTCCCATACGGGCGAGATGGTGGTGGTGGTGGTGGTGGTGCCGATTTTGACTACGTTGT RMLC		
F	*PCR 1*	RMLN FR:CCACCAGAACCACCACCACCAGAACCACCACCACCATCTCGCCCGTATGGAAGA	$(GGGGS)_3$	(Deng et al., 2016)
	PCR 2	FF: GTTCTGGTGGTGGTGGTTCTGGTGGTGGTGGTTCTGCCGATTTTGACTACGTTGT RMLC		
G	*PCR 1*	RMLN GR: AGAACCACCACCACCTGGAGCTGGAGCTGGAGCTGGAGCTGGAGCATCTCGCCCGTATGGGAAGA	$(AP)_5(GGGGS)_1$	(Chen et al., 2013)
	PCR 2	GF:GCTCCAGCTCCAGCTCCAGCTCCAGCTCCAGGTGGTGGTGGTTCTGCCGATTTTGACTACGTTGT RMLC		
H	*PCR 1*	RMLN HR1: CAGGCATACGGCTGAATTGG	$(AP)_{15}(GGGGS)_2$	(Chen et al., 2013)
	PCR 2	HF1: GCCTCCCGCTGACAACCATA RMLC		
	PCR linker	HF2: GACGGCCAGCTAGATATGGA HR2: ATGTACCGCTGGGATAAATTC		
I	*PCR 1*	RMLN IR: GAACTCTCCAGTTGGTGTGGGAGTTGGGGTTGGAGTTCCATCTCGCCCGTATGGGAAGA	GTPTPTPTPTGEF	(Gustavsson et al., 2001)
	PCR 2	IF: GGAACTCCAACCCCAACTCCCACACCAACTGGAGAGTTCGCCGATTTTGACTACGTTGT RMLC		
J	*PCR UPO*	RMLN JR: AGAACCACCACCACCGAACTCTCCAGTTGGTGTGGGAGTTGGGGTTGGAGTTCCATCTCGCCCGTATGGGAAGA	GTPTPTPTPTGEF GGGGS	(Gustavsson et al., 2001)
	PCR AAO	JF: AACTCCCACACCAACTGGAGAGTTCGGTGGTGGTGGTTCTGCCGATTTTGACTACGTTG RMLC		
K	*PCR UPO*	RMLN KR: ACAACGTAGTCAAAATCGGCACCTCTTGGATCGTTTAACAAAGCGAAAAAATCTCGCCCGTATGGGAAGA	FFALLNDPRG	*Linker Database* (George and Heringa, 2002)
	PCR AAO	KF:TCTTCCCATACGGGCGAGATTTTTTCGCTTTGTTAAACGATCCAAGAGGTGCCGATTTTGACTACGTTGT RMLC		

L	*PCR* *UPO*	RMLN LR: ACAACGTAGTCAAAATCGGCCAAATCCTCTTCCTTTTTGTAAGTAACAGCATCTCGCCCGTATGGGAAGA	AVTYKKEEDL	*Linker Database* (George and Heringa, 2002)
	PCR *AAO*	LF:TCTTCCCATACGGGCGAGATGCTGTTACTTACAAAAAGGAAGAGGATTTGGCCGATTTTGACTACGTTGT RMLC		

The recovered DNA fragments were cloned under the control of the GAL1 promoter of the pJRoC30 expression shuttle vector, with the use of *Bam*HI and *Xho*I to linearize the plasmid and to remove the parent gene. The linearized vector was loaded onto a preparative agarose gel and purified with the NucleoSpin Gel and PCR Clean-up kit. The PCR products (200 ng each) were mixed with the linearized plasmid (100 ng) and transformed into *S. cerevisiae* for *in vivo* gene reassembly and cloning by IVOE (Alcalde, 2010). **Figure 3.2**.

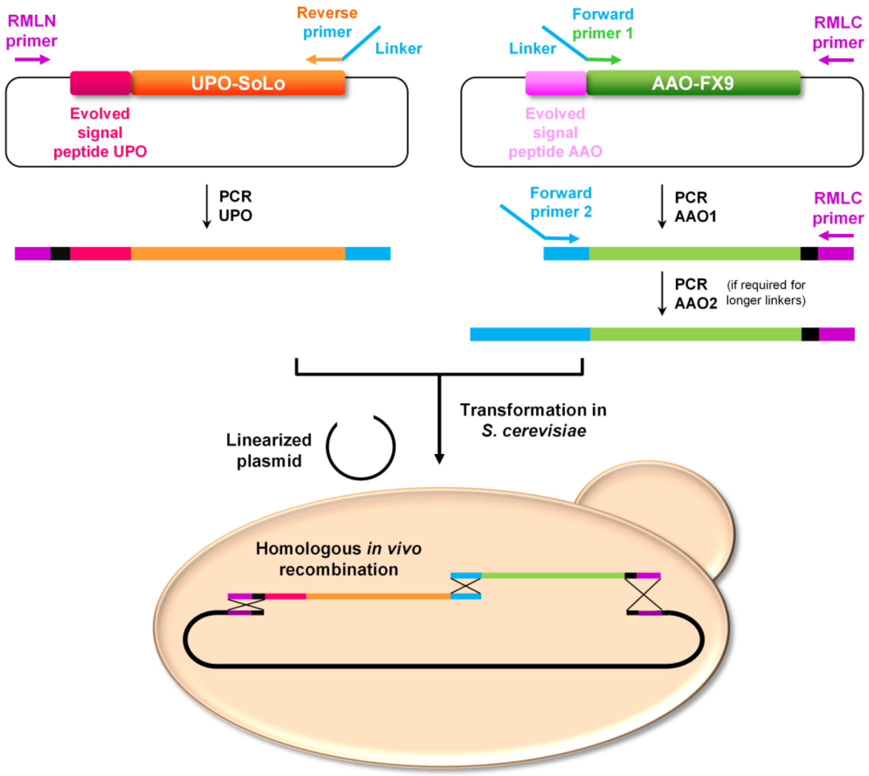
RMLN primer
Reverse primer
Linker
UPO-SoLo
Evolved signal peptide UPO
Forward primer 1
Linker
RMLC primer
AAO-FX9
Evolved signal peptide AAO
PCR UPO
Forward primer 2
PCR AAO1
RMLC primer
PCR AAO2
(if required for longer linkers)
Transformation in S. cerevisiae
Linearized plasmid
Homologous in vivo recombination

Figure 3.2. Cloning strategy for the creation of the different linkers based on homologous DNA recombination *in vivo*. Constructions A, B, B', C, D and H were created with three PCRs due to the length of the linker.

After selecting the best candidates for protein characterization, they were cloned with a His tag in C-terminal of the fusion protein. For this purpose, two PCRs were performed, being the first one the template for the second one. His tag coding sequence is underlined in each primer. PCR 1.His: 50 µL final volume, DMSO (3%), primer RHis1 (5'-ctaatgatgatgatgatgatgctgatcagccttgataagatcggct-3') (0.5 µM), RMLN (0.5 µM), dNTPs (1 mM, 0.25 mM each), high-fidelity DNA polymerase iProof (0.02 U mL^{-1}) and the template (construction F9, F12, F17, G and H) (10 ng). PCR 2.His: 50 µL final volume, DMSO (3%), primer RHis2 (5'-cataactaattacatgatgcggccctctagatgcatgctcgagcggccgcctaatgatgatgatgatgatgctgatc-3') (0.5 µM), RMLN (0.5 µM), dNTPs (1 mM, 0.25 mM each), high-fidelity

DNA polymerase iProof (0.02 U mL^{-1}) and the template (PCR 1.His) (10 ng). PCR reactions were carried out in a gradient thermocycler using the following parameters: 98 °C for 30 s (1 cycle); 98 °C for 20 s, 45 °C (PCR 1.His) or 50 °C (PCR 2.His) for 30 s, and 72 °C for 120 s (30 cycles); and 72 °C for 20 min (1 cycle). PCR products were prepared and transformed as described before. The H construction was further cloned in *P. pastoris* BSYBG11 under the P_{DF} promoter with the same signal peptide used in *S. cerevisiae*. P_{DF} is an orthologous promoter of P_{DC}, *P. pastoris CAT1* promoter (PCAT1-500). Expression conditions were the ones described before with minor modifications (Fischer et al., 2019).

3.4.2. Activity screening assays

i) ABTS/H_2O_2 assay: Aliquots of 20 µL of yeast supernatants were added to 180 µL reaction mixture for ABTS screening containing 100 mM sodium citrate-phosphate pH 4.0, 5 mM ABTS and 2 mM H_2O_2. The plates were measured in kinetic or endpoint mode at 418 nm ($\varepsilon ABTS^{\cdot +}=36{,}000\ M^{-1}\ cm^{-1}$) (Spectramax Plus, Molecular Devices). UPO activity is defined as the amount of enzyme that converts 1 µmol of ABTS to $ABTS^{\cdot +}$ per min under the reaction conditions.

ii) 4-methoxybenzyl alcohol/ABTS-HRP coupled assay: Aliquots of 20 µL of yeast supernatants were added to 180 µL of HRP-ABTS reagent (final concentrations of HRP-ABTS reagent in the well: 1 mM 4-methoxybenzyl alcohol, 2.5 mM ABTS, 1 µg of HRP mL^{-1} (horseradish peroxidase) in 100 mM phosphate buffer [pH 6.0]). The plates were incubated at room temperature and measured in kinetic or endpoint mode at 418 nm. AAO activity is defined as the amount of enzyme that converts 1 µmol of alcohol to aldehyde with the stoichiometric formation of H_2O_2 per min under the reaction conditions.

iii) 4-methoxybenzyl alcohol/ABTS assay: Aliquots of 20 µL of yeast supernatants were added to 180 µL reaction mixture containing 100 mM sodium citrate-phosphate pH 4.0, 5 mM ABTS and 1 mM 4-methoxybenzyl alcohol. The plates were incubated at room temperature and measured in endpoint mode at 418 nm.

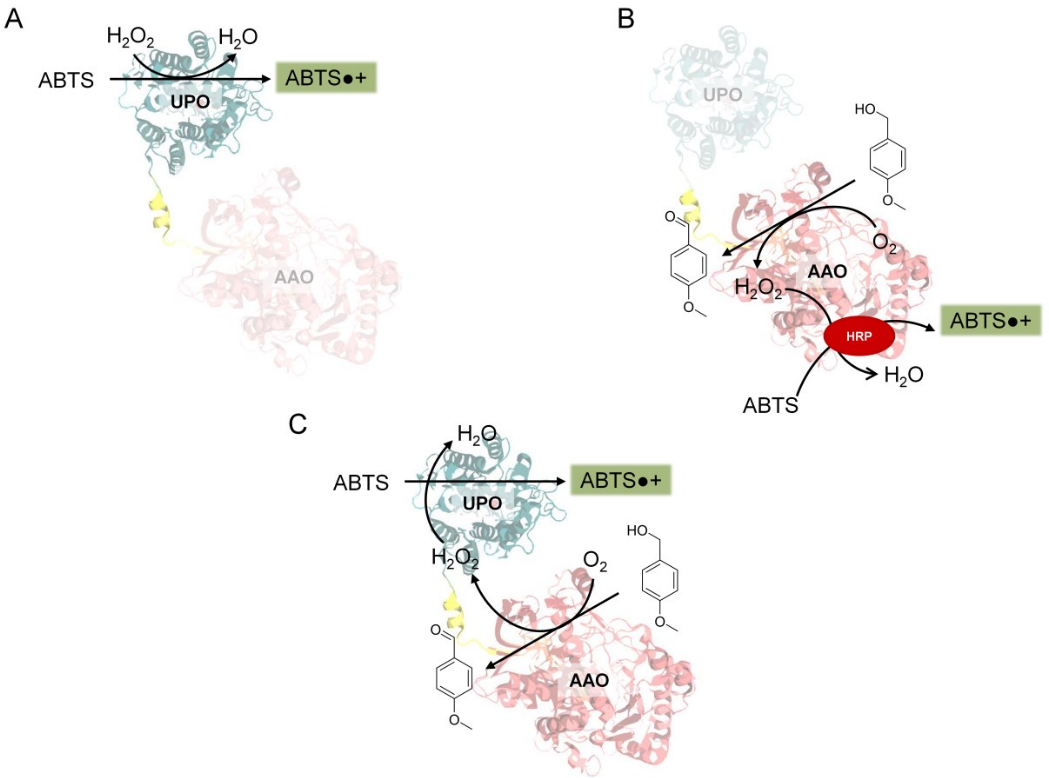

Figure 3.3. Screening of enzyme fusions. (**A**) ABTS/H_2O_2 assay. (**B**) 4-methoxybenzyl alcohol/ABTS-HRP coupled assay. (**C**) 4-methoxybenzyl alcohol/ABTS assay. Assays A and B uncouple the activity of AAO or UPO, respectively, whereas assay C allows the activity of the whole fusion to be assessed. Assay B is performed in 100 mM phosphate buffer pH 6.0 where UPO´s activity towards ABTS is not detectable.

3.4.3. Expression and purification of enzyme fusions

i) Expression in microplate and selection of the constructs: Individual clones were picked and cultured in sterile 96-well plates containing 50 µL of minimal medium (SC). In each plate, column 6 was inoculated with SoLo (UPO), column 7 with FX9 (AAO) and well H1 was not inoculated (culture media control). Plates were sealed to prevent evaporation and incubated at 30 °C, 225 rpm, and 80% relative humidity in a humidity shaker (Minitron-INFORS; Biogen, Spain). After 48 h, 150 µL of expression medium were added to each well, followed by culture for additional 48 h at 25 °C. The plates were centrifuged at 2,000 rpm (at 4 °C) and finally, 20 µL portions of the supernatants were screened for activity with the AAO, UPO and enzyme fusion mix assays. The plasmids from positive wells were recovered with a Zymoprep yeast plasmid miniprep kit I. Since the product of the Zymoprep was impure and the DNA extracted was very low concentrated, the shuttle vectors were transformed into supercompetent *E. coli* XL2-Blue cells and plated onto LB-ampicillin plates. Single colonies were selected to inoculate 5 mL of LB-ampicillin medium and incubated overnight at 37 °C and 225 rpm. The plasmids from the best mutants were extracted (NucleoSpin plasmid kit), sent for DNA sequencing (GATC Biotech-Eurofins, Luxembourg) and transformed into *S. cerevisiae* for flask production.

ii) Large scale production and purification: Single colonies from the *S. cerevisiae* clones containing the constructs were picked from a SC drop-out plate, inoculated in minimal medium (10 mL), incubated for 48 h at 30 °C and 230 rpm. An aliquot of cells was removed and used to inoculate minimal medium (100 mL) in a 500 mL shake flask (at OD_{600} ~0.25). The cells completed two growth phases (8 h) and then expression medium (900 mL) was inoculated with the pre-culture (100 mL) (OD_{600} of 0.1). After incubating for 72 h at 25 °C and 150 rpm (maximal enzyme activity; OD_{600} = 25-30), in 2,500 mL baffled Ultra Yield flasks (Thomson Instruments Inc., CA, USA). The cells were recovered by centrifugation at 8,000 rpm (at 4 °C) and the supernatant was double-filtered (using both glass membrane and a nitrocellulose membrane of 0.45 µm pore size). Enzyme fusions were purified by immobilized metal-ion affinity chromatography (IMAC) using HisTrap FF columns (GE Healthcare, ON, Canada) coupled to an ÄKTA purifier system. Binding buffer contained 20 mM Bis-Tris pH 7.4, 250 mM NaCl, 10 mM imidazole and elution buffer 20 mM Bis-Tris pH 7.4, 250 mM NaCl, 200 mM imidazole. IMAC-purified enzyme fusions were dialyzed for desalting and further purification by size-exclusion chromatography (SEC) using a Superdex 75 Increase 10/300 GL SEC column (GE Healthcare) in running buffer (50 mM potassium phosphate pH 7, 150 mM NaCl) at 0.8 mL min^{-1}. Fractions presenting both UPO and AAO activity were pooled, concentrated and dialyzed against stability buffer (20 mM potassium phosphate pH 7); resulting in pure orange proteins (this coloration is due to the presence of heme group –red- and FAD –yellow- inside the protein). Samples were loaded onto 4-20% precast polyacrylamide gel under denaturing conditions (Bio-Rad). Enzymes were deglycosilated with PNGase F (New England Biolabs, MA, USA) following the commercial protocol under denaturing conditions. The concentration of UPO for total turnover numbers calculations (TTNs) was determined using the CO (carbon monoxide) difference spectrum. It was performed at 25 °C using Tris/HCl buffer (20 mM, pH 7.0) and sodium dithionite (50 mM). Samples were bubbled with CO for 60 sec (1-2 bubbles per sec). The CO difference spectra were recorded between 400 nm and 500 nm. From the absorbance difference between 445 nm and 490 nm, the peroxygenase concentration can be calculated using an extinction coefficient of ε445-490=107 mM-1 cm-1. FX9 (AAO) and SoLo (UPO) were produced and purified as described elsewhere (Viña-Gonzalez et al., 2018) or according to **Section**

3.3.2. Concentrations of the enzymes were determined with Bio-Rad protein reagent and BSA (bovine serum albumin) as standard.

3.4.4. Kinetic characterization

ABTS kinetic constants were estimated at 25 ºC in sodium phosphate/citrate buffer (pH 4.0, 100 mM) containing H_2O_2 (2 mM). 4-methoxybenzyl alcohol (**2e**), 4-chlorobenzyl alcohol (**2c**) and 4-fluorobenzyl alcohol (**2a**) kinetics were measured in potassium phosphate buffer (pH 6.0, 100 mM) containing H_2O_2 (2 mM) just in the case of UPO measurements. Reactions were performed in triplicate, and substrate oxidations were followed through spectrophotometric changes (ε_{418} ABTS•+=36,000 M^{-1} cm^{-1}; ε_{285} 4-methoxybenzaldehyde=16,950 M^{-1} $cm^{-1;}$ ε_{252} 4-fluorobenzaldehyde=13,700 M^{-1} cm^{-1} and ε_{260} 4-chlorobenzaldehyde=15,862 M^{-1} cm^{-1}) (Ferreira et al., 2005). In the case of dextromethorphan kinetics with SoLo and H enzyme fusion, they were estimated at 25 ºC in potassium phosphate buffer (pH 6.0, 100 mM) containing H_2O_2 (2 mM) and 0.5-10 mM dextromethorphan. The reactions were stopped by the addition of Purpald® after 40-480 seconds depending on substrate concentration. Dextrorphan production was measured indirectly using Purpald® reagent (it reacts with formaldehyde -byproduct of dextromethorphan demethylation- giving a purple color measurable at 550 nm). Aliquots of 10 µL were withdrawn from each well and mixed with 140 µL of *dd*H_2O, later 50 µL of 100 mM Purpald® dissolved in NaOH 2N were added, mixed 2 min and immediately measured at 550 nm. Formaldehyde concentration determination was evaluated with a calibration curve (**Figure 3.4**). To calculate the K_m and k_{cat} values, the average V_{max} was represented against substrate concentration and fitted to a single rectangular hyperbola function with SigmaPlot 10.0, where parameter a was equal to k_{cat} and parameter b was equal to K_m.

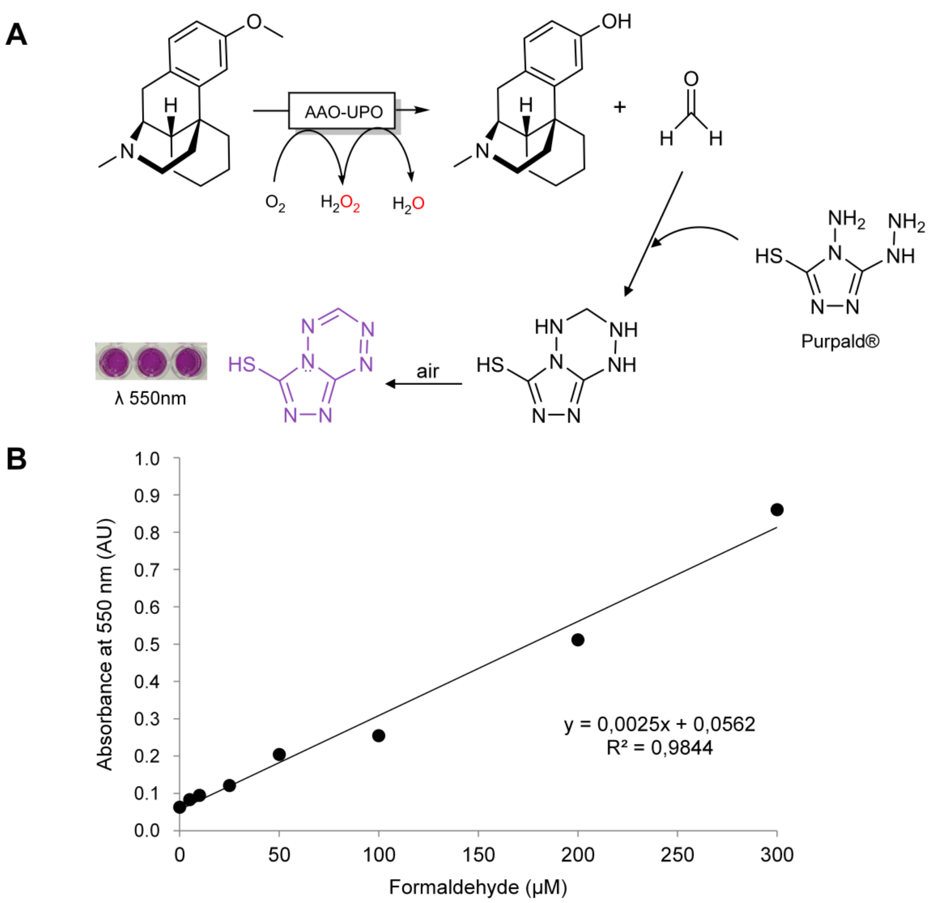

Figure 3.4. Purpald® assay (**A**) and calibration curve (**B**).

3.4.5. Evaluation of the enzyme fusion system

T_{50} values were calculated as described in **Section 3.2.2**. Dextrorphan synthesis was determined on Shimadzu GC-2010 Plus gas chromatograph with an AOC-20i Auto injector with FID detector (Shimadzu, Japan) using nitrogen as carrier gas with a previously described method (van Schie et al., 2020). The reactions were performed in GC vials of 1.5 mL in a final volume of 0.3 mL. For the evaluation of the performance of different alcohols within the cascade, reactions contained 10 mM of each primary alcohol (**2a-f**), 0.04 µM of H (peroxygenase concentration measured with CO difference spectrum) and 10 mM of dextromethorphan hydrobromide in 100 mM potassium phosphate buffer pH 7 were carried out. Comparison of enzyme fusions was performed with 10 mM of **2a**, 0.05 µM of each enzyme fusion and 10 mM of dextromethorphan hydrobromide in 100 mM potassium phosphate buffer pH 7. Optimized reaction conditions were achieved with 2 mM of **2a**, 0.04 µM of enzyme fusion H (peroxygenase concentration measured with CO difference spectrum) and 10 mM of dextromethorphan hydrobromide in 100 mM potassium phosphate buffer pH 7.0. Concerning alcohol feeding experiments, initial reaction mixtures contained 0.04 μM of H and 10 mM of dextromethorphan hydrobromide in 100 mM potassium phosphate buffer pH 7. **2a** was added inside the vial with a tubing connected to a syringe pump (1 μL h^{-1}) at 3 different rates (0.5, 1 and 2 mM h^{-1}), achieved with a different stock concentration of alcohol inside the syringes (**Figure 3.5**). All reactions were incubated at 30 °C, 600 rpm, 24 h in a ThermoMixer® C and were performed at least by duplicate. Time course reactions contained 15 mM of **2a**, 0.1 μM of H and 10 mM of dextromethorphan hydrobromide in 100 mM potassium phosphate buffer pH 7. Reactions were extracted with ethyl acetate at different time points to stop the reactions (0.5, 1, 2, 4, 8 and 24 hours).

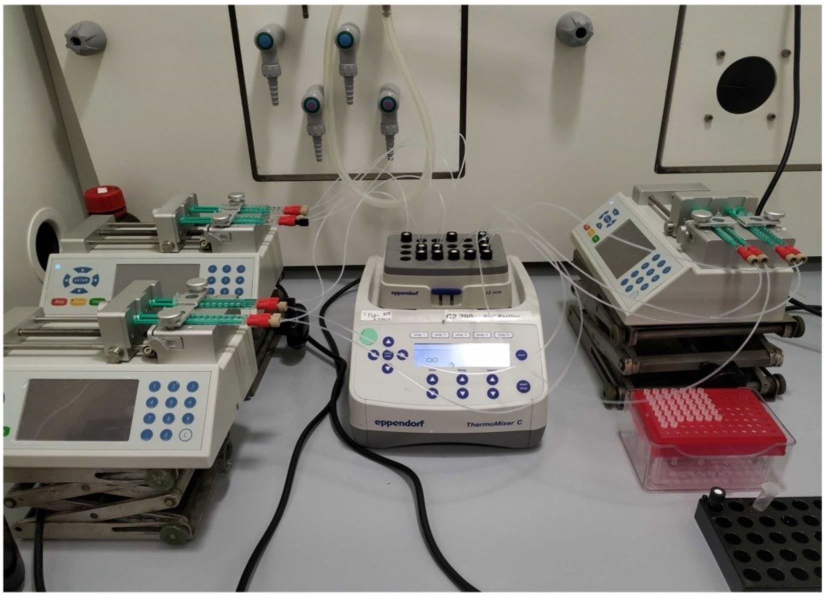

Figure 3.5. Reaction setup for dextrorphan production with different alcohol feeding.

H enzyme fusion performance compared to the use of both enzymes separately (FX9 and SoLo) was evaluated in triplicate in GC vials of 1.5 mL in a final volume of 0.2 mL containing 10 mM of **2a**, 10 mM of dextromethorphan hydrobromide in 100 mM potassium phosphate buffer pH 6 and 0.1 μM of H (peroxygenase concentration measured with CO difference spectrum) (UPO_AAO) or 0.1 μM of FX9 (AAO) and 0.1 μM of SoLo (UPO) (UPO+AAO). Reactions were incubated at 30 °C, 600 rpm, 1h in a ThermoMixer® C. Aliquots of 7.5 μL were withdrawn from each vial at time points 15, 30, 45 and 60 min for product determination using Purparld®. The aliquots were added to 142.5 μL of *dd*H_2O (1/20 dilution), later 50 μL of 100 mM Purpald® dissolved in NaOH 2N were added, mixed 2 min and immediately measured at 550 nm as described before.

RESULTS AND DISCUSSION

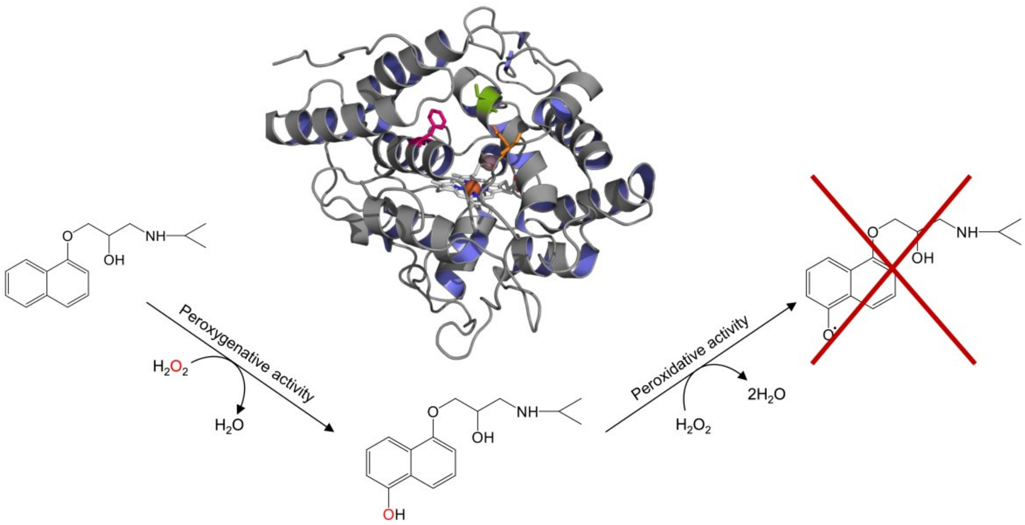
NH
OH
O
Peroxygenative activity
H2O2
H2O
NH
OH
O
OH
Peroxidative activity
H2O2
2H2O
NH
OH
O
O·

4. Results and discussion

4.1. Chapter 1: Selective synthesis of the human drug metabolite 5´-hydroxypropranolol by an evolved self-sufficient peroxygenase.

Propranolol is a widely used beta-blocker that is metabolized by human liver P450 monooxygenases into equipotent hydroxylated human drug metabolites (HDMs). It is paramount for the pharmaceutical industry to evaluate the toxicity and activity of these metabolites but unfortunately, their synthesis has hitherto involved the use of severe conditions, with poor reaction yields and unwanted byproducts. Unspecific peroxygenases (UPOs) catalyze the selective oxyfunctionalization of C-H bonds and they are of particular interest in synthetic organic chemistry. Here, we describe the engineering of UPO from *Agrocybe aegerita* for the efficient synthesis of 5´-hydroxypropranolol (5´-OHP). We employed a structure-guided evolution approach combined with computational analysis, with the aim of avoiding unwanted phenoxyl radical coupling without having to dope the reaction with radical scavengers. The evolved biocatalyst showed a catalytic efficiency enhanced by two orders of magnitude and 99% regioselectivity for the synthesis of 5´-OHP. When the UPO mutant was combined with an H_2O_2 *in situ* generation system using methanol as sacrificial electron donor, total turnover numbers of up to 264,000 were achieved, offering a cost-effective and readily scalable method to rapidly prepare 5´-OHP.

This chapter is based on the publication: Gomez de Santos, P., Cañellas, M., Tieves, F., Younes, S.H.H., Molina-Espeja, P., Hofrichter, M., Hollmann, F., Guallar, V., Alcalde, M., 2018. Selective Synthesis of the Human Drug Metabolite 5´-Hydroxypropranolol by an Evolved Self-Sufficient Peroxygenase. *ACS Catal.* 8, 4789–4799.

4.1.1 Screening method and benchmarking

As mentioned in the introduction, the products of peroxygenase activity on aromatics like propranolol, become substrates of UPO’s peroxidase activity, which ultimately leads to the formation of a complex mixture of phenoxyl radicals (including semiquinones) and their disproportionation (quinones) and coupling products. This mixture is further clouded by non-enzymatic polymerization, affecting the final yields and the purification of the target compounds (Ullrich and Hofrichter, 2007). Such problems might be partially circumvented by doping the reaction with expensive phenoxyl radical scavengers (*e.g.* ascorbic acid), although this solution is far from practical in terms of developing a cost-effective strategy (**Scheme 4.1**).

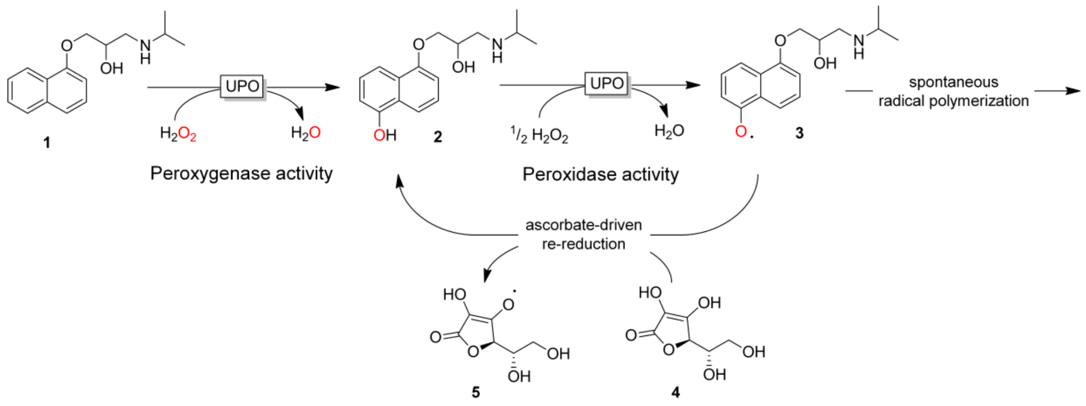

Scheme 4.1. Transformation of propranolol by UPO in the presence of ascorbic acid as a radical scavenger. Peroxygenase activity converts propranolol (**1**) into 5´-OHP (**2**), a substrate of the peroxidase activity of the enzyme that leads to the formation of phenoxyl radicals (**3**), which can in turn undergo non-enzymatic coupling and polymerization. The inclusion of ascorbic acid (**4**) in the reaction mixture can alleviate the formation of unwanted side-products by reducing the conversion of (**3**) to (**2**) while it is oxidized into ascorbyl radical (**5**).

As a starting point for the present study, we used a colorimetric screening assay based on 4-aminoantypirine (4-AAP) (Otey and Joern, 2003) to benchmark the wildtype UPO (*Aae*UPO (Ullrich et al., 2004)), PaDa-I (Molina-Espeja et al., 2014) and JaWa (Molina-Espeja et al., 2016a) mutants in the reaction with propranolol, assessing the variants in terms of their activity in the presence and absence of ascorbic acid (AA); (**Figure 4.1**). Significantly, the JaWa mutant outperformed both the *Aae*UPO and PaDa-I variants by ~4-fold (both the presence and absence of AA). Given that JaWa showed TTN of 50,000 in the transformation of naphthalene into 1-naphthol, the structural similarities between naphthalene and propranolol, and the location of the G241D mutation at the entrance of the heme access channel, we searched for new catalytic motifs to be subjected to focused evolution.

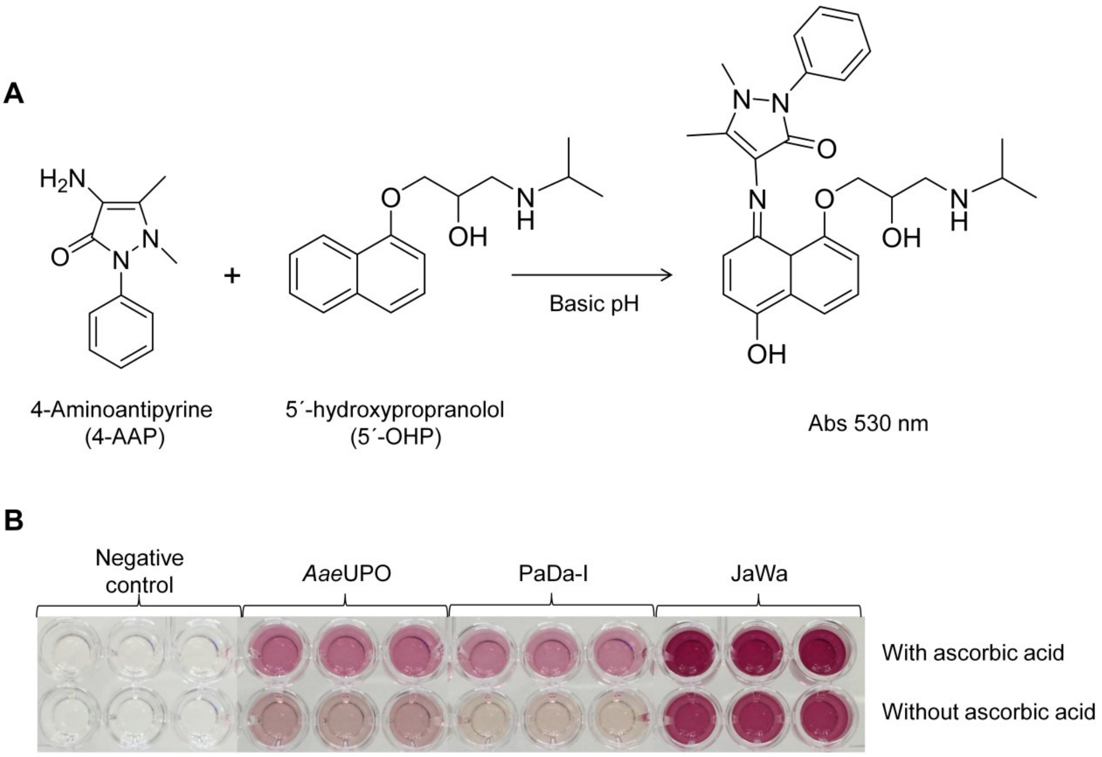
A
H2N
O
N
N
+
O
OH
N
H
Basic pH
N
N
O
N
O
OH
N
H
OH
4-Aminoantipyrine
(4-AAP)
5´-hydroxypropranolol
(5´-OHP)
Abs 530 nm
B
Negative
control
AaeUPO
PaDa-I
JaWa
With ascorbic acid
Without ascorbic acid

Figure 4.1. Screening assay to detect 5´-OHP with 4-AAP. (A) The dual screening assay allowed us to select clones with weaker peroxidase activity on 5´-OHP and enhanced peroxygenase activity on propranolol. We used the ratio between the activities in the presence and absence of AA as a discriminatory factor of the assay. (B) Benchmarking of the reaction with propranolol and different UPO variants, in the presence and absence of AA.

4.1.2. Directed evolution studies

Molecular docking simulations (Chemical Computing Group ULC, 2010) with propranolol underlined the possibility that along with Phe191, the G241D mutation favored the anchoring of propranolol (**Figure 4.2**). Accordingly, we selected the D187-V248 segment for random mutagenesis and DNA recombination by MORPHING (Gonzalez-Perez et al., 2014b), excluding the introduction of destabilizing mutations in the remaining protein structure.

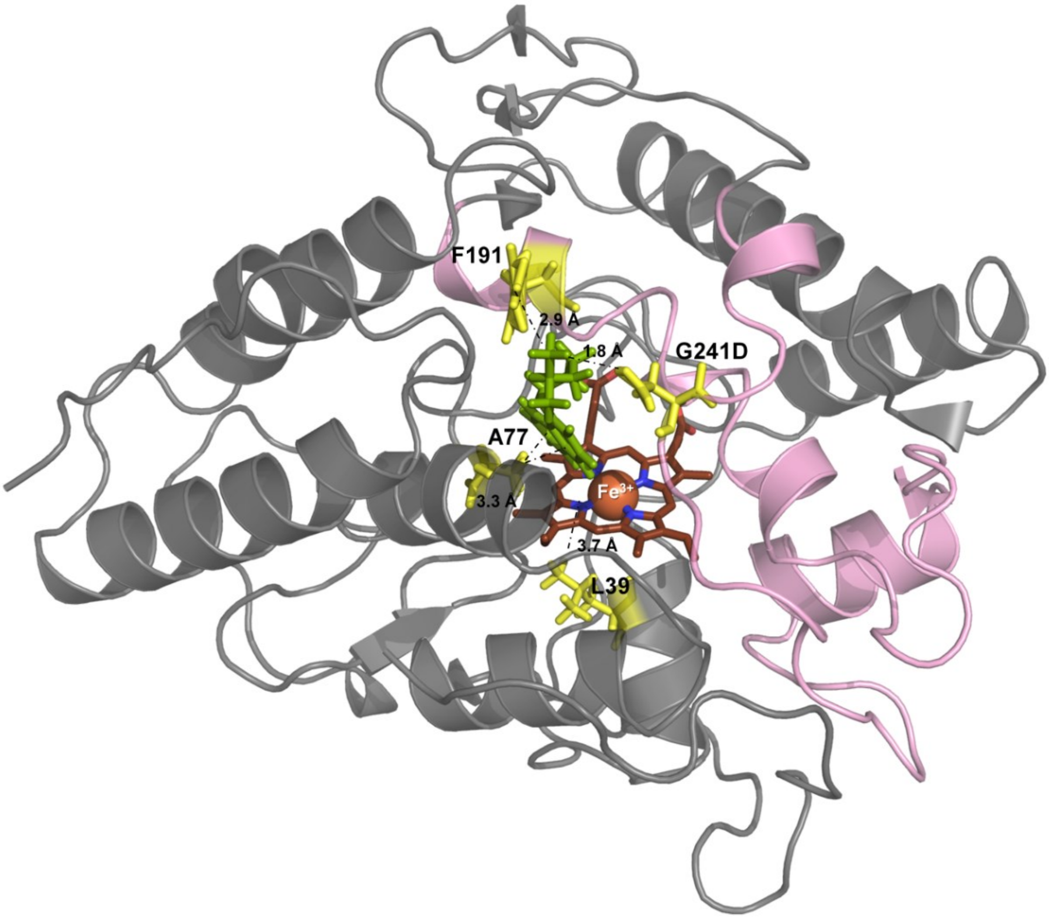

Figure 4.2. The UPO structure (JaWa mutant) is shown as a grey cartoon and the relevant amino acids are indicated in yellow, together with the distances between them and the propranolol molecule (in green) or to the heme group (in dark red). The F191 position and G241D substitution seem to be involved in positioning the aliphatic branch of propranolol, while A77 apparently interacts with the aromatic rings and L39 lies underneath the heme. The D187-V248 segment (in pink) was subjected to MORPHING, harboring the α-helix where F191 is located and the loop of G241D. Docking simulations were performed using Molecular Operating Environment (MOE) software and the crystal structure of the evolved UPO at a resolution of 1.2 Å (Ramirez-Escudero et al., 2018).

We constructed two mutant libraries with different mutational loads (**Figure 4.3.A**) and screened them using the 4-AAP assay which was validated and adapted to microplate (**Figure 4.4** and **4.5**). As selection criterion, we imposed that UPO variants had to oxidize propranolol exceeding a threshold of 1.5-fold of parental's activity. After two consecutive re-screenings, the six selected clones that satisfied the activity threshold carried the same single substitution (F191S), which did not jeopardize thermostability as the T_{50} value for both the parental JaWa and the mutant was maintained at ~60 ºC (**Figure 4.3.B** and **C**). This mutation improved the formation of 5´-OHP in the absence of AA up to 230% and most importantly, the ratio between both reactions enhanced 1.8-fold in the presence and absence of AA.

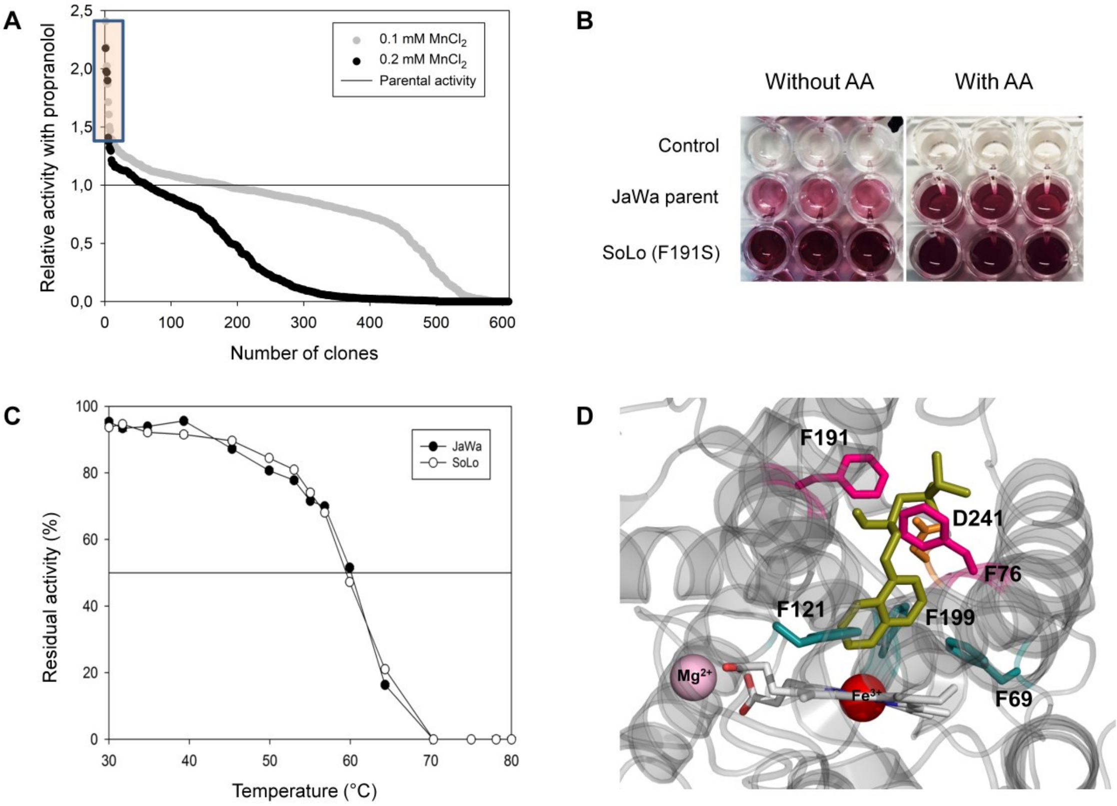

Figure 4.3. (**A**) Mutagenic landscapes obtained by MORPHING at different mutational frequencies. The activity of the clones is plotted in descending order and the solid line shows the activity of the parental type in the assay. The clones selected for rescreening are framed. (**B**) Activity of the parental UPO and the SoLo mutant in the 4-AAP assay, in the presence and absence of AA. (**C**) Kinetic thermostability of the JaWa and SoLo variants. T_{50} was defined as the temperature at which the enzyme maintained 50% of its activity after 10 min incubation. Each point and standard deviation comes from three independent experiments. (**D**) Positions subjected to saturation mutagenesis. The UPO structure is shown as a grey cartoon: the heme group is in CPK colors with Fe^{3+} as a red sphere, the Phe triad is in turquoise, the Phe191 and Phe76 pair delimiting the entrance to the heme is in pink, and Asp241 is orange. The structural Mg^{2+} is represented as a pink sphere and propranolol is in green.

Without ascorbic acid

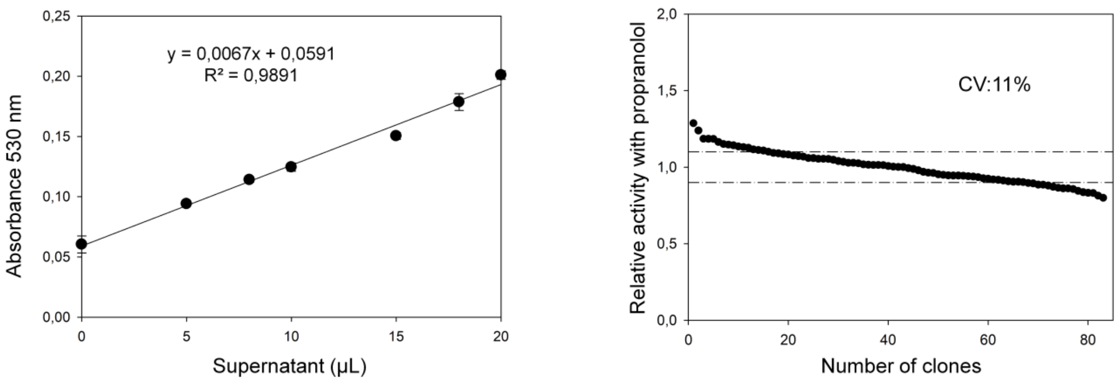

With ascorbic acid

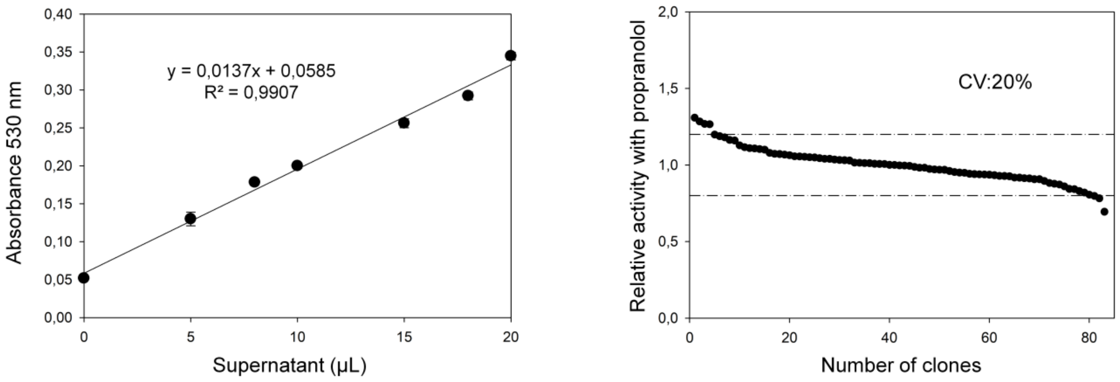

Figure 4.4. Validation of the screening assay. (Left) Linearity of the assay, (Right) Coefficient of variance (CV) of the spectrophotometric assay. The landscapes correspond to 83 independent clones containing JaWa parental type, grown in microtiter format. The activity of the clones is plotted in descending order; dashed lines indicate the CV for each assay.

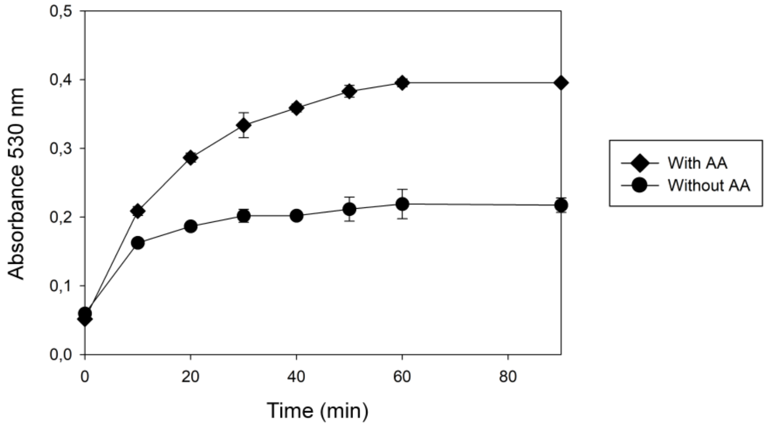

Figure 4.5. Optimization of the incubation time with and without AA.

Given that Phe191 and Phe76 are responsible for defining the entrance to the heme access channel, whereas the aromatic triad formed by Phe69, Phe121 and Phe199 is involved in orienting the substrate for catalysis (Piontek et al., 2013), all these residues were studied by saturation mutagenesis using as template the F191S variant (**Figure 4.3.D**). We first designed a combinatorial saturation mutagenesis library of Phe191 and Phe76 in which the most active clones exclusively incorporated again the F191S substitution. When individual saturation mutagenesis was performed at Phe69, Phe121 and Phe199, a set of non-functional libraries was obtained (80% inactive clones), with no further beneficial substitutions identified (**Figure 4.6**).

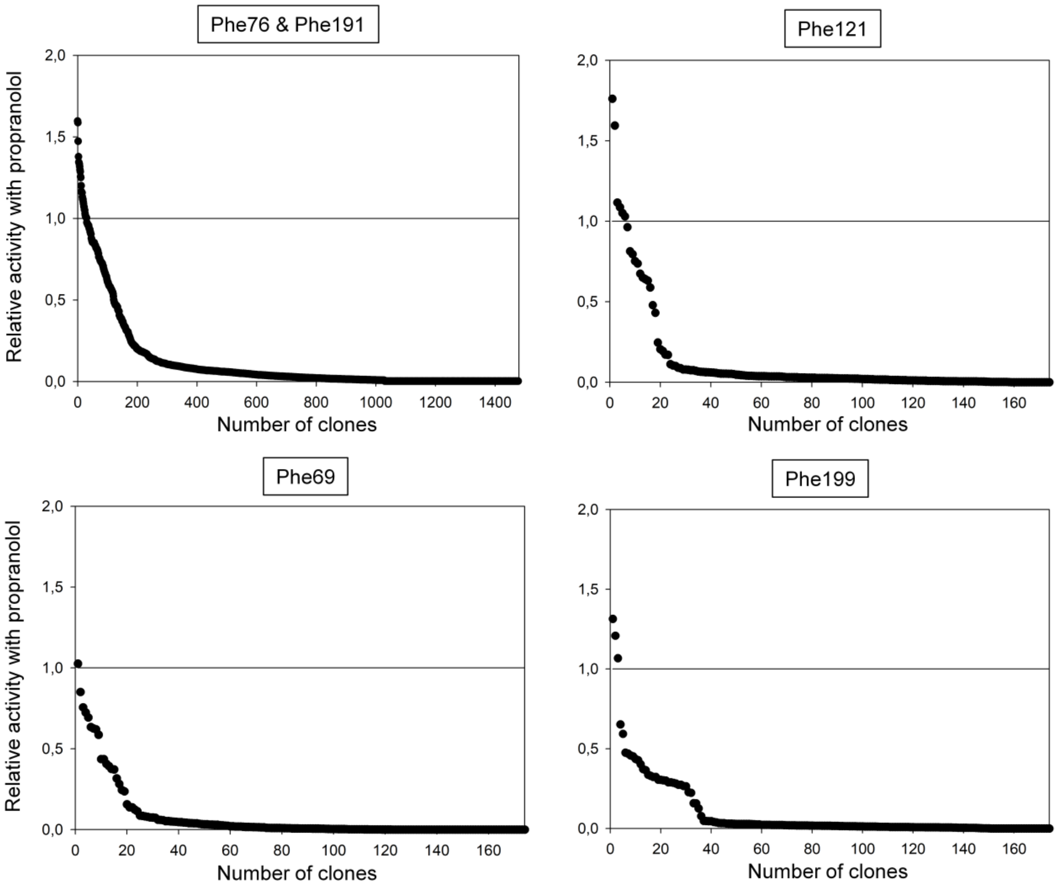

Figure 4.6. Mutagenic landscapes of saturation mutagenesis libraries. The activity of the clones is plotted in descending order; horizontal solid line indicates the activity of parental type.

The mutant clone containing the F191S mutation (named SoLo), JaWa, PaDa-I and *Aae*UPO were all produced, purified to homogeneity [Reinheitszahl, *Rz* (A_{418}/A_{280})~2.2], and characterized biochemically and computationally at the atomic level. We first analyzed the transformation of propranolol by HPLC-PDA (**Figure 4.7.C**) and notably, the regioselectivity for 5´-OHP shifted from 91% in *Aae*UPO to 99% in PaDa-I, JaWa and SoLo. When boosting the UPO by periodic dosing with 2 mM H_2O_2 over the course of the reaction, without supplying AA, TTN of 3,000, 15,000 and 45,000 were achieved for the *Aae*UPO, JaWa and SoLo mutants, respectively, roughly representing a 15-fold improvement of SoLo relative to the wildtype *Aae*UPO (**Figure 4.7.A, B**). More significantly, in the absence of AA the SoLo mutant still outperformed the TTN of the wildtype doped with AA more than 3-fold (*viz*. 45,000 and 14,000 TTN for SoLo in the absence of AA and *Aae*UPO in the presence of AA, respectively).

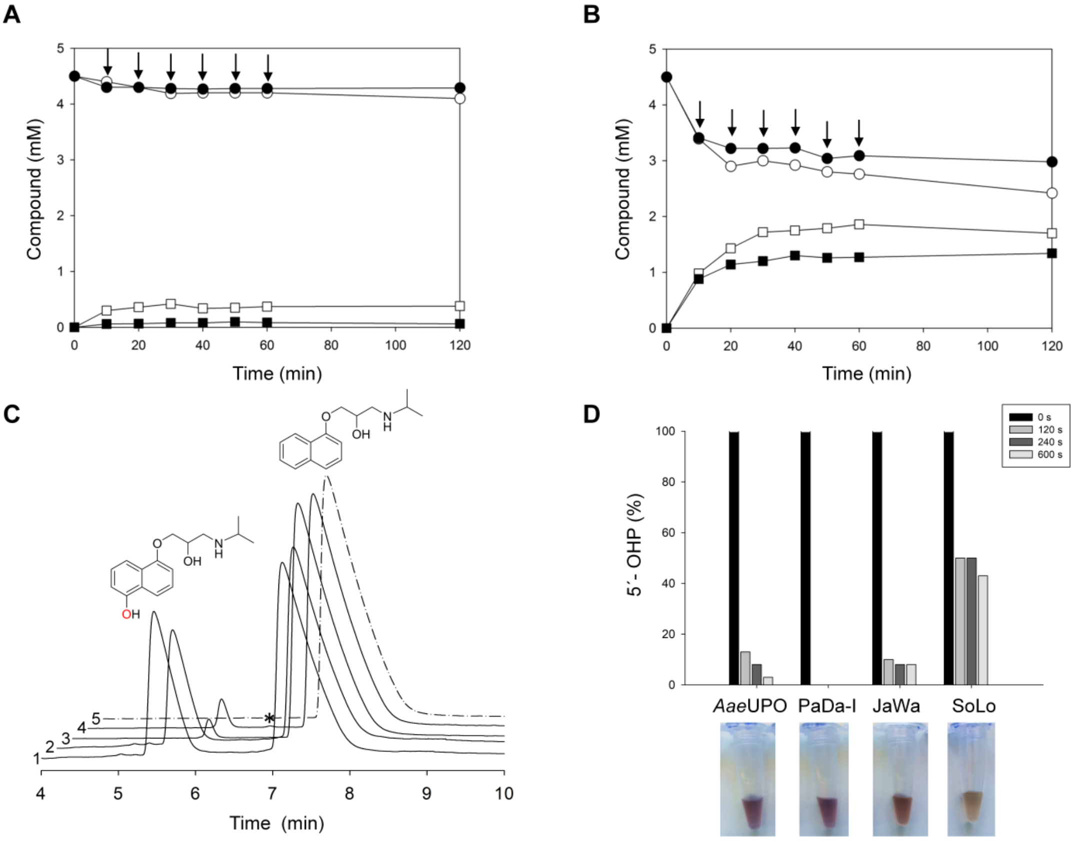

Figure 4.7. Propranolol conversion by native and mutant UPOs. (**A**) and (**B**) time course of the reactions over 120 min at pH 7.0 with the wildtype *Aae*UPO and the SoLo mutant, respectively. White circles, propranolol (with AA); black circles, propranolol (without AA); white squares, 5´-OHP (with AA); black squares, propranolol (without AA); arrows, periodic pulses of 2 mM H_2O_2. The total turnover numbers (TTN, µmol product µmol enzyme^{-1}) were estimated from the 5´-OHP concentration after 120 min. (**C**) The HPLC elution profiles after a reaction time of 60 min in the absence of AA: 1, SoLo; 2, JaWa; 3, PaDa-I; 4, *Aae*UPO; 5, Control without enzyme; *, traces of DIP. (**D**) Conversion of 5´-OHP into phenoxyl radicals and polymers.

Kinetic parameters were measured for the one-electron oxidation of ABTS (peroxidase activity), the two-electron oxidation of propranolol into 5´-OHP (peroxygenase activity) and for H_2O_2 with benzyl alcohol as peroxygenase substrate (**Table 4.1**). SoLo showed a striking 14-fold and 17-fold drop in the catalytic efficiency (k_{cat}/K_m) with ABTS relative to *Aae*UPO and PaDa-I, respectively, while maintaining similar performance as JaWa. The strong enhancement in the K_m, with a maximal 23-fold increase relative to *Aae*UPO was mostly responsible for this effect. Kinetic differences for propranolol were even more dramatic and the catalytic efficiencies for JaWa and SoLo were two orders of magnitude higher than for *Aae*UPO and PaDa-I, mostly due to the important 5- to 10-fold decrease in the K_m for this substrate. The kinetics for H_2O_2 in the peroxygenation of benzyl alcohol did not differ among the UPO variants.

Table 4.1. Steady kinetic parameters of UPO variants.

Substrate	Kinetic constant	***Aae*UPO**	**PaDa-I**	**JaWa**	**SoLo**
ABTS	K_m (μM)	25 ± 2	50 ± 6	181 ± 22	568 ± 91
	k_{cat} (s^{-1})	221 ± 6	546 ± 19	125 ± 5	365 ± 23
	k_{cat}/K_m ($M^{-1} s^{-1}$)	8.8×10^6	11.0×10^6	6.9×10^5	6.4×10^5
Propranolol	K_m (μM)	2,239 ± 333	2,268 ± 220	244 ± 92	391 ± 97
	k_{cat} (s^{-1})	150 ± 12	212 ± 11	765 ± 76	497 ± 35
	k_{cat}/K_m ($M^{-1} s^{-1}$)	6.7×10^4	9.3×10^4	3.1×10^6	1.3×10^6
H_2O_2	K_m (μM)	1,370 ± 162	1,530 ± 80	1,250 ± 300	1,430 ± 153
	k_{cat} (s^{-1})	290 ± 15	676 ± 24	447 ± 40	446 ± 23
	k_{cat}/K_m ($M^{-1} s^{-1}$)	2.1×10^5	4.4×10^5	3.6×10^5	3.1×10^5

4.1.3. Computational analysis

In order to study the differences found between the *Aae*UPO, PaDa-I, JaWa and SoLo variants during propranolol hydroxylation at the atomic level, we turned to molecular modeling employing PELE (Protein Energy Landscape Exploration), a Monte Carlo algorithm capable of effectively sampling the protein-ligand conformational space (Madadkar-Sobhani and Guallar, 2013). We first modeled propranolol diffusion to the active site for each variant, finding that binding energies and distances largely correlate with the experimental K_m (**Figure 4.8 and Supporting Movie**). To facilitate oxygenation, ideally the distances between the C_5 propranolol carbon atom and the catalytic heme-ferryl oxygen should be around (or below) 4 Å. JaWa, with the lowest K_m for propranolol, clearly presents the best "catalytic minimum", with a distance around 3.5 Å and a binding energy at *c.a.* -70kcal/mol. On the other hand, *Aae*UPO and PaDa-I, with noticeably higher K_m, have markedly worse binding energy profiles, which would result in the necessity of adding more substrate to reach correct catalytic positions. Moreover, when we analyzed the relative distance distribution of substrate's C_5 atom in the active site (**Figure 4.8**), we obtained a similar tendency: the relative frequency of structures below 4 Å is significantly higher for JaWa and SoLo variants.

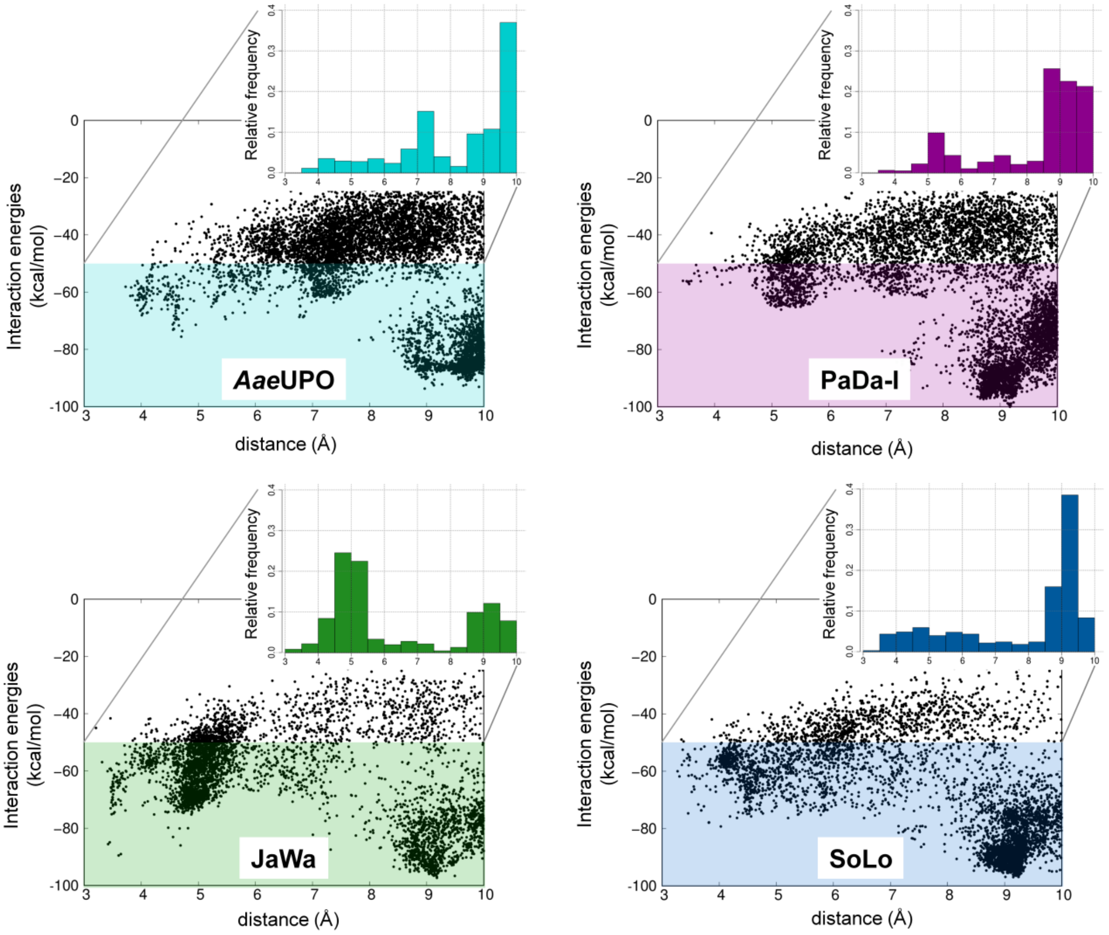

Figure 4.8. Computational analysis of propranolol diffusion in native and mutant UPOs. Interaction energies (in kcal·mol-1) vs. ligand distances (in Å) from PELE simulations with propranolol in *Aae*UPO, PaDa-I, JaWa and SoLo UPO variants. The distances are between the reactive O atom in the heme compound I and the C5 atom of propranolol. The top-right (inset) plots show the relative population for all the structures with interaction energies below -50 kcal·mol-1 using binning widths of 0.5 Å.

In addition, simulations provided important insights into the influence of the G241D mutation present in both JaWa and SoLo but absent in *Aae*UPO and PaDa-I (**Supporting Movie**), which facilitates the anchoring of the substrate in a more favorable orientation for hydroxylation. Besides, the Phe191 residue seems to tighten the stabilization of this catalytic orientation in the JaWa variant which is in agreement with the slight kinetic differences between both variants for propranolol. To obtain further structural insights into the changes caused by F191S mutation, 100 ns molecular dynamics (MD) were performed with JaWa and SoLo. MD pocket method (Schmidtke et al., 2011) was used to track heme's cavity volume changes along the MD trajectories, showing a widening of the SoLo variant pocket compared to Jawa of ~50 Å^3 (**Figures 4.9.C, D, E**). The most obvious reason behind the cavity broadening is the mutation Phe191 to a less bulky amino acid such as serine. Moreover, structure visual inspection in JaWa, shows that Phe191 tends to be placed in the hydrophobic heme cavity, causing a displacement of the α-helix hosting it and reducing the heme pocket volume. In the SoLo variant, such movement does not occur since Ser191 is kept buried into the protein by a hydrogen bond interaction within its hosting α-helix (**Figures 4.9.A, B**).

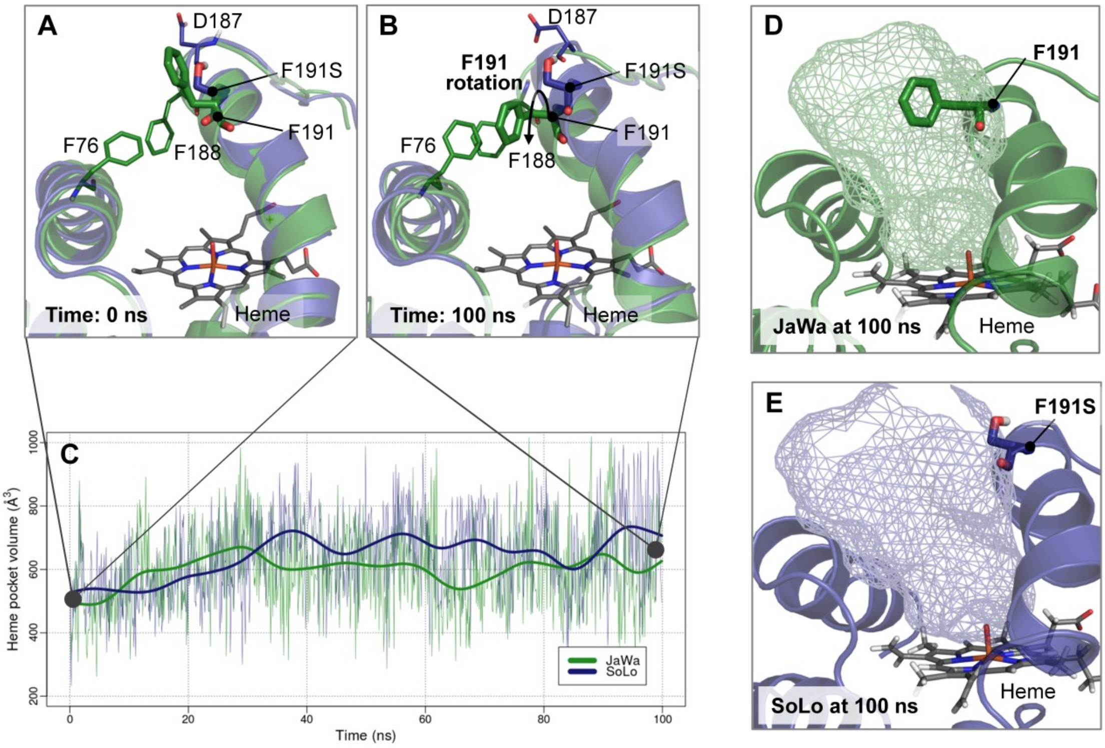

Figure 4.9. F191S induced structural changes along 100 ns MD. (**A**) and (**B**) JaWa and SoLo (colored in green and dark blue respectively) comparison at the beginning (0 ns, A) and at the end (100 ns, B) of the MD simulation. Simulations show that while F191 residue in JaWa causes a displacement of the α-helix hosting it and leads to the reduction of the heme cavity, in the SoLo variant F191S avoids the heme pocket hydrophobicity and tends to be buried into the α-helix holding it, interacting mainly with nearby residues (an hydrogen bond with D187 is conserved 87% among the MD). (**C**) Heme cavity volume tracking along 100 ns MD simulations for JaWa and SoLo variants, calculated with MDpocket every 0.1 ns. Smoothed volume of the pocket is shown in thick lines. (**D**) and (**E**) Heme binding pocket volume representation as a mesh surface for JaWa and SoLo variants respectively after 100 ns MD simulation.

However, we still wanted to ascertain why there was more 5´-OHP formed by SoLo than by JaWa, particularly given that the latter had an even higher catalytic efficiency for propranolol (**Table 4.1**). We hypothesized that the F191S mutation, which widens the access channel (**Figure 4.9** and **4.10.B**), could play an important role in by-passing the unwanted peroxidase activity on 5´-OHP (**2**) and the ensuing formation of the phenoxyl radical (**3**), thereby increasing the *P*:*p* ratio (numbering according to **Scheme 4.1.**). To unveil the weaker peroxidase activity of SoLo, we measured the disappearance of **2** by HPLC-PDA during the reaction with the different variants in the absence of AA (**4**), using

2 as the departure reducing substrate. Pleasingly, the rate of converting **2** into **3** was noteworthy for all the variants except SoLo, which maintained a concentration of the substrate 10-fold higher than that of the rest of the variants after 10 minutes of the reaction (**Figure 4.7.D**). These noticeable differences became readily visible because the polymeric products formed through the non-enzymatic coupling of the phenoxyl radicals are colored (see inset in **Figure 4.7.D**). These results were confirmed computationally by PELE whereby the 5´-OHP diffusion addressed the significantly smaller concentration of this peroxidase substrate at lower distances (<5 Å) from the heme catalytic center in SoLo compared to JaWa, as well as shorter residence times in the binding site (**Figure 4.10.A**) which results in the inefficient 5´-OHP oxidation by SoLo variant. Taken together, our results unequivocally show that while the F191S mutation acts as the main driver of the remarkable decrease in peroxidase activity on **2**, the G241D change is mostly responsible for the improved peroxygenase activity on **1** (**Figure 4.8**).

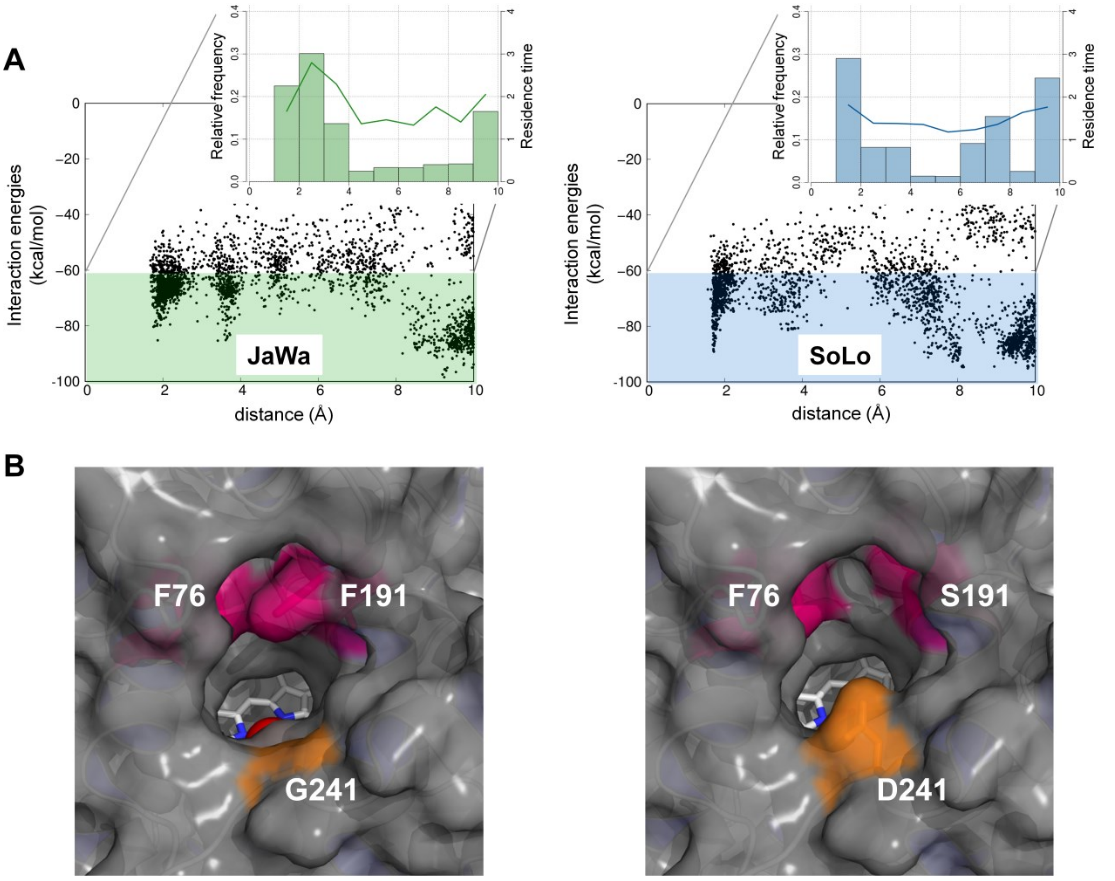

Figure 4.10. (**A**) Computational analysis of 5´-OHP diffusion in JaWa and SoLo UPO variants. Interaction energies (in kcal·mol^{-1}) *vs.* ligand distances (in Å) from PELE simulations with 5´-OHP in JaWa and SoLo UPO variants. The distances are between the reactive O atom in the heme compound I and the C$_5$ atom of 5´-OHP. The top-right inset bars show the relative distance distribution of those structures with energies below -60 kcal·mol^{-1}, along with a line indicating the

average residence time of 5´-OHP in the binding site, calculated using binning widths of 1Å. (**B**) Differences in the heme access channel of UPO variants. The Phe residues defining the entrance of the heme channel of PaDa-I (left), with G241D in orange and F191S mutations in SoLo (right). The G241D mutation is present in the JaWa and SoLo variants, whereas F191S appears only in SoLo (neither *Aae*UPO nor PaDa-I mutant contain such substitutions). Protein modeling based on the crystal structure of the evolved PaDa-I variant at a resolution of 1.5 Å (Ramirez-Escudero et al., 2018).

4.1.4. Reaction engineering

To address the well-known lability of heme-containing enzymes (including UPOs) against H_2O_2, we evaluated two strategies using either *in situ* generation of H_2O_2 from ambient O_2 or using *tert*-butyl hydroperoxide (*tert*-BuOOH) as milder peroxide source. For *in situ* H_2O_2 generation we utilized a bienzymatic cascade comprising alcohol oxidase (AOx) and formaldehyde dismutase (FDM) for the double oxidation of methanol to formic acid (generating two equivalents of H_2O_2, **Scheme 4.2**) (Fernández-Fueyo et al., 2016a).

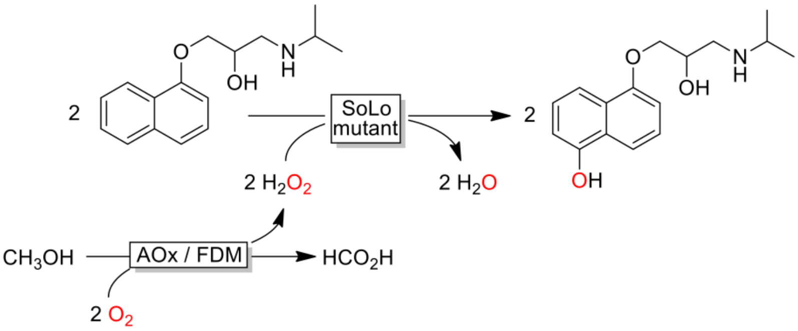

Scheme 4.2. Enzymatic cascade for *in situ* H_2O_2 generation. Alcohol oxidase (AOx) and formaldehyde dismutase (FDM) perform the double oxidation of methanol to formic acid for the generation of two equivalents of H_2O_2 (Fernández-Fueyo et al., 2016b) which are used by the UPO mutant (SoLo) for the formation of 5´-OHP.

With such system, TTN as high as 264,000 and 226,000 were achieved with and without AA, respectively. Also the second strategy, *i.e.* using *tert*-BuOOH as milder oxidant, proved successful (**Figure 4.11**). On semi-preparative scale, 20 and 10 mM of 5´-OHP were produced (20 and 40% analytical yield, respectively) with and without AA, respectively. The final product was isolated and further purified via a one-step flash chromatography step yielding 10.5 mg of pure 5´-OHP (as confirmed by ^{1}H-NMR, Annex **Figure 9.1**) in overall 15.2 % isolated yield. It should, however, be emphasized that neither the synthetic reaction, nor the isolation and purification procedure were optimized.

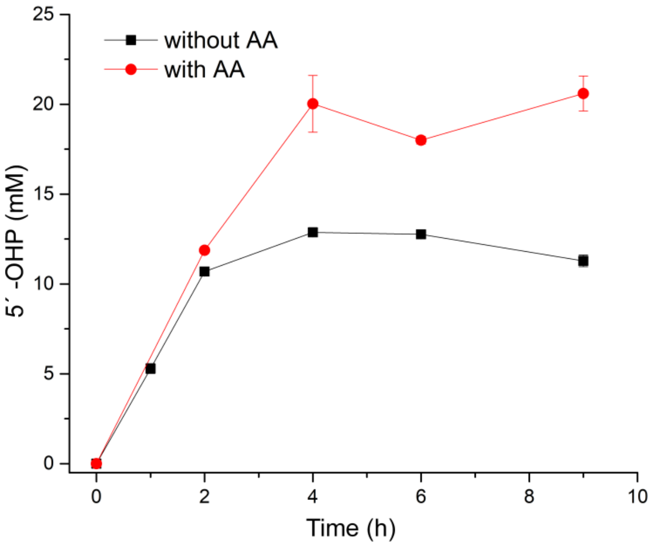

Figure 4.11. Semi-preparative production of 5´-OHP with SoLo mutant and *tert*-BuOOH. The reaction started by the addition of 5 mM *tert*-BuOOH and every hour, 5 mM tert-BuOOH was added to the reaction (further information can be found in the Material and methods).

4.1.5. Conclusions

Using H_2O_2 as a final electron acceptor and exclusive oxygen donor, UPO carries out a variety of oxygen-transfer reactions and as such, it is considered by many to be "taking the baton" from P450s in the field of synthetic organic chemistry (Bormann et al., 2015; Hofrichter et al., 2015; Molina-Espeja et al., 2017; Wang et al., 2017). In this study, we designed a highly active and stable UPO variant that behaves as a self-sufficient and efficient biocatalyst for the selective synthesis of 5´-OHP, irrespective of the presence of radical scavengers in the reaction. The UPO mutant shows the highest regioselectivity and TTN for the synthesis of 5´-OHP reported so far. When we compare it with the best engineered P450 BM3 heme domain peroxygenase, SoLo mutant surpasses it roughly by 9,000-fold (Otey et al., 2006). More significantly, with the assistance of a H_2O_2 *in situ* generation system based on an enzyme cascade reaction with methanol as the sacrificial electron donor for the reductive activation of O_2 (Fernández-Fueyo et al., 2016b), this UPO variant outperforms any natural or engineered hydroxylating catalyst described to date going one step closer to the industrial needs (Molina-Espeja et al., 2016b).

4.2. Chapter 2: Benchmarking of laboratory evolved unspecific peroxygenases for the synthesis of human drug metabolites.

By mimicking the role of human liver P450 monooxygenases, fungal unspecific peroxygenases (UPOs) can perform a range of highly selective oxyfunctionalization reactions on pharmacological compounds, including *O*-dealkylations and hydroxylations, thereby simulating drug metabolism. Here we have benchmarked human drug metabolite (HDM) synthesis by several evolved UPO mutants (**Figure 4.12**), focusing on dextromethorphan, naproxen and tolbutamide. The HDM from dextromethorphan was prepared at the semi-preparative scale as a proof of production. The structural analysis of mutations involved in the synthesis of HDMs highlights the heme access channel as the main feature on which to focus when designing evolved UPOs. These variants are becoming emergent tools for the cost-effective synthesis of HDMs from next-generation drugs.

This chapter is based on the publication: Gomez de Santos, P., Cervantes, F.V., Tieves, F., Plou, F.J., Hollmann, F., Alcalde, M., 2019. Benchmarking of laboratory evolved unspecific peroxygenases for the synthesis of human drug metabolites. *Tetrahedron* 75, 1827–1831.

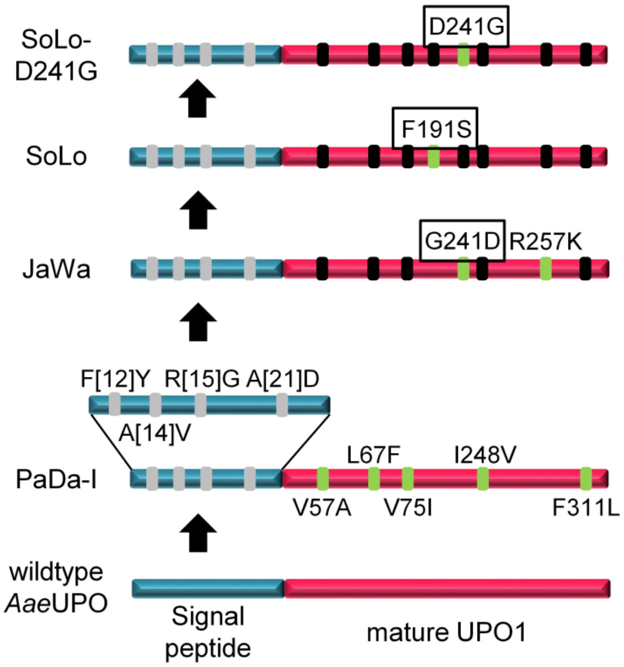

Figure 4.12. Evolved variants used in this chapter. The signal peptide is represented in blue and the mature protein in pink, along with the different mutations: green rectangles identify new mutations; black rectangles highlight the accumulated mutations; and grey rectangles indicate the mutations in the signal peptide.

4.2.1. Dextromethorphan, naproxen and tolbutamide conversion

The evolved PaDa-I, JaWa and SoLo UPO mutants were produced and purified to homogeneity (*Rz* A_{418}/A_{280} ~2.2), and their activity was tested on dextromethorphan (**1**), an antitussive drug with sedative and dissociative properties. Native *Aae*UPO converts this pharmaceutical agent into dextrorphan (**2**) by *O*-dealkylation, its authentic HDM (**Figure 4.13**) (Poraj-Kobielska et al., 2011).

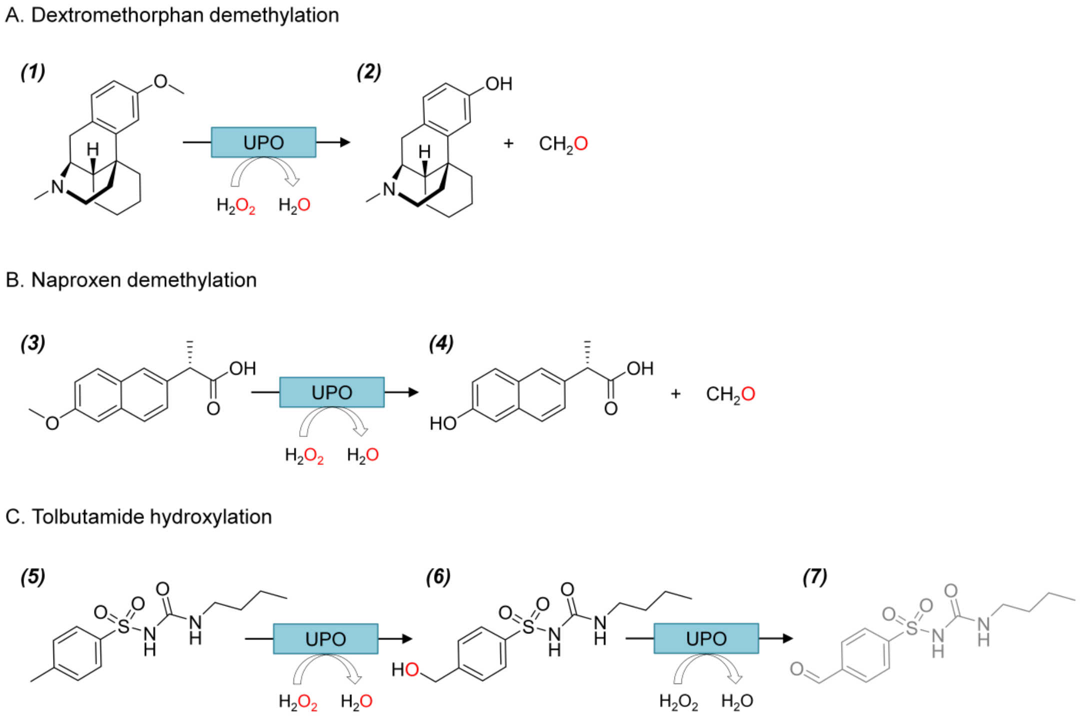
A. Dextromethorphan demethylation
(1)
(2)
UPO
H_2O_2
H_2O
H
N
O
OH
+
CH_2O
B. Naproxen demethylation
(3)
(4)
OH
O
HO
UPO
H_2O_2
H_2O
+
CH_2O
C. Tolbutamide hydroxylation
(5)
(6)
(7)
UPO
H_2O_2
H_2O
HO
O
S
N
H

Figure 4.13. Drugs transformed by UPOs and their corresponding products. (**A**) *Aae*UPO transforms dextromethorphan (**1**) to dextrorphan (**2**) or (**B**) naproxen (**3**) to *O*-desmethylnaproxen **4** by *O*-dealkylation. (**C**) Stepwise conversion of tolbutamide (**5**) into hydroxytolbutamide (**6**) is achieved by attacking the benzylic carbon, although it may be subsequently overoxidized to 4-formyl-tolbutamide (**7**).

Previous engineered P450 BM3 variants were tested towards (**1**) but the product obtained was not the authentic HDM (**2**) (Lewis et al., 2010; van Vugt-Lussenburg et al., 2006). The reactions of the selected UPO mutants were analyzed by HPLC/PDA (**Figure 4.14**) and the products determined by HPLC/MS (see Material and methods). In all cases, the substrate conversion indicated that each of the mutants outperformed the native *Aae*UPO (16%): PaDa-I, 57%; SoLo 75%; and JaWa, 82% (**Table 4.2**).

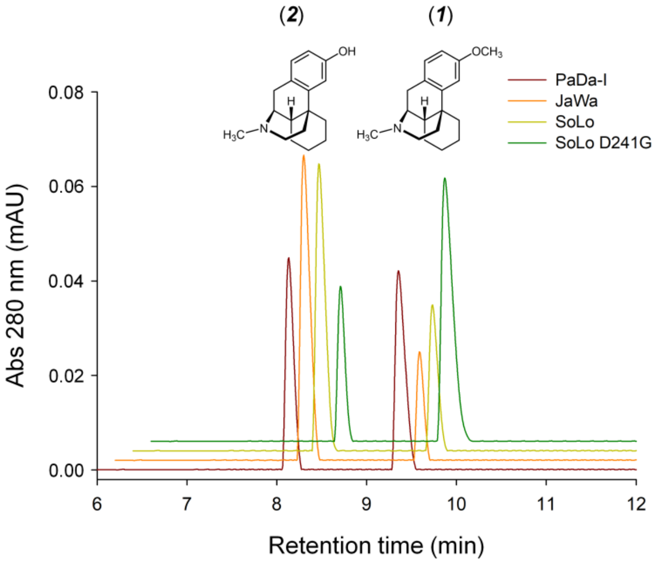

Figure 4.14. Dextromethorphan conversion by evolved UPOs. HPLC elution profiles after a 60 min reaction time: (**1**) dextromethorphan; (**2**) dextrorphan.

Given its excellent behavior under operational conditions during the synthesis of the HDM 5´-OHP (Gomez de Santos et al., 2018), the SoLo variant was then evaluated further on a semi-preparative scale. By applying a gradual supply of H_2O_2 to avoid oxidative damage, we produced up to 102.1 mg of (**2**) from (**1**), with a yield of 75.2%. We then tested the selective demethylation of naproxen (**3**), a non-steroidal anti-inflammatory drug, achieving the highest substrate conversion with the PaDa-I secretion variant (36%), followed by JaWa (25%) and SoLo (12%), yet in all the cases less than that of the native *Aae*UPO (57%) (**Table 4.2**) but higher than other reported engineered P450 BM3 variants in terms of TTN (Lewis et al., 2010).

We also assayed tolbutamide (**5**), a Na$^+$-channel blocker, the hydroxylation of which was mediated by *Aae*UPO through the attack of the benzylic carbon, giving rise to the HDM hydroxytolbutamide (**6**) (**Figure 4.13**). In this case the substrate conversion were 20%, 14%, 19% and 15% for PaDa-I, JaWa, SoLo and native *Aae*UPO, respectively. Although JaWa was associated with the lowest conversion, it did display a notable lack of overoxidation (*i.e.* a further two-electron oxidation reaction of (**6**) to 4-formyl-tolbutamide (**7**)), which may be an important property when considering the large-scale production and purification of (**6**). The total turnover numbers (TTNs, reported as μmol product/μmol enzyme) for each evolved mutant and reaction were within the same range, from 1,200 (for SoLo in the production of *O*-desmethylnaproxen) to 8,200 (for JaWa in the production of dextrorphan) (**Table 4.2**).

Table 4.2. Substrates converted to described products confirmed by mass spectrometry. Reactions performed in 1 mL final volume with 0.1 µM of each enzyme, substrate (1 mM, dissolved in 10% acetonitrile), potassium phosphate buffer (100 mM, pH 7.0), ascorbic acid (4 mM) and a single dosage of H_2O_2 (1 mM).

Substrate (*m/z*)	Product (*m/z*)	**PaDa-I (% product)**	**JaWa (% product)**	**SoLo (% product)**	***Aae*UPO* (% product)**	**SoLo-D241G (% product)**
Dextromethorphan $[M+H]^+$ 272	Dextrorphan $[M+H]^+$ 258	57	82	75	16	37
Naproxen $[M-H]^-$ 229	*O*-desmethylnaproxen $[M-H]^-$ 215	36	25	12	57	25
Tolbutamide $[M+H]^+$ 271	Hydroxytolbutamide $[M+H]^+$ 287	20	14	19	15	21
	4-formyl-tolbutamide $[M+H]^+$ 285	15	-	4	n.q.	16

* data obtained from (Poraj-Kobielska et al., 2011)
(-): not detected
n.q.: not quantified

4.2.2. Mutational analysis and SoLo-D241G

The striking differences in substrate conversion between the distinct evolved variants, generated over 8 rounds of directed evolution, led us to analyze the role of the mutations located around the catalytic cavity (**Figure 4.15**). The heme channel of *Aae*UPO is furnished with 10 aromatic residues, of which Phe76 and Phe191 define its access, while Phe69, Phe121 and Phe199 are involved in positioning the substrate for catalysis (Piontek et al., 2013). In the crystal structure of the PaDa-I variant, we noted that the F311L mutation is implicated in broadening the access channel, and it is also responsible for the dual conformational state of Phe191, conferring unheralded plasticity to the heme entrance in some of the evolved UPO variants (Ramirez-Escudero et al., 2018). Such flexibility at the heme access channel is not a feature of the native *Aae*UPO and accordingly, it is reasonable to think that these modifications might explain the improved yields with dextromethorphan (**1**) given its bulk. It is also worth noting that JaWa and SoLo produced higher yields with (**1**) than PaDa-I, differences that could be attributed to the G241D mutation situated at the entrance of the heme channel that is carried by both JaWa and SoLo but that is absent in PaDa-I (**Figure 4.15**).

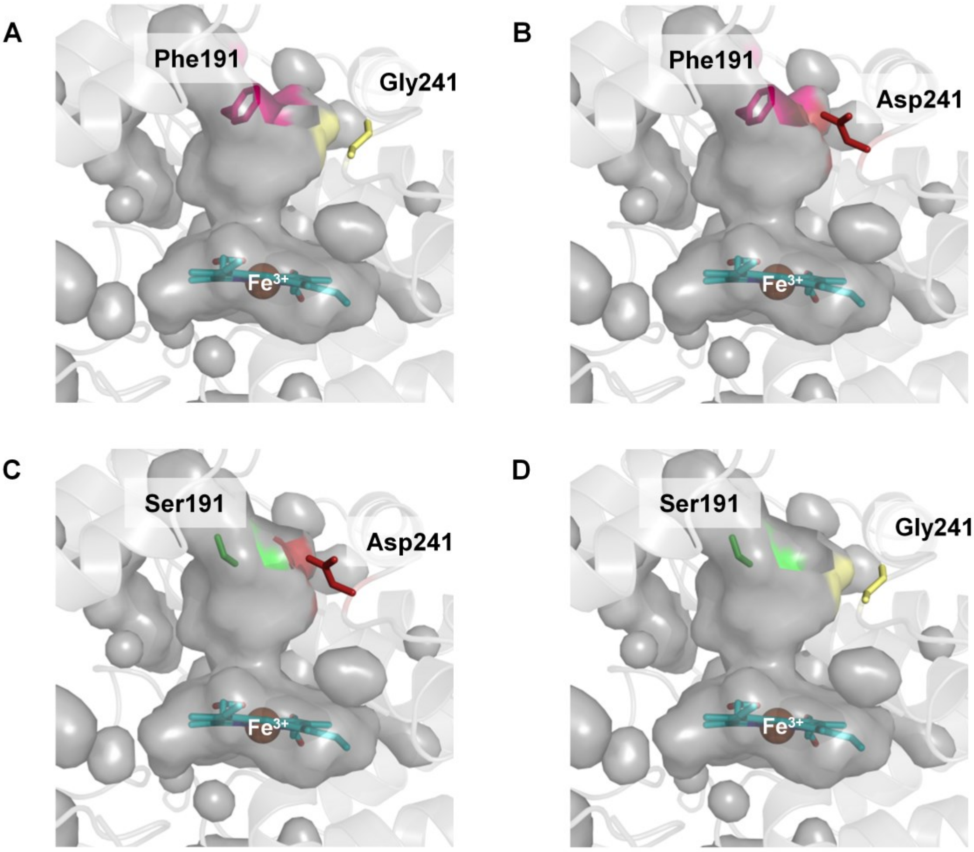

Figure 4.15. The heme access channel of the evolved UPOs. PaDa-I (**A**), JaWa (**B**), SoLo (**C**) and SoLo-D241G (**D**). The UPO structures are shown as a light grey cartoon with the heme access channel/pocket as a grey surface, and the relevant amino acids are indicated in pink (Phe191), yellow (Gly241), dark red (Asp241) and green (Ser191). The model was visualized with Pymol (http://pymol.org) based on the crystal structure of the PaDa-I mutant at a resolution of 1.5 Å, PDB entry: 5OXU (Ramirez-Escudero et al., 2018).

In our previous evolution experiments with JaWa and SoLo, computational analysis revealed that G241D favored substrate anchoring (for naphthalene and propranolol, respectively), better orientating these substrates for oxygenation. To confirm that this beneficial effect also applies to (**1**), we reverted the G241D mutation in SoLo by site-directed mutagenesis (**Figure 4.12**). The SoLo-D241G mutant produced much lower conversion from (**1**) (from 75% to 37%), albeit still above those of native *Aae*UPO (16%, **Table 1**). The SoLo-D241G mutant also showed lower product formation than PaDa-I (37% *vs.* 57%), indicating that the F191S mutation in SoLo must be responsible for this effect, which is again consistent with the small differences between the JaWa (lacking F191S mutation) and SoLo mutants (**Figure 4.15**). In terms of naproxen (**3**) conversion, the effect of reverting the G241D mutation was the opposite of that observed for (**1**), increasing roughly two-fold in the case of SoLo-D241G (**Table 4.1**). As indicated previously, positions 191 and 241 seem to be crucial for this phenomenon, with Phe191 and Gly241 of PaDa-I representing the best combination for this substrate among the evolved variants. Finally, when tolbutamide (**5**) was tested as the substrate, the three mutants rendered similar amounts of hydroxytolbutamide (**6**). Interestingly, PaDa-I showed a 15% overoxidation activity on (**6**), producing 4-formyl-tolbutamide (**7**), while SoLo and JaWa generated only traces of this product. The reverted SoLo-D241G variant also produced similar conversions to SoLo in terms of (**5**) hydroxylation (21 and 19%, respectively), although this variant enhanced overoxidation to the levels seen with PaDa-I (**Table 4.2**). This difference might indicate that the G241D mutation shortens the residence time of (**6**) in the heme cavity, thereby suppressing overoxidation.

4.2.3. Conclusions

Evolved UPO variants with different substrate scopes are suitable biocatalysts to synthesize known and novel HDMs. The heme access channel of these evolved variants is malleable and it can be adapted through additional evolutionary campaigns to achieve cost-effective production of HDMs. Accordingly, future structure-guided evolution experiments focusing on this region may expand the substrate range of UPOs towards next-generation drugs with different chemical structures.

4.3. Chapter 3: Evolved peroxygenase-aryl alcohol oxidase fusions for self-sufficient oxyfunctionalization reactions.

Fungal peroxygenases are deemed emergent biocatalysts for selective C-H bond oxyfunctionalization reactions. In this study we have engineered a functional and stable self-sufficient chimeric peroxygenase fusion. The bifunctional biocatalyst carried a laboratory evolved version of the fungal peroxygenase fused to an evolved fungal aryl-alcohol oxidase that supplies H_2O_2 *in situ*. Enzyme fusion libraries with peptide linkers of different size and amino acid composition were designed while attached leader sequences favored secretion in yeast. The most promising functional enzyme fusions were characterized biochemically and further tested for the synthesis of dextrorphan, a metabolite of the antitussive drug dextromethorphan. This reaction system was optimized to control the aromatic alcohol transformation rate and therefore the H_2O_2 supply to achieve total turnover numbers of 62,000, the highest value reported for the biocatalytic synthesis of dextrorphan to date.

This chapter is based on the publication: Gomez de Santos, P., Lázaro, S., Viña-González, J., Hoang, M.D., Sánchez-Moreno, I., Glieder, A., Hollmann, F., Alcalde, M., 2020. Evolved peroxygenase-aryl alcohol oxidase fusions for self-sufficient oxyfunctionalization reactions. *ACS Catal.* In press.

4.3.1. Point of departure to construct the chimeric fusion enzymes: the laboratory evolved AAO and UPO variants

We previously generated several secretion mutants by laboratory evolution of the AAO from *Pleurotus eryingii* and the UPO from *Agrocybe aegerita*. These evolved enzymes are highly active, stable and functionally expressed at reasonable titers in yeast, which make them suitable templates for the design of UPO_AAO fusions. The FX9 mutant was used as the AAO partner, which was the product of 5 rounds of directed, structure-guided evolution to enhance its functional expression: 4 mg L^{-1} in *Saccharomyces cerevisiae* and ~25 mg L^{-1} in *Pichia pastoris* in fed-batch bioreactor (Viña-Gonzalez et al., 2018, 2015). FX9 carries the mutations F[3]S-N[25]D-T[50]A-F[52]L-H91N-L170M, of which the mutations in the chimeric leader sequence preαproK that promoted secretion are underlined (Viña-Gonzalez et al., 2015). Concerning UPO, we chose the SoLo variant which shows a reduced peroxidase activity *vs.* several aromatic alcohols as a result of three consecutive directed evolution campaigns: i) for secretion by yeast, achieving titers of 8 mg L^{-1} by *S. cerevisiae* and over 200 mg L^{-1} by *P. pastoris* in a bioreactor (Molina-Espeja et al., 2015, 2014);

ii) for production of the agrochemical 1-naphthol (Molina-Espeja et al., 2016a); and iii) for HDM synthesis (Gomez de Santos et al., 2019, 2018; Molina-Espeja et al., 2016b). Accordingly, SoLo carries the F[12]Y-A[14]V-R[15]G-A[21]D-V[57]A-L67F-V75I-F191S-G241D-I248V-R257K-F311L mutations, the underlined residues lying in the evolved signal peptide (evSp).

4.3.2. Construction of the enzyme fusion libraries

There are three key issues to consider when constructing enzyme fusions: the component partner enzymes, the connections between them, and their order in the fusion protein. The enzymatic partners were chosen in terms of their cooperative activity, in this case UPO playing the leading role as the oxyfunctionalization partner and AAO as supporting role in the generation of H_2O_2. Rather than directly connecting UPO to AAO, *i.e.* placing the genes together without a stop codon, we inserted a peptide linker to connect one to the other in order to avoid misfolding and/or a loss of expression (Amet et al., 2008; Zhao et al., 2008). Given that not only the specific amino acids in this linker but also its length may be crucial, we focused on both flexible and rigid linkers of different sizes and composition. Flexible linkers allow some degree of movement between the enzyme partners and they are mainly composed of repetitive stretches of small or hydrophilic amino acids like Gly. By contrast, rigid linkers are stiff structures (*e.g.* α-helical structures or multiple Pro residues) that may separate functional domains more efficiently, albeit with a loss of flexibility (Chen et al., 2013).

As the fusion must be exported by yeast cells, the choice of a leader sequence that drives adequate secretion is also important. Accordingly, we designed 4 constructs (A, B, C and D) to compare the secretion driven by both the evolved leader sequences, preαproK from AAO and evSp from UPO, as well as the effect of the different linkers on the expression of each fusion in distinct orientations, **Table 4.3**. The different constructs were cloned *in vivo* into *S. cerevisiae* and screened for UPO activity using the ABTS/H_2O_2 assay, for AAO activity with the 4-methoxybenzyl alcohol/ABTS-HRP coupled assay, and for both AAO and UPO activities with the 4-methoxybenzyl alcohol/ABTS assay, **Figure 3.4** in Material and methods.

Table 4.3. Fusion library I. The order of the enzymes, and the leader sequences and linkers used are indicated.

Construct	Leader sequence	N-terminal partner	Linker	C-terminal partner	UPO activity *	AAO activity *	UPO_AAO activity*
A	evSp	UPO	LA(EAAAK)$_4$AAA	AAO	++	-	-
B	evSp	UPO	LA(EAAAK)$_5$AAA	AAO	++	-	-
B'	evSp	UPO	LA(EAAAK)$_5$AAA(GGGGR)$_1$	AAO	+++	+++	+++
C	preαproK	AAO	(GGGGR)$_1$LA(EAAAK)$_4$AAA	UPO	-	+	-
D	preαproK	AAO	(GGGGR)$_1$LA(EAAAK)$_5$AAA	UPO	-	+	-

*Activity was measured in supernatants of independent cultures grown in 96-well plates using the ABTS/H_2O_2 assay for UPO, the 4-methoxybenzyl alcohol/ABTS-HRP coupled assay for AAO, or the 4-methoxybenzyl alcohol/ABTS assay for the UPO_AAO fusion, see also **Figure 4.13**. Each construct contained a leader sequence followed by the two enzyme partners connected by a linker, and they were measured in independent 96-well cultures.

The A and B constructs carried the evSp leader followed by the UPO gene, which was joined to the AAO gene by a rigid linker of 25 (A construct) or 30 (B construct) amino acids. By contrast, in constructs C and D the preαproK leader preceded the AAO gene, which was connected to the UPO gene by a linker that combined flexible and rigid regions of 30 (C construct) and 35 (D) amino acids. Constructs A and B displayed UPO activity but no AAO activity, whereas some AAO activity was detected for the C and D constructs, suggesting that a linker with a flexible region connected to the N-terminal domain of AAO may be important to maintain AAO functional.

Indeed, this might protect the H-bonding between the FAD cofactor and the N-terminal of the AAO, which is crucial for the correct AAO folding (Fernandez et al., 2009). Accordingly, we designed a new construct B', which was similar to B but that included a flexible linker ending (GGGGR). For this construct, we analyzed different linker lengths: As the distance between the partners is important, the number of repetitions in the linker regions was explored by harnessing the high frequency of homologous DNA recombination in *S. cerevisiae*. In this way, the linker sequence was designed so that the yeast´s DNA recombination machinery was prone to generate a library of fusions *in vivo* that contains linkers with different numbers of amino acid repetitions, see Material and methods, **Figure 3.2**.

This strategy was successful and after screening the library, we identified a construct B' UPO_AAO fusion with both activities that were coupled by a linker of 110 residues (LA(EAAAK)$_{20}$AAA(GGGGR)$_{1}$). When this fusion was purified, three active fractions were isolated that corresponded to the UPO, AAO and the UPO_AAO fusion activity. The existence of these fractions indicated that the linker was attacked by proteases, possibly in the Golgi compartment where *STE13*, a membrane-bound dipeptidyl aminopeptidase, can cleave the EA motifs (Romanos et al., 1992). This problem was solved by constructing a second library of UPO_AAO fusions in which the linker did not have cleavage sites for Golgi proteases, while still promoting possible recombination mismatches in the linkers to adjust their length (constructs E and F) and conserving a flexible region to connect to the N-terminal AAO, **Table 4.4**.

Table 4.4. Linkers tested in library II of the UPO_AAO fusions.

Constructs*	Linker	Source
E	(G)$_{8}$	(Chen et al., 2013)
F	(GGGGS)$_{3}$	(Deng et al., 2016)
G	(AP)$_{5}$(GGGGS)$_{1}$	(Chen et al., 2013)
H	(AP)$_{15}$(GGGGS)$_{2}$	(Chen et al., 2013)
I	GTPTPTPTPTGEF	(Gustavsson et al., 2001)
J	GTPTPTPTPTGEF(GGGGS)$_{1}$	(Gustavsson et al., 2001)
K	FFALLNDPRG	Linker database (George and Heringa, 2002)
L	AVTYKKEEDL	Linker database (George and Heringa, 2002)

*All fusions were preceded by the evSp leader, with UPO and AAO hierarchically connected by linkers of different characteristics: the E and F linkers were selected to test different degrees of flexibility; the G and H linkers included the AP rigid motif to confer a semi-rigid linkage between the partners; linker I proved to be tolerant to proteases; J is a modified version of I including a flexible region; and K and L are natural linkers from the vanadium peroxygenase from *Curvularia inaequalis*.

After screening fusion library II, we identified 10 functional fusion constructs with both UPO and AAO activities, **Figure 4.16**. The *in vivo* DNA recombination and assembly of the fusion in *S. cerevisia*e led to the isolation of four different F fusions whose activity was directly proportional to the increasing length of the linker: F4 $(GGGGS)_4$; F9 $(GGGGS)_9$; F12 $(GGGGS)_{12}$; and F17 $(GGGGS)_{17}$.

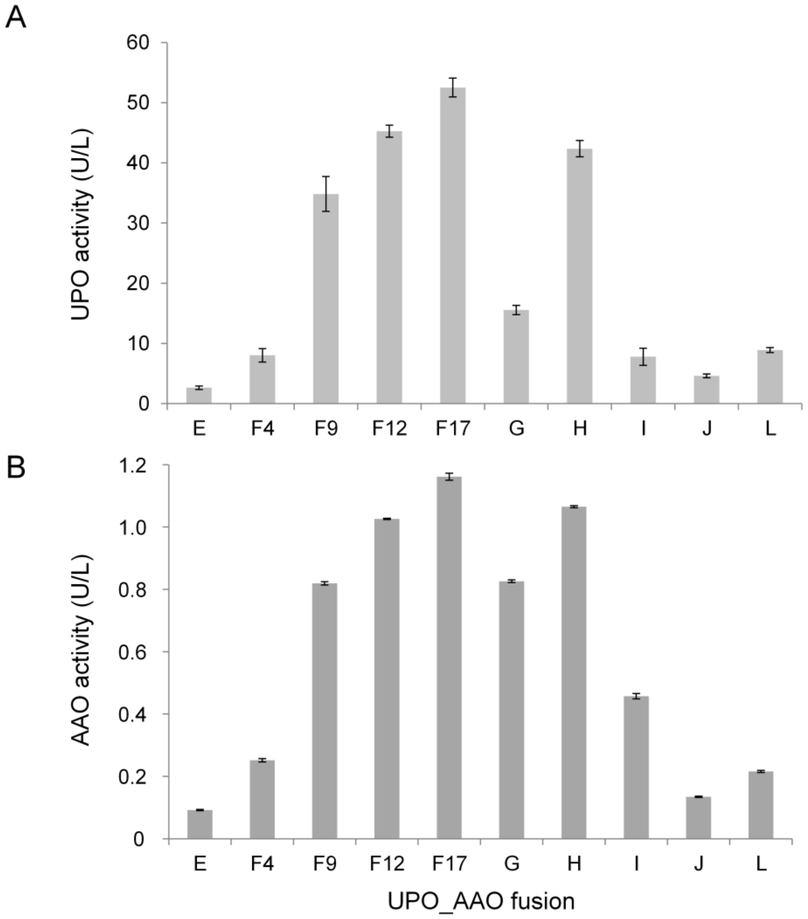

Figure 4.16. Activity of the UPO_AAO fusions. (**A**) UPO Activity, (**B**) AAO activity. Activity was measured in quintuplet from supernatants of independent cultures using the ABTS/H_2O_2 assay for UPO and the 4-methoxybenzyl alcohol/ABTS-HRP coupled assay for AAO. No activity of the K construct was detected.

4.3.3. Production and biochemical characterization

The five best constructs (F9, F12, F17, G and H) were produced, purified and characterized biochemically. Kinetic thermostability was determined by measuring the T_{50} (the temperature at which the enzyme retains 50% of its initial activity after a 10 min incubation). Thermostability was mostly conserved in all the fusions, with T_{50} values ranging from 57.3 to 58.8 ºC vs. 59.5 and 63 ºC for free UPO and AAO, respectively (see Material and methods for details). All fusions were hyperglycosylated by yeast, with sugar moieties constituting roughly 50% of the molecular mass of the enzymes, **Figure 4.17.A**. This was not surprising given that the molecular mass of individual UPO and AAO secreted by yeast are 52,000 and 150,000 Da, of which hyperglycosylation represents 30%

and 60%, respectively (Gomez de Santos et al., 2018; Viña-Gonzalez et al., 2018). The addition of outer chain mannose moieties to complex and large proteins in the Golgi apparatus occurs frequently in the *S. cerevisiae* secretory pathway, as is the case of the chimeric fusions. Disregarding glycosylation and the linkers, the expected size of the UPO_AAO fusions was 97,000 Da, consistent with that of the deglycosylated fusion enzymes. Indeed, the wide smear at ~200,000 Da produced by the different glycoforms in SDS-PAGE, collapsed into tighter bands of ~115,000 to ~125,000 Da after treatment with PNGaseF, **Figure 4.17.B**.

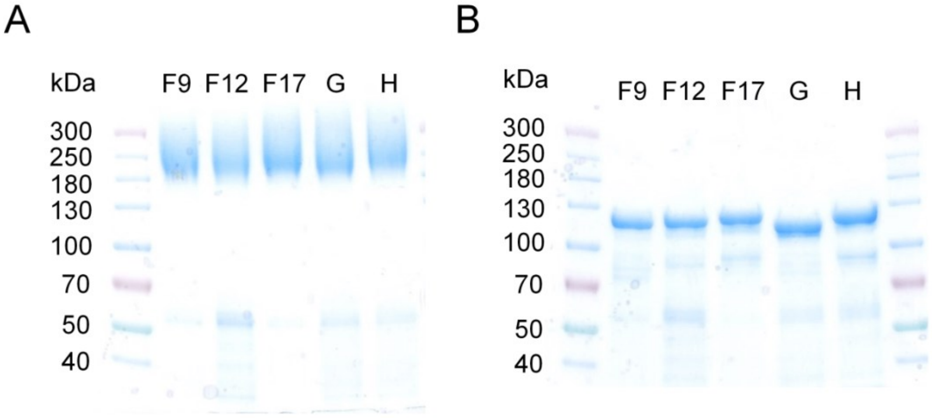

Figure 4.17. Molecular mass of the UPO_AAO fusions. (**A**) purified fusions, (**B**) fusions after treatment with PNGaseF resolved on 4-20% precast polyacrylamide gels.

The expression of the UPO_AAO fusion proteins was weaker than that of the individual secreted enzymes, on average 10 to 15-fold lower depending on the construct. However, expression could be recovered by transferring the system from *S. cerevisiae* to the *Pichia pastoris* BSYBG11 strain and using the carbon source repressed promoter P_{DF} (Fischer et al., 2019). P_{DF} permits methanol independent protein expression, which may favor an alternative *P. pastoris* recombinant protein production due to the toxicity and flammability of methanol. To benchmark the *S. cerevisiae* and *P. pastoris* production systems, the H enzyme fusion was cloned in the methanol-free *P. pastoris* strain, produced and purified.

In contrast to the *S. cerevisiae* variant, the *P. pastoris* variant yielded a ~140,000 Da band that was reduced to a ~125,000 Da species by PNGaseF, highlighting its milder glycosylation (roughly 10%) as would be expected in *P. pastoris*, **Figure 4.18**. In flask, the production yield of this protein increased from 0.22 mg L^{-1} in *S. cerevisiae* to 7 mg L^{-1} in *P. pastoris*, a 32-fold improvement. This value will certainly increase when the strain is fermented in a fed-batch bioreactor due to the higher cell densities obtained in this format: ~100 g dry biomass L^{-1} in bioreactor; ~10 g dry biomass L^{-1} in flask production (Molina-Espeja et al., 2015; Viña-Gonzalez et al., 2018).

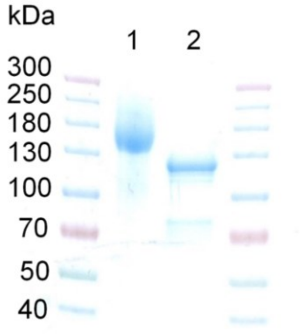

Figure 4.18. SDS PAGE. 4-20% precast polyacrylamide gel (**Lane 1**) πH, H variant produced in *P. pastoris*. (**Lane 2**) Deglycosylated πH with PNGaseF. H variant in *P. pastoris* is glycosylated around a 10%.

We measured the steady kinetic parameters of purified UPO_AAO fusions and the individual secreted enzymes. Compared with AAO alone, the kinetics of the AAO partner were mostly conserved in all the fusions, while the catalytic efficiency of the UPO partner was reduced, with a 1.3- to 4-fold decrease in their activity relative to the individual secreted UPO, an effect that could be related to the strong hyperglycosylation shown in all the fusions (**Figure 4.17**). Moreover, kinetic constants slightly varied among the different fusions, as consequence of the distinct composition and length of the linkers which may affect the orientation between enzyme partners. **Table 4.5**.

Table 4.5. Kinetic parameters of UPO_AAO fusions and the individual enzymes.

Substrate	Kinetic constants	F9	F12	F17	G	H	AAO	UPO
4-methoxybenzyl alcohol (**2e**)	K_m (μM)	28 ± 0.4	38 ± 6	20 ± 3	21 ± 5	21 ± 3	23 ± 2	n.d.
	k_{cat} (s^{-1})	30 ± 1	28 ± 1	44 ± 1	30 ± 2	34 ± 1	41 ± 1	n.d.
	k_{cat}/K_m (mM^{-1} s^{-1})	1,061	747	2,183	1,383	1,568	1,782	n.d.
ABTS	K_m (μM)	733 ± 85	1,375 ± 239	1,204 ± 123	778 ± 119	667 ± 82	---	568 ± 91
	k_{cat} (s^{-1})	133 ± 6.5	209 ± 20	376 ± 20	250 ± 17	213 ± 11	---	365 ± 23
	k_{cat}/K_m (mM^{-1} s^{-1})	182	152	313	321	319	---	642

The 4-methoxybenzyl (2e) kinetic constants for free AAO and AAO fusion partner were performed in 100 mM phosphate buffer pH 6.0 at 25°C. ABTS kinetic constants for free UPO and UPO fusion partner were performed in 100 mM citrate phosphate buffer pH 4.0 at 25°C in the presence of 2 mM H_2O_2 (see Material and methods for details). All reactions were performed in triplicate. n.d. not determined.

4.3.4. Production of dextrorphan, a human drug metabolite from dextromethorphan

The fusions were tested in a practical case, the synthesis of dextrorphan, a true HDM of the antitussive drug dextromethorphan. In this cascade reaction, primary aromatic alcohols were used as the substrates of the AAO partner in the fusion as depicted in **Scheme 4.3**.

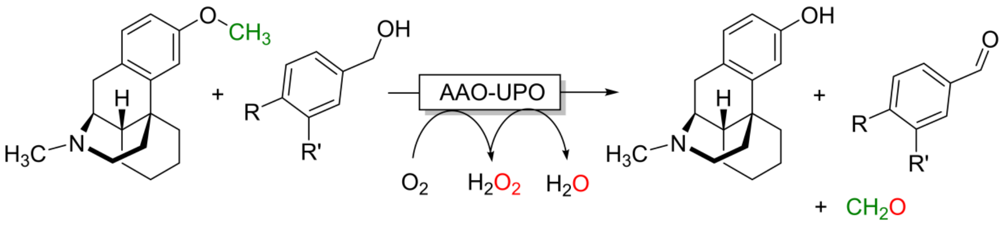

(1) (2a-f) (3) (4a-f)

	2a/4a	2b/4b	2c/4c	2d/4d	2e/4e	2f/4f
R	F	H	Cl	H	OCH_3	OCH_3
R'	H	Cl	H	OCH_3	H	OH

Scheme 4.3. Cascade reaction for the synthesis of dextrorphan. Dextromethorphan (**1**) is transformed by the AAO_UPO fusion into dextrorphan (**3**) through a cascade reaction. An aromatic alcohol (**2a-f**) is oxidized by the AAO partner into the corresponding aldehyde (**4a-f**), generating one equivalent of H_2O_2. The latter is used by the UPO partner to transform (**1**) into (**3**) through *O*-dealkylation, releasing formaldehyde as a byproduct.

Several aromatic alcohols that are substrates of AAO may be also susceptible of transformation by UPO, which could lead to the imbalance of the cascade reaction. Accordingly, to rule out unwanted interactions between the aromatic alcohol and the UPO partner, while balancing the stoichiometric supply of H_2O_2, the following alcohols were tested: 4-fluorobenzyl alcohol (**2a**), 3-chlorobenzyl alcohol (**2b**), 4-chlorobenzyl alcohol (**2c**), 3-methoxybenzyl alcohol (**2d**), 4-methoxybenzyl alcohol (**2e**) and 3-hydroxy-4-methoxybenzyl alcohol (**2f**). The highest conversion was obtained when using the **2a**, **2d** and **2e**, giving rise to total turnover numbers (TTN, reported as µmol dextrorphan/µmol enzyme fusion) of ~40,000 without further optimization, **Figure 4.19.A**.

In previous studies, the catalytic efficiencies of recombinant AAO with these aromatic alcohols were reported as 59 and 65 s^{-1} mM^{-1} (for **2a** and **2d** respectively), 152, 203 and 398 s^{-1} mM^{-1} (for **2f**, **2b** and **2c**) and 5,233 s^{-1} mM^{-1} for **2e** (Ferreira et al., 2005).

This data addresses that the activity of the fusion is not related to the alcohol preferences by the AAO partner, *i.e.* regardless of using the best (**2e**) or the worst (**2a**) alcohol for AAO, similar TTNs with the fusion were achieved, **Figure 4.19.A** (kinetic values with recombinant AAO expressed in *S. cerevisiae* rendered similar values, see **Table 4.6**) . The fact that the AAO shows catalytic efficiencies with differences of two orders of magnitude for the two best alcohols used in the cascade, points the activity of UPO towards these aromatic alcohols as the key driver of the whole cascade reaction (*i.e.* the lower the UPO activity against the aromatic alcohol, the higher the TTN with dextromethorphan). To confirm this hypothesis, we measured kinetic values of the best (**2a**) and the worst (**2c**) alcohols of the cascade, as well as of dextromethorphan (see **Table 4.6**). Indeed, the higher affinity of **2c** for UPO catalytic site when compared to dextromethorphan (with K_m values of 1,670 ± 170 μM and 3,554 ± 725 μM, respectively, **Table 4.6**) addresses **2c** as a strong competitor of dextromethorphan, which limits the performance of the fusion in the production of dextrorphan, **Figure 4.20.A**. By contrast, with **2a** was not even possible to determine the kinetics due to the higher K_m, far beyond the water solubility of the substrate, and becoming therefore an ideal substrate to boost the cascade, **Figure 4.19**.

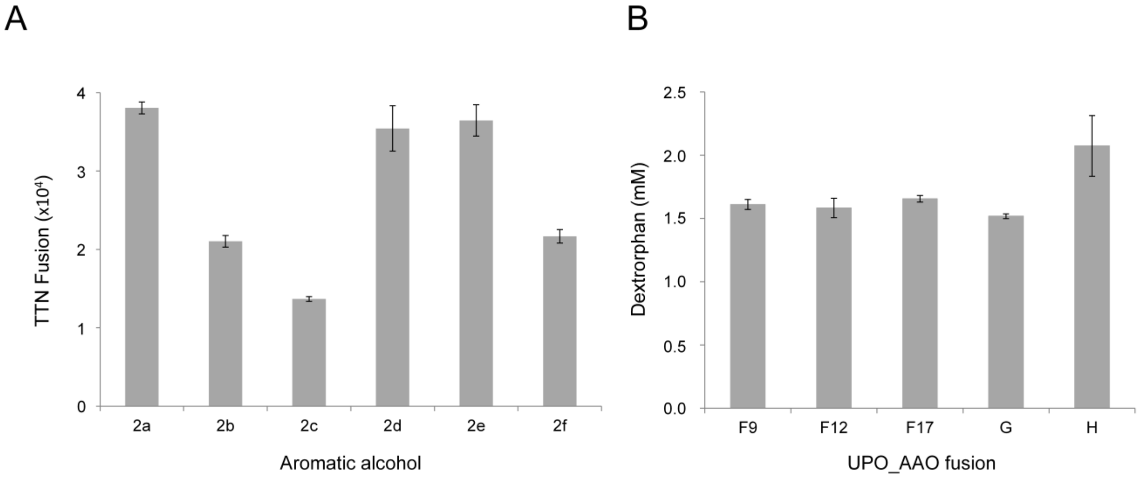

Figure 4.19. Aromatic alcohol selection and fusion enzyme performance in the production of dextrorphan. (**A**) Total turnover numbers (TTN) for the transformation of dextromethorphan into dextrorphan. Reactions were performed in 1.5 mL GC vials, in a final volume of 0.3 mL containing: 10 mM of each aromatic alcohol, 0.04 μM of the H fusion (peroxygenase partner concentration measured with CO difference spectrum), and 10 mM dextromethorphan hydrobromide in 100 mM potassium phosphate buffer [pH 7.0]. (**B**) Comparison of the different UPO_AAO fusions with 2a and dextromethorphan. The reactions were performed in 1.5 mL GC vials, in a final volume of 0.3 mL containing: 10 mM **2a**, 0.05 μM of each UPO_AAO fusion (peroxygenase partner concentration measured with CO difference spectrum), and 10 mM dextromethorphan hydrobromide in 100 mM potassium phosphate buffer [pH 7.0]. All reactions were incubated for 24 h at 30 °C and at 600 rpm. The reactions were performed in duplicate at least and analyzed by GC-FID, as described in the Material and methods.

Table 4.6. Kinetic parameters of H and the individual enzymes with a comparison between the best (**2a**) and the worst (**2c**) alcohol for the cascade.

Substrate	Kinetic constants	H	AAO	UPO
4-fluorobenzyl alcohol (**2a**)	K_m (μM)	630 ± 54	584 ± 19	n.m
	k_{cat} (s^{-1})	25.7 ± 1.1	26.7 ± 0.4	n.m
	k_{cat}/K_m (mM^{-1} s^{-1})	41	46	n.m
4-chlorobenzyl alcohol (**2c**)	K_m (μM)	103 ± 4	104 ± 6	1,670 ± 170
	k_{cat} (s^{-1})	28.1 ± 0.3	33.8 ± 0.5	339.2 ± 16.6
	k_{cat}/K_m (mM^{-1} s^{-1})	272	325	203
Dextromethorphan	K_m (μM)	7,387 ± 2,807	---	3,554 ± 725
	k_{cat} (s^{-1})	2,298 ± 432	---	1,395 ± 121
	k_{cat}/K_m (mM^{-1} s^{-1})	311	---	402

4-fluorobenzyl and 4-chlorobenzyl alcohol kinetic constants for free AAO and AAO fusion partner were estimated in 100 mM phosphate buffer [pH 6.0] at 25 °C. 4-fluorobenzyl and 4-chlorobenzyl alcohol kinetic constants for free UPO were estimated in 100 mM citrate phosphate buffer [pH 6.0] at 25 °C in the presence of 2 mM H_2O_2. Dextromethorphan kinetic constants for free UPO and UPO fusion partner were estimated in 100 mM citrate phosphate buffer [pH 6.0] at 25 °C in the presence of 2 mM H_2O_2 and measured with the Purpald® colorimetric assay (see Material and methods for details). All reactions were performed in triplicate. n.m: not measurable due to the high K_m value and the poor solubility of the substrate at concentrations over 20 mM. See **Figure 4.20**.

Figure 4.20. Kinetic plots of UPO with 4-fluorobenzyl alcohol and 4-chlorobenzyl alcohol. Each point including the standard deviation comes from three independent measurements.

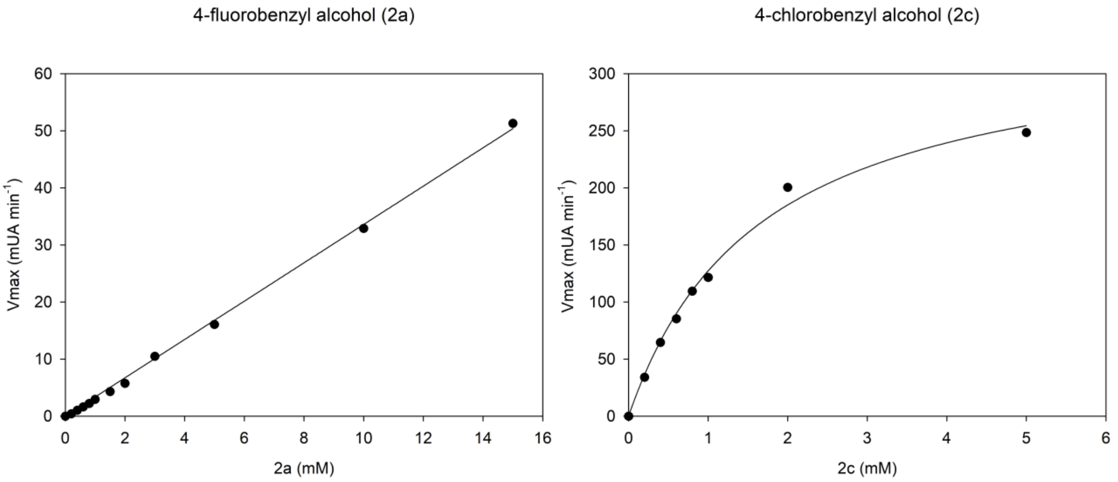

The UPO_AAO fusions were accordingly benchmarked with **2a** as the departure alcohol, with the H fusion producing ~2 mM of dextrorphan with a TTN of 48,300 after optimizing the reaction conditions (see Material and methods for details), **Figure 4.19.B**.

To the best of our knowledge, this value is the highest TTN ever reported for the enzymatic synthesis of dextrorphan, followed far behind by the recently described sulfite oxidase-peroxygenase cascade system (van Schie et al., 2020) with a TTN of 10,540 (*i.e.* 4-fold less than the current chimeric fusion system). This difference is even more dramatic when comparing to the performance of the UPO mutant without the H_2O_2 cascade which only achieved 7,500 TTN (Gomez de Santos et al., 2019). The performance of the H fusion was compared to that of free UPO and AAO enzyme cocktail. After 15 min reaction and applying equal equimolar enzyme concentrations in both the fusion and the free enzyme cocktail, the H fusion doubled the production of dextrorphan. After 45 min reaction, a plateau was reached with TTN of 32,100 and 21,200 for the H fusion and the enzyme cocktail, respectively, **Figure 4.21**. The differences observed between both systems seem to address a substrate channeling effect, minimizing the diffusion of H_2O_2 between the fusion partners, and therefore becoming the main responsible for the improved performance of the fusion. Crystallization of the fusion along with computational ligand diffusion experiments could shed light into this matter.

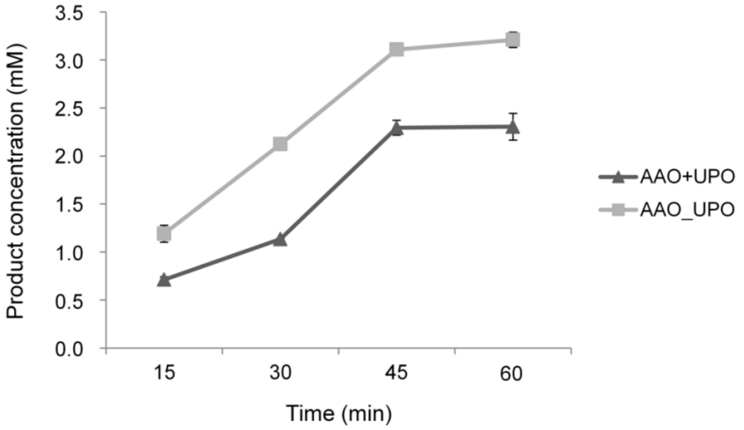

Figure 4.21. Comparison between fused and non-fused enzymes. AAO+UPO: reactions with equimolar concentration of AAO and UPO. AAO_UPO: H enzyme fusion.

To further characterize the enzymatic cascade of the H fusion, a time course reaction was performed, **Figure 4.22**. The yield of dextrorphan produced by the UPO partner remained linear during the first hour, slowing down to reach a maximum after 8h (**Figure 4.22.A**). Oxidation of **2a** to **4a** proceeded significantly faster than the coupled hydroxylation of **1** to **3**, **Figure 4.22**. Hence, *in situ* accumulation of H_2O_2 occurred, which most likely inactivated the UPO subunit of the fusion enzyme thereby limiting its turnover number in dextrorphan synthesis to approx. 25,000. Since the K_m value for the benzyl alcohol substrate is in the millimolar range, we hypothesized that limiting the *in situ* concentration of **2a** (by using a syringe pump) may lead to a more balanced oxidase/peroxygenase activity. Indeed, using the fed-batch strategy (**Figure 3.5** in Material and methods) with **2a** dosing rates of 0.5, 1 and 2 mM h^{-1} resulted in TTN for the dextrorphan synthesis of 62,145, 59,104 and 54,535, respectively. The benefits of controlling the alcohol dosing agrees well with previous studies on P450 OleTJE fused to an alditol oxidase (Matthews et al., 2017).

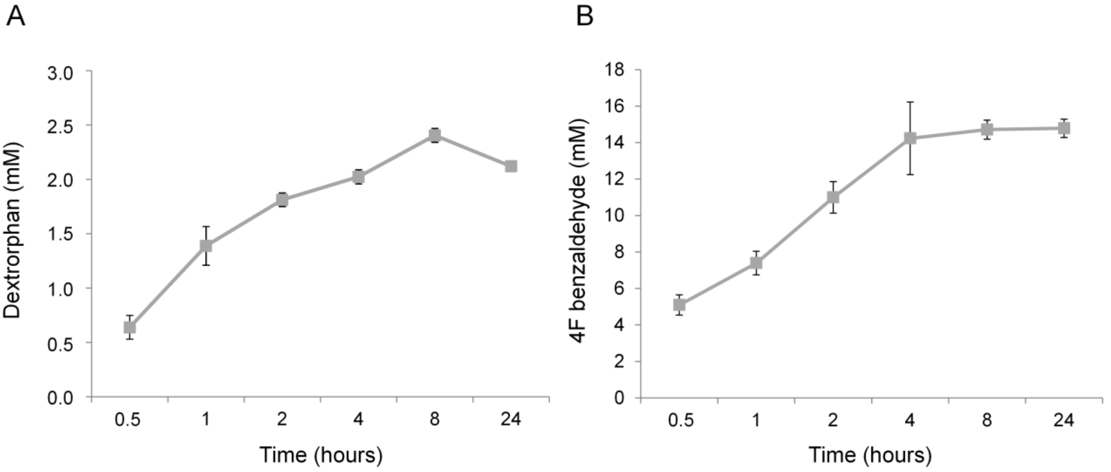

Figure 4.22. Time course of the fusion H reaction. (**A**) Dextrorphan production (UPO activity). (**B**) **2a** oxidation (AAO activity). The reactions were performed in 1.5 mL GC vials, in a final volume of 0.3 mL containing: 15 mM of **2a**, 0.1 μM of H (peroxygenase concentration measured with CO difference spectrum), and 10 mM of dextromethorphan hydrobromide (**1**) in 100 mM potassium phosphate buffer [pH 7]. Reactions were incubated at 30 °C and at 600 rpm in a ThermoMixer® C, and extracted with ethyl acetate at different time points to stop the reactions (0.5, 1, 2, 4, 8 and 24 hours). All reactions were performed at least in duplicate.

4.3.5. Conclusions

Advances in directed evolution in yeast and progress in the engineering of chimeric fusion proteins has allowed us to design the first UPO_AAO fusion that could be employed in the synthesis of a range of pharmaceutical and chemical products. Indeed, the enzymatic production of HDMs is gaining momentum, with peroxygenases and P450 monooxygenases sharing the headlines in this important field of research (Beyer et al., 2018; Fessner et al., 2020; Kiebist et al., 2019, 2017, 2015; Poraj-Kobielska et al., 2011). Given the unique partnership between AAO and UPO, the fusion construct designed here could be further applied and evolved in the laboratory for more complex cascade reactions that harness the activity of both these enzymes, such as the 6-electron oxidation of 5-hydroxymethyl furfural (HMF) to furan-2,5-dicarboxylic acid (FDCA), an attractive building block for renewable plastics (currently under study) (Carro et al., 2015; Viña-Gonzalez et al., 2020). From a more general perspective, the directed evolution of the linker itself or of the whole system could enhance the activities of both partners, fine tuning the generation of H_2O_2 in the context of a given biotransformation.

GLOBAL DISCUSSION

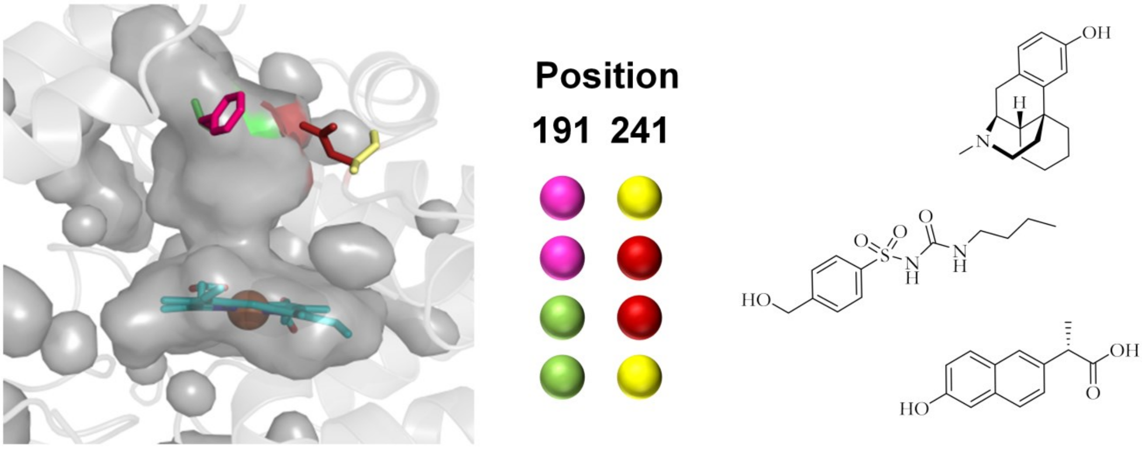
Position
191 241
OH
H
N
O
S
N
H
HO
OH
O

5. Global discussion

In this section, we will briefly discuss about the main results described in previous sections along with the new trends and studies that are arising from the work carried out in this Doctoral Thesis.

5.1. Directed evolution of unspecific peroxygenase for HDMs

The synthesis of HDMs by UPOs is a topic of great interest for the pharma industry. Indeed, by mimicking the role of human liver P450s, UPOs can furnish a broad *palette* of reactions for pharmaceutical studies. That is why the application of UPOs in the synthesis of HDMs is emerging as the most promising alternative to the already well known methods based on chemical, enzymatic -P450s- or whole cell transformations. Under mild and simple operational conditions, UPOs show high turnover numbers and selectivity while acting as soluble and extracellular enzymes. Despite all these advantages, there is still room for improvement because UPO's conversions are poorly accomplished with certain drugs (*e.g.* hardly 25% for propranolol, tolbutamide, dextromethorphan, carbamazepine) (Poraj-Kobielska et al., 2011). Accordingly, in this Doctoral Thesis we have optimized by directed evolution the activity and selectivity of UPO for the synthesis of HDMs of significance for the pharma market.

5.1.1. Propranolol

Unlike P450s, the major HDM product of propranolol biotransformation by wild type *Aae*UPO was shown to be 5´-OHP (91% regioselectivity), along with only minor amounts of DIP, and conversion rates of 23%. We started adapting the previously described screening method for detection of hydroxylated aromatics (Otey and Joern, 2003) with a new purpose: the identification of improved variants towards propranolol, together with avoiding the further one electron oxidation of the hydroxylated product, with the final aim of producing and isolating 5´-OHP at high yields. With this strategy, we pursued not only achieving high activity levels but to simplify the purification of 5´-OHP, as for the pharmaceutical industry activity is pointless if further retrieving of the product is not possible. The use of a double screening assay both in the presence and in the absence of ascorbic acid (AA) -acting as radical scavenger- in the frame of the focused evolution campaign, led us to the SoLo mutant, an enzyme with the highest selectivity hitherto shown for this process (99%), and more importantly, with a catalytic efficiency enhanced by two orders of magnitude and a decreased peroxidase activity over 5´-OHP. This cutback in peroxidase activity was due to the shortening of the residence time of the product inside the heme channel, diminishing the one electron oxidation of 5´-OHP through the peroxidase route, as proved by QM/MM and PELE computational analysis (in collaboration with Prof. Víctor Guallar, from the Barcelona Supercomputing Center).

The unique properties of the evolved *Aae*UPO allowed us to perform reaction engineering studies aimed at improving further the long term -operational- activity for the preparative production of 5´-OHP. Accordingly, the SoLo/propranolol reaction system was subjected to three different approaches: the use of *tert*-butyl hydroperoxide (*tert*-BuOOH) as a milder peroxide source, as well as the coupling of SoLo mutant with either a mono- or a bi-enzymatic cascade for *in situ* H_2O_2 generation (Gomez de Santos et al., 2018; Tieves et al., 2019). The use of *tert*-BuOOH helped to perform a semi-preparative scale production, obtaining the cleanest ^{1}H-NMR spectrum reported so far for this compound. Regarding the study of enzyme cascade reactions, during my stay at the Prof. Frank Hollmann from the Technical University of Delft (TUDelft), we combined alcohol oxidase (AOx) and formaldehyde dismutase (FDM) for the double oxidation of methanol to formic acid, releasing H_2O_2. This H_2O_2 *in situ* supply system, fed the SoLo mutant in the transformation of propranolol to 5´-OHP yielding 264,000 and 226,000 TTNs in the presence and in the absence of AA, respectively (Gomez de Santos et al., 2018). Very recently, we have explored the formate oxidase from *Aspergillus oryzae* (*Ao*FOx) as a new H_2O_2 *in situ* supply system rendering TTNs as high as 420,000 TTN for FOx and 83,000 for SoLo (results not included in this Thesis book, Tieves et al., 2019) (**Figure 5.1.A**). As such, and depending on the peroxide generation system, differences of one order of magnitude could be noticed, which addresses the combination of directed UPO evolution with reaction engineering as the most plausible approach to maximize the UPO's performance.

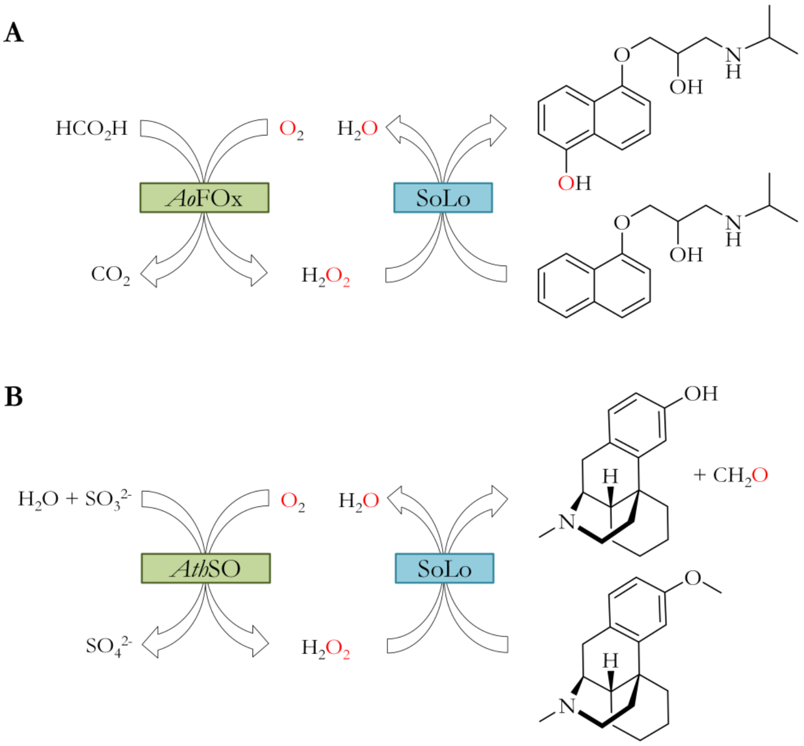

Figure 5.1. Enzymatic *in situ* H_2O_2 generation systems tested with SoLo for the synthesis of 5´-OHP using *Ao*FOx (**A**) and for the synthesis of dextrorphan using *Ath*SO (**B**).

5.1.2. Dextromethorphan, naproxen and tolbutamide

Once we performed the enzyme and reaction engineering of the SoLo mutant, we passed to benchmark this evolved *Aae*UPO with several related mutants for the synthesis of other relevant HDMs: we tested dextromethorphan, naproxen and tolbutamide conversion. Among the most relevant results, dextrorphan production yields from dextromethorphan were 16%, 75% and 82% for wildtype *Aae*UPO, SoLo and JaWa mutants, respectively. With a single dose of H_2O_2, 7,500 TTNs were achieved with SoLo mutant, which we recently coupled to another *in situ* H_2O_2 generation system not included in the Thesis results: the sulfite oxidase from *Arabidopsis thaliana* (*Ath*SO) that uses calcium sulfite (an industrial waste product from scrubbing flue gases) as an electron donor to reduce O_2 into H_2O_2 (van Schie et al., 2020). With this new system, SoLo reached 10,540 TTNs in the transformation of dextrorphan, adding another new method to the pool of H_2O_2 *in situ* generation strategies for UPOs oxyfunctionalization chemistry (**Figure 5.1.B**).

Leaving aside peroxide generation strategies, it is important to highlight that depending on the variant under study, substitutions at the heme channel are behind the modulation of the activity and selectivity towards novel compounds. Indeed, the diversity of amino acids lining the heme channel of both short and long UPOs determine the substrate scope of each peroxygenase, and therefore the re-adaptation of heme pockets can expand the substrate repertoire. As such, focused mutagenesis at the heme channel can unveil new substrate preferences for UPOs. In this direction and in collaboration with Prof. Sarel Fleishman, from the Weizmann Institute of Science (Israel), we are currently developing new *Aae*UPO variants by applying the FuncLib algorithm, an automated method for designing multipoint mutations at enzyme active sites using phylogenetic analysis and Rosetta design calculations -results not included in this Thesis book- (Khersonsky et al., 2018). FuncLib requires a single molecular structure (crystal structure) of the target enzyme and a set of diverse sequence homologs. With this *in silico* method, we were able to identify variants that exhibited changes in activities of orders-of-magnitude without drops in stability. More interestingly, preliminary results also confirm selectivity changes together with an increase in TTNs around 5-10 fold (manuscript in preparation).

5.2. UPO_AAO fusions: a new twist in UPO engineering

Given the successful results obtained by controlling the dosage of H_2O_2, we considered that the design of an UPO fusion enzyme could represent a major breakthrough in UPO engineering. Five constructions of UPO_AAO were functionally expressed in yeast without major alterations in both activities compared to individual enzymes. The H fusion represented an excellent fusion model, which was tested with dextromethorphan and 4-fluorobenzyl alcohol as substrates, achieving 62,145 TTNs in the production of dextrorphan. This number is 6 and 8-fold higher than *Ath*SO (van Schie et al., 2020) or the single shot of H_2O_2, respectively, and similar to the TTNs obtained with *Ao*FOx for propranolol.

We foresee this fusion as a self-sufficient system to produce HDMs at the preparative scale from newly discovered drugs in a straight manner. In the long term, by replacing the fusions modules used in this Doctoral Thesis by other *Aae*UPO and AAO variants, versatile kits for the detection of metabolites could be commercialized (work ongoing).

Conversely, the UPO fusion enzyme can allow one-pot, two-step cascade reactions or the production of two valuable compounds in one single reaction. It is well known that in conventional biocatalysis with H_2O_2-producing oxidases, O_2 is not used efficiently as it is reduced to H_2O_2, forming this useless byproduct whereas with the UPO_AAO enzyme fusion, O_2 could be reduced twice, as the byproduct of the oxidase activity represents the main fuel for peroxygenase, allowing both oxidations -by the oxidase- and C-H oxyfunctionalization reactions -by the peroxygenase-. Thinking bigger and given that the production of H_2O_2 and peroxygenase activity could be unified within a single polypeptide, the bifunctional biocatalyst formed by the fusion of these two independent enzymes could thereafter be subjected to directed co-evolution in order to adapt it to meet specific industrial demands.

An example of a promising cascade where the fusion could be applied is in the production of 2,5-furandicarboxylic acid (FDCA) from 5-hydroxymethylfurfural (HMF). FDCA represents an important building block for the synthesis of PEF, a sustainable alternative to traditional polyesters (such as poly(ethylene-terephthalates), PETs). Indeed, it was successfully proved the stepwise use of native AAO and *Aae*UPO in this whole -6 electron oxidation- cascade reaction, albeit with very poor yields due to the oxidative damage caused by H_2O_2 on UPO (Carro et al., 2015). In this cascade, AAO is in charge of the first two oxidation steps, producing concomitantly 2 equivalents of H_2O_2 which could be used by UPO in the last oxidation step from FFCA to FDCA, **Figure 5.2**. Therefore, a stoichiometric control of the H_2O_2 dosage seems to be fundamental to maintain the UPO active during the whole biotransformation. In this regard, several efforts have been made to design more efficient AAO and UPO variants for the FDCA route.

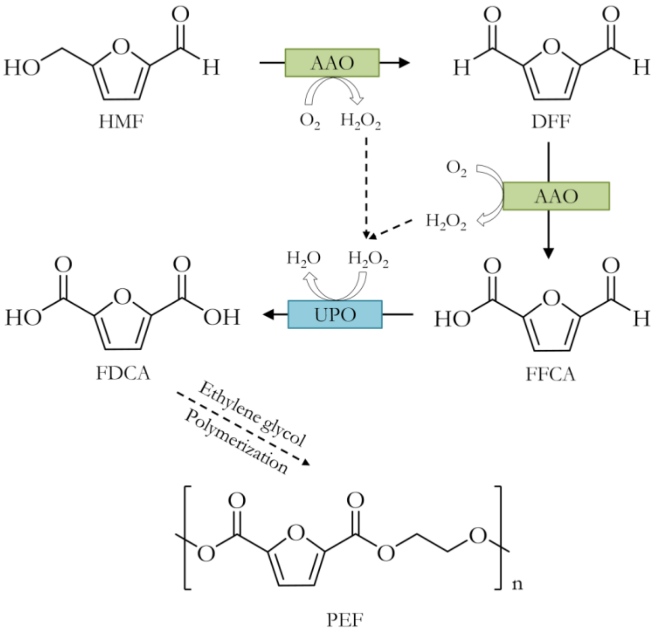

Figure 5.2. Synthesis of poly(ethylene-2,5-furandicarboxylate) (PEF) from 5-hydroxymethylfurfural (HMF). HMF is converted into 2,5-diformylfuran (DFF) by AAO partner releasing one H_2O_2 equivalent. Thereafter, DFF is further transformed by AAO into 2,5-formylfurancarboxylic acid (FFCA) producing a second H_2O_2 equivalent. The *in situ* generated H_2O_2 fuels UPO to perform the last oxidation step towards 2,5-furandicarboxylic acid (FDCA), the main building block for PEF synthesis.

In particular, our laboratory applied directed AAO evolution to disclose the Bantha mutant that converted HMF to DFF with a 3-fold enhancement in the k_{cat} and it was even able to produce low amounts of FDCA (Viña-Gonzalez et al., 2020). Moreover, preliminary results from our group (data not published) have shown a new *Aae*UPO mutant, named JEd-I (Ramirez-Escudero et al., 2018), with better performance compared to the rest of the UPOs reported so far for the FDCA route (**Figure 5.3**). The substitution A316P of JEd-I mutant is placed in a malleable loop in contact with the heme cavity, and it seems to be behind the improved activity although further characterization is needed. Taken together, an enzyme fusion formed by JEd-I (UPO) and Bantha (AAO) could mean a step forward in the synthesis of FDCA from HMF (work ongoing).

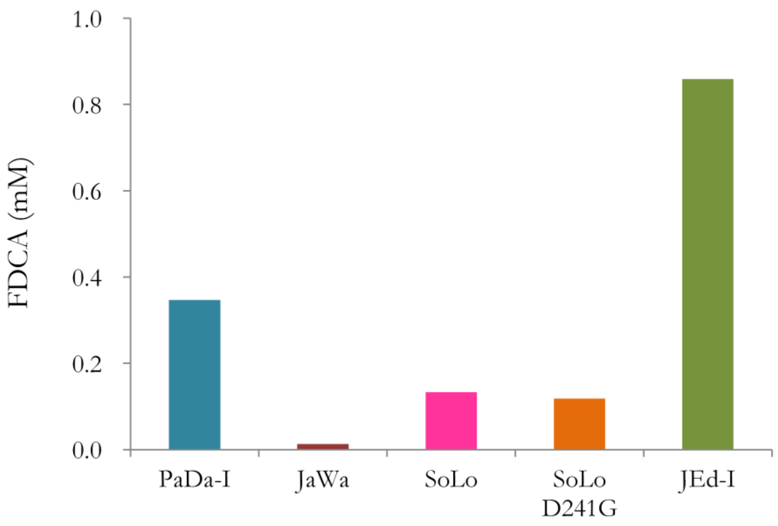

Figure 5.3. Preliminary benchmarking of different UPO variants towards the synthesis of FDCA from FFCA. Reactions were performed for 24h in 100 mM phosphate buffer pH 7, 0.04 mg mL^{-1} of each mutant, 2.5 mM of H_2O_2 and 2.5 mM of FFCA.

CONCLUSIONS

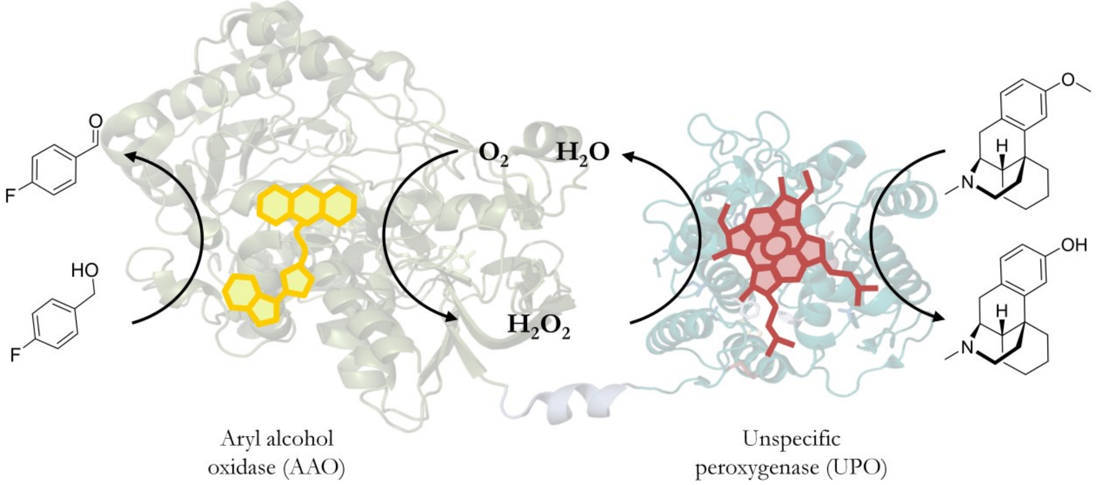
O
F
HO
F
O_2
H_2O
H_2O_2
O
N
H
OH
N
H
Aryl alcohol
oxidase (AAO)
Unspecific
peroxygenase (UPO)

6. Conclusions

1. A sensitive dual high-throughput screening method for the detection of *Aae*UPO variants with enriched peroxygenase activity on propranolol and weak peroxidase activity for the product of interest 5´-OHP was developed, tested and validated.
2. A new mutant for the selective synthesis of 5´-OHP was engineered by focused evolution combined with computational analysis (named SoLo). This mutant showed a catalytic efficiency enhanced by two orders of magnitude and 99% regioselectivity for the synthesis of 5´-OHP, together with a diminished peroxidase activity towards 5´-OHP.
3. When SoLo was coupled to an *in situ* H_2O_2 generation system using methanol as sacrificial electron donor, TTN of 264,000 were achieved, offering a cost-effective and readily scalable method to rapidly prepare 5´-OHP.
4. The benchmarking of several evolved *Aae*UPO mutants in the preparation of HDMs from relevant pharma compounds (dextromethorphan, naproxen and tolbutamide) highlighted the heme access channel as the main feature on which to focus the *Aae*UPO design.
5. In the engineering of functional UPO_AAO fusions, several combinations of UPO and AAO, containing different signal peptides and linkers of different length and nature, were designed and explored with the help of a sensitive screening assay that allowed the breakdown of the different activities within each fusion.
6. The five most interesting UPO_AAO fusions were biochemically characterized and further tested in the synthesis of dextrorphan using a cascade fed by different aromatic alcohols.
7. Reaction engineering of the most promising fusion (H construct) was carried out to achieve total turnover numbers of 62,000, the highest value for the enzymatic synthesis of dextrorphan reported to date. H outperformed both single enzymes (UPO and AAO) working in equimolar concentration.
8. H fusion was functionally expressed in *P. pastoris* to reach production levels of 7 mg L^{-1} in flask, which represents a 32-fold improvement compared to that of *S. cerevisiae*. This value will certainly increase when the strain is fermented in a fed-batch bioreactor.

7. Conclusiones

1. Se ha desarrollado, probado y validado un método sensible *high-throughtput* (cribado de alto rendimiento) para la detección de variantes de *Aae*UPO con una actividad peroxigenasa aumentada sobre el sustrato propranolol y una actividad peroxidasa disminuida sobre el producto de interés 5´-OHP.
2. Se ha obtenido un nuevo mutante (llamado SoLo) mediante evolución dirigida enfocada combinada con análisis computacionales para la síntesis selectiva de 5´-OHP. Este mutante posee una eficiencia catalítica mejorada en dos órdenes de magnitud y una regioselectividad del 99% para la síntesis de 5´-OHP. Además posee una actividad peroxidasa sobre este producto disminuida.
3. Al acoplar a SoLo a un sistema de generación de H_2O_2 *in situ*, utilizando metanol como donante de electrones, se alcanzó un TTN (número de recambio total) de 264,000, ofreciendo un método rentable y escalable para la preparación de 5´-OHP.
4. Se realizó una evaluación comparativa de diferentes variantes evolucionadas de *Aae*UPO para la preparación de HDMs de compuestos farmacéuticos relevantes (dextrometorfano, naproxeno y tolbutamida). Estos experimentos mostraron que el canal de acceso al grupo hemo es el motivo principal en el que centrarse para el diseño de *Aae*UPO.
5. Se diseñó un método de cribado sensible para la detección de actividad UPO y AAO por separado y combinadas para el diseño de enzimas de fusión funcionales UPO_AAO. Se probaron diferentes combinaciones de UPO y AAO con diversos péptidos señales y *linkers* de diversa naturaleza y tamaño.
6. Las cinco fusiones UPO_AAO más interesantes fueron caracterizadas bioquímicamente y ensayadas para la síntesis de dextrorfano utilizando una cascada con diferentes alcoholes aromáticos.
7. Tras la realización de ingeniería de la reacción, la fusión más prometedora (construcción H) alcanzó unos TTN de 62,000, el valor más alto alcanzado mediante métodos enzimáticos hasta la fecha. Además, se realizó una comparación de la proteína de fusión H y las enzimas añadidas sin fusionar, obteniendo un mejor rendimiento con el uso de la enzima de fusión.
8. La fusión H fue expresada funcionalmente en *P. pastoris*, alcanzando unos niveles de producción de 7 mg L^{-1} en matraz, valor que representa una mejora de 32 veces respecto a la producción en *S. cerevisiae*. Este valor además mejorará cuando sea producida en biorreactor.

REFERENCES

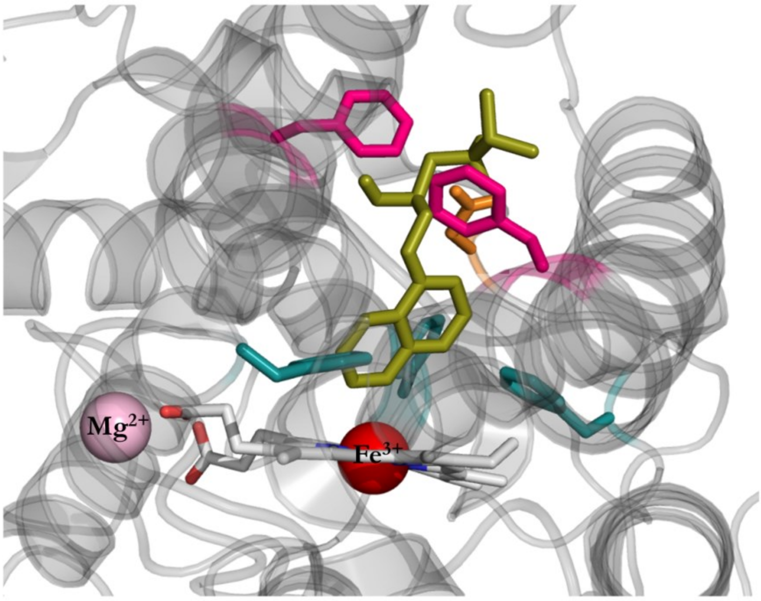

8. References

Aalbers, F.S., Fraaije, M.W., 2019a. Enzyme Fusions in Biocatalysis: Coupling Reactions by Pairing Enzymes. *ChemBioChem* 20, 20–28.

Aalbers, F.S., Fraaije, M.W., 2019b. Design of Artificial Alcohol Oxidases: Alcohol Dehydrogenase-NADPH Oxidase Fusions for Continuous Oxidations. *ChemBioChem* 20, 51–56.

Al-Majed, A.A., Bakheit, A.H.H., Abdel Aziz, H.A., Alajmi, F.M., AlRabiah, H., 2017. Chapter Six - Propranolol, in: Brittain, H.G. (Ed.), Profiles of Drug Substances, Excipients and Related Methodology. Academic Press, pp. 287–338.

Alcalde, M., 2015. Engineering the ligninolytic enzyme consortium. *Trends Biotechnol.* 33, 155–162.

Alcalde, M., 2010. Mutagenesis Protocols in Saccharomyces cerevisiae by In Vivo Overlap Extension, in: Braman, J. (Ed.), In Vitro Mutagenesis Protocols: Third Edition. Humana Press, Totowa, NJ, pp. 3–14.

Amet, N., Lee, H.-F., Shen, W.-C., 2008. Insertion of the Designed Helical Linker Led to Increased Expression of Tf-Based Fusion Proteins. *Pharm. Res.* 26, 523.

Anandakrishnan, R., Aguilar, B., Onufriev, A. V, 2012. H++ 3.0: automating pK prediction and the preparation of biomolecular structures for atomistic molecular modeling and simulations. *Nucleic Acids Res.* 40, W537–W541.

Anh, D.H., 2008. Novel extracellular haloperoxidase-peroxygenases from the coprophilous fungi Coprinus radians and Coprinus verticillatus: production, purification and biochemical characterization. Ph.D. Thesis, International Graduate School of Zittau.

Anh, D.H., Ullrich, R., Benndorf, D., Svatoś, A., Muck, A., Hofrichter, M., 2007. The Coprophilous Mushroom Coprinus radians Secretes a Haloperoxidase That Catalyzes Aromatic Peroxygenation. *Appl. Environ. Microbiol.* 73, 5477–5485.

Aranda, C., Olmedo, A., Kiebist, J., Scheibner, K., del Río, J.C., Martínez, A.T., Gutiérrez, A., 2018. Selective Epoxidation of Fatty Acids and Fatty Acid Methyl Esters by Fungal Peroxygenases. *ChemCatChem* 10, 3964–3968.

Aranda, E., Kinne, M., Kluge, M., Ullrich, R., Hofrichter, M., 2009. Conversion of dibenzothiophene by the mushrooms Agrocybe aegerita and Coprinellus radians and their extracellular peroxygenases. *Appl. Microbiol. Biotechnol.* 82, 1057–1066.

Atrakchi, A.H., 2009. Interpretation and Considerations on the Safety Evaluation of Human Drug Metabolites. *Chem. Res. Toxicol.* 22, 1217–1220.

Babot, E.D., del Río, J.C., Kalum, L., Martínez, A.T., Gutiérrez, A., 2015a. Regioselective Hydroxylation in the Production of 25-Hydroxyvitamin D by Coprinopsis cinerea Peroxygenase. *ChemCatChem* 7, 283–290.

Babot, E.D., del Río, J.C., Cañellas, M., Sancho, F., Lucas, F., Guallar, V., Kalum, L., Lund, H., Gröbe, G., Scheibner, K., Ullrich, R., Hofrichter, M., Martínez, A.T., Gutiérrez, A., 2015b. Steroid Hydroxylation by Basidiomycete Peroxygenases: a Combined Experimental and Computational Study. *Appl. Environ. Microbiol.* 81, 4130–4142.

Babot, E.D., del Río, J.C., Kalum, L., Martínez, A.T., Gutiérrez, A., 2013. Oxyfunctionalization of aliphatic compounds by a recombinant peroxygenase from Coprinopsis cinerea. *Biotechnol. Bioeng.* 110, 2323–2332.

Baillie, T.A., Cayen, M.N., Fouda, H., Gerson, R.J., Green, J.D., Grossman, S.J., Klunk, L.J., LeBlanc, B., Perkins, D.G., Shipley, L.A., 2002. Drug Metabolites in Safety Testing. *Toxicol. Appl. Pharmacol.* 182, 188–196.

Bassanini, I., Ferrandi, E.E., Vanoni, M., Ottolina, G., Riva, S., Crotti, M., Brenna, E., Monti, D., 2017. Peroxygenase-Catalyzed Enantioselective Sulfoxidations. *European J. Org. Chem.* 2017, 7186–7189.

Beyer, N., Kulig, J.K., Bartsch, A., Hayes, M.A., Janssen, D.B., Fraaije, M.W., 2017. P450BM3 fused to phosphite dehydrogenase allows phosphite-driven selective oxidations. *Appl. Microbiol. Biotechnol.* 101, 2319–2331.

Beyer, N., Kulig, J.K., Fraaije, M.W., Hayes, M.A., Janssen, D.B., 2018. Exploring PTDH–P450BM3 Variants for the Synthesis of Drug Metabolites. *ChemBioChem* 19, 326–337.

Bikle, D.D., 2014. Vitamin D Metabolism, Mechanism of Action, and Clinical Applications. *Chem. Biol.* 21, 319–329.

Bloom, J.D., Arnold, F.H., 2009. In the light of directed evolution: Pathways of adaptive protein evolution. *Proc. Natl. Acad. Sci.* 106, 9995–10000.

Bochevarov, A.D., Harder, E., Hughes, T.F., Greenwood, J.R., Braden, D.A., Philipp, D.M., Rinaldo, D., Halls, M.D., Zhang, J., Friesner, R.A., 2013. Jaguar: a High-

Performance Quantum Chemistry Software Program with Strengths in Life and Materials Sciences. *Int. J. Quantum Chem.* 113, 2110.

Bormann, S., Gomez Baraibar, A., Ni, Y., Holtmann, D., Hollmann, F., 2015. Specific oxyfunctionalisations catalysed by peroxygenases: opportunities, challenges and solutions. *Catal. Sci. Technol.* 5, 2038–2052.

Bornscheuer, U.T., Huisman, G.W., Kazlauskas, R.J., Lutz, S., Moore, J.C., Robins, K., 2012. Engineering the third wave of biocatalysis. *Nature* 485, 185–194.

Burek, B.O., de Boer, S.R., Tieves, F., Zhang, W., van Schie, M., Bormann, S., Alcalde, M., Holtmann, D., Hollmann, F., Bahnemann, D.W., Bloh, J.Z., 2019. Photoenzymatic Hydroxylation of Ethylbenzene Catalyzed by Unspecific Peroxygenase: Origin of Enzyme Inactivation and the Impact of Light Intensity and Temperature. *ChemCatChem* 11, 3093–3100.

Carro, J., Ferreira, P., Rodríguez, L., Prieto, A., Serrano, A., Balcells, B., Ardá, A., Jiménez-Barbero, J., Gutiérrez, A., Ullrich, R., Hofrichter, M., Martínez, A.T., 2015. 5-hydroxymethylfurfural conversion by fungal aryl-alcohol oxidase and unspecific peroxygenase. *FEBS J.* 282, 3218–3229.

Carro, J., González-Benjumea, A., Fernández-Fueyo, E., Aranda, C., Guallar, V., Gutiérrez, A., Martínez, A.T., 2019. Modulating Fatty Acid Epoxidation vs Hydroxylation in a Fungal Peroxygenase. *ACS Catal.* 9, 6234–6242.

Chemical Computing Group ULC, 2010. Molecular Operating Environment (MOE).

Chen, X., Zaro, J.L., Shen, W.-C., 2013. Fusion protein linkers: Property, design and functionality. *Adv. Drug Deliv. Rev.* 65, 1357–1369.

Colpa, D.I., Lončar, N., Schmidt, M., Fraaije, M.W., 2017. Creating Oxidase-Peroxidase Fusion Enzymes as a Toolbox for Cascade Reactions. *Chembiochem* 18, 2226–2230.

D.E. Shaw Research, 2009. Desmond Molecular Dynamics System, version 2.2, Schrödinger, New York.

de Visser, S.P., Ogliaro, F., Harris, N., Shaik, S., 2001. Multi-State Epoxidation of Ethene by Cytochrome P450: A Quantum Chemical Study. *J. Am. Chem. Soc.* 123, 3037–3047.

Deng, Y., Sun, M., Xu, S., Zhou, J., 2016. Enhanced (S)-linalool production by fusion expression of farnesyl diphosphate synthase and linalool synthase in Saccharomyces cerevisiae. *J. Appl. Microbiol.* 121, 187–195.

Eiben, S., Kaysser, L., Maurer, S., Kühnel, K., Urlacher, V.B., Schmid, R.D., 2006. Preparative use of isolated CYP102 monooxygenases—A critical appraisal. *J. Biotechnol.* 124, 662–669.

Fernández-Fueyo, E., Ni, Y., Gomez Baraibar, A., Alcalde, M., van Langen, L.M., Hollmann, F., 2016a. Towards preparative peroxygenase-catalyzed oxyfunctionalization reactions in organic media. *J. Mol. Catal. B Enzym.* 134, 347–352.

Fernández-Fueyo, E., Ni, Y., Gomez Baraibar, A., Ullrich, R., Hofrichter, M., Yanase, H., Alcalde, M., van Berkel, W.J.H., Hollmann, F., 2016b. Peroxygenase-Catalyzed Oxyfunctionalization Reactions Promoted by the Complete Oxidation of Methanol. *Angew. Chemie Int. Ed.* 55, 798–801.

Fernandez, I.S., Ruiz-Duenas, F.J., Santillana, E., Ferreira, P., Martinez, M.J., Martinez, A.T., Romero, A., 2009. Novel structural features in the GMC family of oxidoreductases revealed by the crystal structure of fungal aryl-alcohol oxidase. *Acta Crystallogr. Sect. D* 65, 1196–1205.

Ferreira, P., Medina, M., Guillén, F., Martínez, M.J., Van Berkel, W.J.H., Martínez, Á.T., 2005. Spectral and catalytic properties of aryl-alcohol oxidase, a fungal flavoenzyme acting on polyunsaturated alcohols. *Biochem. J.* 389, 731–738.

Fessner, N., Srdic, M., Weber, H., Schmid, C., Schoenauer, D., Schwaneberg, U., Glieder, A., 2020. Preparative-Scale Production of Testosterone Metabolites by Human Liver Cytochrome P450 3A4. *Adv. Synth. Catal.* 362, 2725.

Fischer, J.E., Hatzl, A.-M., Weninger, A., Schmid, C., Glieder, A., 2019. Methanol Independent Expression by Pichia Pastoris Employing De-repression Technologies. *JoVE* e58589.

Freakley, S.J., Kochius, S., van Marwijk, J., Fenner, C., Lewis, R.J., Baldenius, K., Marais, S.S., Opperman, D.J., Harrison, S.T.L., Alcalde, M., Smit, M.S., Hutchings, G.J., 2019. A chemo-enzymatic oxidation cascade to activate C–H bonds with in situ generated H2O2. *Nat. Commun.* 10, 4178.

Fritts, C.A., Waldroup, P.W., 2003. Effect of Source and Level of Vitamin D on Live Performance and Bone Development in Growing Broilers1. *J. Appl. Poult. Res.* 12, 45–52.

George, R.A., Heringa, J., 2002. An analysis of protein domain linkers: their classification and role in protein folding. *Protein Eng. Des. Sel.* 15, 871–879.

Gomez de Santos, P., Cañellas, M., Tieves, F., Younes, S.H.H., Molina-Espeja, P., Hofrichter, M., Hollmann, F., Guallar, V., Alcalde, M., 2018. Selective Synthesis of the Human Drug Metabolite 5'-Hydroxypropranolol by an Evolved Self-Sufficient Peroxygenase. *ACS Catal.* 8, 4789–4799.

Gomez de Santos, P., Cervantes, F.V., Tieves, F., Plou, F.J., Hollmann, F., Alcalde, M., 2019. Benchmarking of laboratory evolved unspecific peroxygenases for the synthesis of human drug metabolites. *Tetrahedron* 75, 1827–1831.

González-Benjumea, A., Carro, J., Renau-Mínguez, C., Linde, D., Fernández-Fueyo, E., Gutiérrez, A., Martínez, A.T., 2020. Fatty acid epoxidation by Collariella virescens peroxygenase and heme-channel variants. *Catal. Sci. Technol.* 10, 717–725.

Gonzalez-Perez, D., Alcalde, M., 2014. Assembly of evolved ligninolytic genes in Saccharomyces cerevisiae. *Bioengineered* 5, 254–263.

Gonzalez-Perez, D., Garcia-Ruiz, E., Alcalde, M., 2012. Saccharomyces cerevisiae in directed evolution. *Bioengineered* 3, 174–179.

Gonzalez-Perez, D., Garcia-Ruiz, E., Ruiz-Dueñas, F.J., Martinez, A.T., Alcalde, M., 2014a. Structural Determinants of Oxidative Stabilization in an Evolved Versatile Peroxidase. *ACS Catal.* 4, 3891–3901.

Gonzalez-Perez, D., Molina-Espeja, P., Garcia-Ruiz, E., Alcalde, M., 2014b. Mutagenic Organized Recombination Process by Homologous In Vivo Grouping (MORPHING) for Directed Enzyme Evolution. *PLoS One* 9, e90919.

Green, M.R., Sambrook, J., 2012. Molecular Cloning: A Laboratory Manual, 4th ed. Cold Spring Harbor Laboratory Press, U.S.A.

Greenslade, F.C., Newquist, K.L., 1978. In vitro measurement of the beta-adrenergic blocking properties of ORF 12592, the 5-hydroxy analog of propranolol. *Arch Int Pharmacodyn Ther* 233, 270–280.

Gröbe, G., Ullrich, R., Pecyna, M.J., Kapturska, D., Friedrich, S., Hofrichter, M., Scheibner, K., 2011. High-yield production of aromatic peroxygenase by the agaric fungus Marasmius rotula. *AMB Express* 1, 31.

Gustavsson, M., Lehtiö, J., Denman, S., Teeri, T.T., Hult, K., Martinelle, M., 2001. Stable linker peptides for a cellulose-binding domain–lipase fusion protein expressed in Pichia pastoris. *Protein Eng. Des. Sel.* 14, 711–715.

Gutiérrez, A., Babot, E.D., Ullrich, R., Hofrichter, M., Martínez, A.T., del Río, J.C., 2011. Regioselective oxygenation of fatty acids, fatty alcohols and other aliphatic compounds by a basidiomycete heme-thiolate peroxidase. *Arch. Biochem. Biophys.* 514, 33–43.

Hanano, A., Burcklen, M., Flenet, M., Ivancich, A., Louwagie, M., Garin, J., Blée, E., 2006. Plant Seed Peroxygenase Is an Original Heme-oxygenase with an EF-hand Calcium Binding Motif. *J. Biol. Chem.* 281, 33140–33151.

Hernández-Ortega, A., Ferreira, P., Martínez, A.T., 2012. Fungal aryl-alcohol oxidase: a peroxide-producing flavoenzyme involved in lignin degradation. *Appl. Microbiol. Biotechnol.* 93, 1395–1410.

Hobisch, M., van Schie, M.M.C.H., Kim, J., Andersen, K.R., Alcalde, M., Kourist, R., Park, C.B., Hollmann, F., Kara, S., 2020. Solvent-Free Photobiocatalytic Hydroxylation of Cyclohexane. *ChemCatChem* 12, 40009.

Hofrichter, M., Kellner, H., Herzog, R., Karich, A., Liers, C., Scheibner, K., Kimani, V.W., Ullrich, R., 2020. Fungal Peroxygenases: A Phylogenetically Old Superfamily of Heme Enzymes with Promiscuity for Oxygen Transfer Reactions, in: Nevalainen, H. (Ed.), Grand Challenges in Fungal Biotechnology. Springer International Publishing, Cham, pp. 369–403.

Hofrichter, M., Kellner, H., Pecyna, M.J., Ullrich, R., 2015. Fungal Unspecific Peroxygenases: Heme-Thiolate Proteins That Combine Peroxidase and Cytochrome P450 Properties, in: Hrycay, E.G., Bandiera, S.M. (Eds.), Monooxygenase, Peroxidase and Peroxygenase Properties and Mechanisms of Cytochrome P450. Springer International Publishing, Cham, pp. 341–368.

Hofrichter, M., Ullrich, R., 2014. Oxidations catalyzed by fungal peroxygenases. *Curr. Opin. Chem. Biol.* 19, 116–125.

Holtmann, D., Hollmann, F., 2016. The Oxygen Dilemma: A Severe Challenge for the Application of Monooxygenases? *ChemBioChem* 17, 1391–1398.

Huang, L., Aalbers, F.S., Tang, W., Röllig, R., Fraaije, M.W., Kara, S., 2019. Convergent

Cascade Catalyzed by Monooxygenase–Alcohol Dehydrogenase Fusion Applied in Organic Media. *ChemBioChem* 20, 1653–1658.

Jones, G., 2013. Extrarenal Vitamin D Activation and Interactions Between Vitamin D2, Vitamin D3, and Vitamin D Analogs. *Annu. Rev. Nutr.* 33, 23–44.

Karich, A., Scheibner, K., Ullrich, R., Hofrichter, M., 2016. Exploring the catalase activity of unspecific peroxygenases and the mechanism of peroxide-dependent heme destruction. *J. Mol. Catal. B Enzym.* 134, 238–246.

Khersonsky, O., Lipsh, R., Avizemer, Z., Ashani, Y., Goldsmith, M., Leader, H., Dym, O., Rogotner, S., Trudeau, D.L., Prilusky, J., Amengual-Rigo, P., Guallar, V., Tawfik, D.S., Fleishman, S.J., 2018. Automated Design of Efficient and Functionally Diverse Enzyme Repertoires. *Mol. Cell* 72, 178–186.

Kiebist, J., Hofrichter, M., Zuhse, R., Scheibner, K., 2019. Oxyfunctionalization of pharmaceuticals by fungal peroxygenases, in: Grundwal, P. (Ed.), Pan Standford Series on Biocatalysis. Pan Stanford Publishing, pp. 643–680.

Kiebist, J., Holla, W., Heidrich, J., Poraj-Kobielska, M., Sandvoss, M., Simonis, R., Gröbe, G., Atzrodt, J., Hofrichter, M., Scheibner, K., 2015. One-pot synthesis of human metabolites of SAR548304 by fungal peroxygenases. *Bioorg. Med. Chem.* 23, 4324–4332.

Kiebist, J., Schmidtke, K., Zimmermann, J., Kellner, H., Jehmlich, N., Ullrich, R., Zänder, D., Hofrichter, M., Scheibner, K., 2017. A Peroxygenase from Chaetomium globosum Catalyzes the Selective Oxygenation of Testosterone. *ChemBioChem* 18, 563–569.

Kille, S., Acevedo-Rocha, C.G., Parra, L.P., Zhang, Z.-G., Opperman, D.J., Reetz, M.T., Acevedo, J.P., 2013. Reducing Codon Redundancy and Screening Effort of Combinatorial Protein Libraries Created by Saturation Mutagenesis. *ACS Synth. Biol.* 2, 83–92.

Kinne, M., 2010. The extracellular peroxygenase of the agaric fungus Agrocybe aegerita: catalytic properties and physiological background with particular emphasis on ether cleavage. PhD Thesis. International Graduate School of Zittau, Zittau, Germany.

Kinne, M., Poraj-Kobielska, M., Ralph, S.A., Ullrich, R., Hofrichter, M., Hammel, K.E., 2009. Oxidative Cleavage of Diverse Ethers by an Extracellular Fungal Peroxygenase. *J. Biol. Chem.* 284, 29343–29349.

Kinne, M., Poraj-Kobielska, M., Ullrich, R., Nousiainen, P., Sipilä, J., Schreibner, K., Hammel, K., Hofrichter, M., 2011. Oxidative cleavage of non-phenolic b-O-4 lignin model dimers by an extracellular aromatic peroxygenase. *Holzforschung* 65, 673–679.

Klebanoff, S.J., 2005. Myeloperoxidase: friend and foe. *J. Leukoc. Biol.* 77, 598–625.

Lee, D.-S., Yamada, A., Sugimoto, H., Matsunaga, I., Ogura, H., Ichihara, K., Adachi, S., Park, S.-Y., Shiro, Y., 2003. Substrate Recognition and Molecular Mechanism of Fatty Acid Hydroxylation by Cytochrome P450 from Bacillus subtilis: Crystallographic, Spectroscopic, and Mutational Studies. *J. Biol. Chem.* 278, 9761–9767.

Lewis, J.C., Mantovani, S.M., Fu, Y., Snow, C.D., Komor, R.S., Wong, C.-H., Arnold, F.H., 2010. Combinatorial Alanine Substitution Enables Rapid Optimization of Cytochrome P450BM3 for Selective Hydroxylation of Large Substrates. *ChemBioChem* 11, 2502–2505.

Li, W., Rozzell, D., Kambourakis, S., Mayhew, M., 2009. Biosynthesis of Drug Metabolites, in: Liese, A., Lin, G.-Q., Tao, J. (Eds.), Biocatalysis for the Pharmaceutical Industry. John Wiley & Sons (Asia), Singapore, pp. 183–211.

Li, Y., Ma, Y., Li, P., Zhang, X., Ribitsch, D., Alcalde, M., Hollmann, F., Wang, Y., 2020. Enantioselective Sulfoxidation of Thioanisole by Cascading a Choline Oxidase and a Peroxygenase in the Presence of Natural Deep Eutectic Solvents. *Chempluschem* 85, 254–257.

Linde, D., Olmedo, A., González-Benjumea, A., Estévez, M., Renau-Mínguez, C., Carro, J., Fernández-Fueyo, E., Gutiérrez, A., Martínez, A.T., 2020. Two New Unspecific Peroxygenases from Heterologous Expression of Fungal Genes in Escherichia coli. *Appl. Environ. Microbiol.* 86, e02899-19.

Madadkar-Sobhani, A., Guallar, V., 2013. PELE web server: atomistic study of biomolecular systems at your fingertips. *Nucleic Acids Res.* 41, W322–W328.

Madhavi Sastry, G., Adzhigirey, M., Day, T., Annabhimoju, R., Sherman, W., 2013. Protein and ligand preparation: parameters, protocols, and influence on virtual screening enrichments. *J. Comput. Aided. Mol. Des.* 27, 221–234.

Martin-Diaz, J., 2019. Evolución dirigida de la peroxigenasa inespecífica de agrocybe aegerita: tolerancia a disolventes orgánicos mediante deriva genética neutral y evolución adaptativa. PhD Thesis. Universidad Autónoma de Madrid, Madrid, Spain.

Martin-Diaz, J., Paret, C., García-Ruiz, E., Molina-Espeja, P., Alcalde, M., 2018. Shuffling the Neutral Drift of Unspecific Peroxygenase in Saccharomyces cerevisiae. *Appl. Environ. Microbiol.* 84, e00808-18.

Martínez, A.T., Ruiz-Dueñas, F.J., Camarero, S., Serrano, A., Linde, D., Lund, H., Vind, J., Tovborg, M., Herold-Majumdar, O.M., Hofrichter, M., Liers, C., Ullrich, R., Scheibner, K., Sannia, G., Piscitelli, A., Pezzella, C., Sener, M.E., Kılıç, S., van Berkel, W.J.H., Guallar, V., Lucas, M.F., Zuhse, R., Ludwig, R., Hollmann, F., Fernández-Fueyo, E., Record, E., Faulds, C.B., Tortajada, M., Winckelmann, I., Rasmussen, J.-A., Gelo-Pujic, M., Gutiérrez, A., del Río, J.C., Rencoret, J., Alcalde, M., 2017. Oxidoreductases on their way to industrial biotransformations. *Biotechnol. Adv.* 35, 815–831.

Mate, D. M., Gonzalez-Perez, D., Mateljak, I., Gomez de Santos, P., Vicente, A.I., Alcalde, M., 2017. Chapter 8 The Pocket Manual of Directed Evolution Tips and Tricks, in: Biotechnology of Microbial Enzymes. pp. 185–213.

Mate, D.M., Palomino, M.A., Molina-Espeja, P., Martin-Diaz, J., Alcalde, M., 2017. Modification of the peroxygenative:peroxidative activity ratio in the unspecific peroxygenase from Agrocybe aegerita by structure-guided evolution. *Protein Eng. Des. Sel.* 30, 191–198.

Matthews, S., Tee, K.L., Rattray, N.J., McLean, K.J., Leys, D., Parker, D.A., Blankley, R.T., Munro, A.W., 2017. Production of alkenes and novel secondary products by P450 OleTJE using novel H2O2-generating fusion protein systems. *FEBS Lett.* 591, 737–750.

Melzer, A., Kimani, V.W., Ullrich, R., 2018. Psathyrella aberdarensis, a new species of Psathyrella (Agaricales) from a Kenyan National Park. *Austrian J. Mycol.* 27, 23–30.

Molina-Espeja, P., Cañellas, M., Plou, F.J., Hofrichter, M., Lucas, F., Guallar, V., Alcalde, M., 2016a. Synthesis of 1-Naphthol by a Natural Peroxygenase Engineered by Directed Evolution. *ChemBioChem* 17, 341–349.

Molina-Espeja, P., Garcia-Ruiz, E., Gonzalez-Perez, D., Ullrich, R., Hofrichter, M., Alcalde, M., 2014. Directed Evolution of Unspecific Peroxygenase from Agrocybe aegerita. *Appl. Environ. Microbiol.* 80, 3496–3507.

Molina-Espeja, P., Gomez de Santos, P., Alcalde, M., 2017. Directed Evolution of

Unspecific Peroxygenase, in: Alcalde, M. (Ed.), Directed Enzyme Evolution: Advances and Applications. Springer International Publishing, Cham, pp. 127–143.

Molina-Espeja, P., Ma, S., Mate, D.M., Ludwig, R., Alcalde, M., 2015. Tandem-yeast expression system for engineering and producing unspecific peroxygenase. *Enzyme Microb. Technol.* 73–74, 29–33.

Molina-Espeja, P., Plou, F.J., Alcalde, M., Gomez de Santos, P., 2016b. Mutants of unspecific peroxygenase with high monooxygenase activity and uses thereof. Patent WO/2017/081355.

Molina-Espeja, P., Viña-Gonzalez, J., Gomez-Fernandez, B.J., Martin-Diaz, J., Garcia-Ruiz, E., Alcalde, M., 2016c. Beyond the outer limits of nature by directed evolution. *Biotechnol. Adv.* 34, 754–767.

National Research Council, 2015. Industrialization of Biology: A Roadmap to Accelerate the Advanced Manufacturing of Chemicals. The National Academies Press, Washington, DC.

Oldenburg, K.R., Vo, K.T., Michaelis, S., Paddon, C., 1997. Recombination-mediated PCR-directed plasmid construction in vivo in yeast. *Nucleic Acids Res.* 25, 451–452.

Olmedo, A., Aranda, C., del Río, J.C., Kiebist, J., Scheibner, K., Martínez, A.T., Gutiérrez, A., 2016. From Alkanes to Carboxylic Acids: Terminal Oxygenation by a Fungal Peroxygenase. *Angew. Chemie Int. Ed.* 55, 12248–12251.

Olmedo, A., Río, J.C. Del, Kiebist, J., Ullrich, R., Hofrichter, M., Scheibner, K., Martínez, A.T., Gutiérrez, A., 2017. Fatty Acid Chain Shortening by a Fungal Peroxygenase. *Chemistry* 23, 16985–16989.

Omura, T., 2005. Heme–thiolate proteins. *Biochem. Biophys. Res. Commun.* 338, 404–409.

Otey, C.R., Bandara, G., Lalonde, J., Takahashi, K., Arnold, F.H., 2006. Preparation of human metabolites of propranolol using laboratory-evolved bacterial cytochromes P450. *Biotechnol. Bioeng.* 93, 494–499.

Otey, C.R., Joern, J.M., 2003. High-Throughput Screen for Aromatic Hydroxylation, in: Arnold, F.H., Georgiou, G. (Eds.), Directed Enzyme Evolution: Screening and Selection Methods. Humana Press, Totowa, NJ, pp. 141–148.

Peter, S., 2013. Oxyfunctionalization of alkanes, alkenes and alkynes by unspecific peroxygenase (EC 1.11.2.1). PhD Thesis. Internationalen Hochschulinstitutes Zittau and Technischen Universität Dresden, Dresden, Germany.

Peter, S., Karich, A., Ullrich, R., Gröbe, G., Scheibner, K., Hofrichter, M., 2014. Enzymatic one-pot conversion of cyclohexane into cyclohexanone: Comparison of four fungal peroxygenases. *J. Mol. Catal. B Enzym.* 103, 47–51.

Peter, S., Kinne, M., Ullrich, R., Kayser, G., Hofrichter, M., 2013. Epoxidation of linear, branched and cyclic alkenes catalyzed by unspecific peroxygenase. *Enzyme Microb. Technol.* 52, 370–376.

Peter, S., Kinne, M., Wang, X., Ullrich, R., Kayser, G., Groves, J.T., Hofrichter, M., 2011. Selective hydroxylation of alkanes by an extracellular fungal peroxygenase. *FEBS J.* 278, 3667–3675.

Piontek, K., Strittmatter, E., Ullrich, R., Gröbe, G., Pecyna, M.J., Kluge, M., Scheibner, K., Hofrichter, M., Plattner, D.A., 2013. Structural Basis of Substrate Conversion in a New Aromatic Peroxygenase: Cytochrome P450 functionality with benefits. *J. Biol. Chem.* 288, 34767–34776.

Poraj-Kobielska, M., Kinne, M., Ullrich, R., Scheibner, K., Kayser, G., Hammel, K.E., Hofrichter, M., 2011. Preparation of human drug metabolites using fungal peroxygenases. *Biochem. Pharmacol.* 82, 789–796.

Ramirez-Escudero, M., Molina-Espeja, P., Gomez de Santos, P., Hofrichter, M., Sanz-Aparicio, J., Alcalde, M., 2018. Structural Insights into the Substrate Promiscuity of a Laboratory-Evolved Peroxygenase. *ACS Chem. Biol.* 13, 3259–3268.

Rauch, M.C.R., Tieves, F., Paul, C.E., Arends, I.W.C.E., Alcalde, M., Hollmann, F., 2019. Peroxygenase-Catalysed Epoxidation of Styrene Derivatives in Neat Reaction Media. *ChemCatChem* 11, 4519–4523.

Romanos, M.A., Scorer, C.A., Clare, J.J., 1992. Foreign gene expression in yeast: a review. *Yeast* 8, 423–488.

Ruiz-Dueñas, F.J., Ferreira, P., Martínez, M.J., Martínez, A.T., 2006. In vitro activation, purification, and characterization of Escherichia coli expressed aryl-alcohol oxidase, a unique H2O2-producing enzyme. *Protein Expr. Purif.* 45, 191–199.

Ruiz-Dueñas, F.J., Martínez, Á.T., 2009. Microbial degradation of lignin: how a bulky recalcitrant polymer is efficiently recycled in nature and how we can take advantage of this. *Microb. Biotechnol.* 2, 164–177.

Schmidtke, P., Bidon-Chanal, A., Luque, F.J., Barril, X., 2011. MDpocket: open-source cavity detection and characterization on molecular dynamics trajectories. *Bioinformatics* 27, 3276–3285.

Schrödinger, 2011. QSite, version 5.7, Schrödinger, LLC, New York.

Serrano, A., Sancho, F., Viña-González, J., Carro, J., Alcalde, M., Guallar, V., Martínez, A.T., 2019. Switching the substrate preference of fungal aryl-alcohol oxidase: towards stereoselective oxidation of secondary benzyl alcohols. *Catal. Sci. Technol.* 9, 833–841.

Siebers, N., Palmer, M., Silberg, D.G., Jennings, L., Bliss, C., Martin, P.T., 2018. Absorption, Distribution, Metabolism, and Excretion of [14C]-Volixibat in Healthy Men: Phase 1 Open-Label Study. *Eur. J. Drug Metab. Pharmacokinet.* 43, 91–101.

Steinbrecht, S., Kiebist, J., König, R., Thiessen, M., Schmidtke, K.-U., Kammerer, S., Küpper, J.-H., Scheibner, K., 2020. Synthesis of cyclophosphamide metabolites by a peroxygenase from Marasmius rotula for toxicological studies on human cancer cells. *AMB Express* 10, 128.

Tang, M.-C., Fu, C.-Y., Tang, G.-L., 2012. Characterization of SfmD as a Heme Peroxidase That Catalyzes the Regioselective Hydroxylation of 3-Methyltyrosine to 3-Hydroxy-5-methyltyrosine in Saframycin A Biosynthesis. *J. Biol. Chem.* 287, 5112–5121.

Tieves, F., Willot, S.J.-P., van Schie, M.M.C.H., Rauch, M.C.R., Younes, S.H.H., Zhang, W., Dong, J., Gomez de Santos, P., Robbins, J.M., Bommarius, B., Alcalde, M., Bommarius, A.S., Hollmann, F., 2019. Formate Oxidase (FOx) from Aspergillus oryzae: One Catalyst Enables Diverse H2O2-Dependent Biocatalytic Oxidation Reactions. *Angew. Chemie - Int. Ed.* 58, 7873–7877.

Turner, N.J., 2009. Directed evolution drives the next generation of biocatalysts. *Nat. Chem. Biol.* 5, 567–573.

Ullrich, R., Dolge, C., Kluge, M., Hofrichter, M., 2008. Pyridine as novel substrate for regioselective oxygenation with aromatic peroxygenase from Agrocybe aegerita. *FEBS Lett.* 582, 4100–4106.

Ullrich, R., Hofrichter, M., 2007. Enzymatic hydroxylation of aromatic compounds. *Cell.*

Mol. Life Sci. 64, 271–293.

Ullrich, R., Hofrichter, M., 2005. The haloperoxidase of the agaric fungus Agrocybe aegerita hydroxylates toluene and naphthalene. *FEBS Lett.* 579, 6247–6250.

Ullrich, R., Nüske, J., Scheibner, K., Spantzel, J., Hofrichter, M., 2004. Novel Haloperoxidase from the Agaric Basidiomycete Agrocybe aegerita Oxidizes Aryl Alcohols and Aldehydes. *Appl. Environ. Microbiol.* 70, 4575–4581.

Ullrich, R., Poraj-Kobielska, M., Scholze, S., Halbout, C., Sandvoss, M., Pecyna, M.J., Scheibner, K., Hofrichter, M., 2018. Side chain removal from corticosteroids by unspecific peroxygenase. *J. Inorg. Biochem.* 183, 84–93.

van Schie, M.M.C.H., Kaczmarek, A.T., Tieves, F., Gomez de Santos, P., Paul, C.E., Arends, I.W.C.E., Alcalde, M., Schwarz, G., Hollmann, F., 2020. Selective Oxyfunctionalisation Reactions Driven by Sulfite Oxidase-Catalysed In Situ Generation of H2O2. *ChemCatChem* 12, 3186–3189.

van Schie, M.M.C.H., Zhang, W., Tieves, F., Choi, D.S., Park, C.B., Burek, B.O., Bloh, J.Z., Arends, I.W.C.E., Paul, C.E., Alcalde, M., Hollmann, F., 2019. Cascading g-C3N4 and Peroxygenases for Selective Oxyfunctionalization Reactions. *ACS Catal.* 9, 7409–7417.

van Vugt-Lussenburg, B.M.A., Damsten, M.C., Maasdijk, D.M., Vermeulen, N.P.E., Commandeur, J.N.M., 2006. Heterotropic and homotropic cooperativity by a drug-metabolising mutant of cytochrome P450 BM3. *Biochem. Biophys. Res. Commun.* 346, 810–818.

Viña-Gonzalez, J., Elbl, K., Ponte, X., Valero, F., Alcalde, M., 2018. Functional expression of aryl-alcohol oxidase in Saccharomyces cerevisiae and Pichia pastoris by directed evolution. *Biotechnol. Bioeng.* 115, 1666–1674.

Viña-Gonzalez, J., Gonzalez-Perez, D., Ferreira, P., Martinez, A.T., Alcalde, M., 2015. Focused Directed Evolution of Aryl-Alcohol Oxidase in Saccharomyces cerevisiae by Using Chimeric Signal Peptides. *Appl. Environ. Microbiol.* 81, 6451–6462.

Viña-Gonzalez, J., Jimenez-Lalana, D., Sancho, F., Serrano, A., Martinez, A.T., Guallar, V., Alcalde, M., 2019. Structure-Guided Evolution of Aryl Alcohol Oxidase from Pleurotus eryngii for the Selective Oxidation of Secondary Benzyl Alcohols. *Adv. Synth. Catal.* 361, 2514–2525.

Viña-Gonzalez, J., Martinez, A.T., Guallar, V., Alcalde, M., 2020. Sequential oxidation of 5-hydroxymethylfurfural to furan-2,5-dicarboxylic acid by an evolved aryl-alcohol oxidase. *Biochim. Biophys. Acta - Proteins Proteomics* 1868, 140293.

Wang, Y., Lan, D., Durrani, R., Hollmann, F., 2017. Peroxygenases en route to becoming dream catalysts. What are the opportunities and challenges? *Curr. Opin. Chem. Biol.* 37, 1–9.

Willot, S.J.-P., Hoang, M.D., Paul, C.E., Alcalde, M., Arends, I.W.C.E., Bommarius, A.S., Bommarius, B., Hollmann, F., 2020. FOx News: Towards Methanol-driven Biocatalytic Oxyfunctionalisation Reactions. *ChemCatChem* 12, 2713–2716.

Willot, S.J.P., Fernández-Fueyo, E., Tieves, F., Pesic, M., Alcalde, M., Arends, I.W.C.E., Park, C.B., Hollmann, F., 2019. Expanding the Spectrum of Light-Driven Peroxygenase Reactions. *ACS Catal.* 9, 890–894.

Yayci, A., Baraibar, Á.G., Krewing, M., Fueyo, E.F., Hollmann, F., Alcalde, M., Kourist, R., Bandow, J.E., 2020. Plasma-Driven in Situ Production of Hydrogen Peroxide for Biocatalysis. *ChemSusChem* 13, 2072–2079.

Yoon, J., Kim, J., Tieves, F., Zhang, W., Alcalde, M., Hollmann, F., Park, C.B., 2020. Piezobiocatalysis: Ultrasound-Driven Enzymatic Oxyfunctionalization of C–H Bonds. *ACS Catal.* 10, 5236–5242.

Yourno, J., Kohno, T., Roth, J.R., 1970. Enzyme Evolution: Generation of a Bifunctional Enzyme by Fusion of Adjacent Genes. *Nature* 228, 820–824.

Zaitseva, E.M., Zaitsev, E.N., Kowalczykowski, S.C., 1999. The DNA Binding Properties of Saccharomyces cerevisiae Rad51 Protein . *J. Biol. Chem.* 274, 2907–2915.

Zhang, W., Burek, B.O., Fernández-Fueyo, E., Alcalde, M., Bloh, J.Z., Hollmann, F., 2017. Selective Activation of C−H Bonds in a Cascade Process Combining Photochemistry and Biocatalysis. *Angew. Chemie Int. Ed.* 56, 15451–15455.

Zhang, W., Fernández-Fueyo, E., Ni, Y., van Schie, M., Gacs, J., Renirie, R., Wever, R., Mutti, F.G., Rother, D., Alcalde, M., Hollmann, F., 2018. Selective aerobic oxidation reactions using a combination of photocatalytic water oxidation and enzymatic oxyfunctionalisations. *Nat. Catal.* 1, 55–62.

Zhao, H.L., Yao, X.Q., Xue, C., Wang, Y., Xiong, X.H., Liu, Z.M., 2008. Increasing the homogeneity, stability and activity of human serum albumin and interferon-α2b fusion protein by linker engineering. *Protein Expr. Purif.* 61, 73–77.

Zöllner, A., Buchheit, D., Meyer, M.R., Maurer, H.H., Peters, F.T., Bureik, M., 2010. Production of human phase 1 and 2 metabolites by whole-cell biotransformation with recombinant microbes. *Bioanalysis* 2, 1277–1290.

Zweifel, M., Thürlimann, B., Riniker, S., Weder, P., von Moos, R., Pagani, O., Bigler, M., Rothgiesser, K.M., Pilop, C., Hawle, H., Brauchli, P., Tapia, C., Schoenfeld, W., Sessa, C., Swiss Group for Clinical Cancer, R., 2017. Phase I trial of the androgen receptor modulator CR1447 in breast cancer patients. *Endocr. Connect.* 6, 549–556.

ANNEX

9. Annex

9.1. ^{1}H NMR spectrum for Chapter 1

Figure 9.1. ^{1}H NMR of 5´-OHP after product isolation.

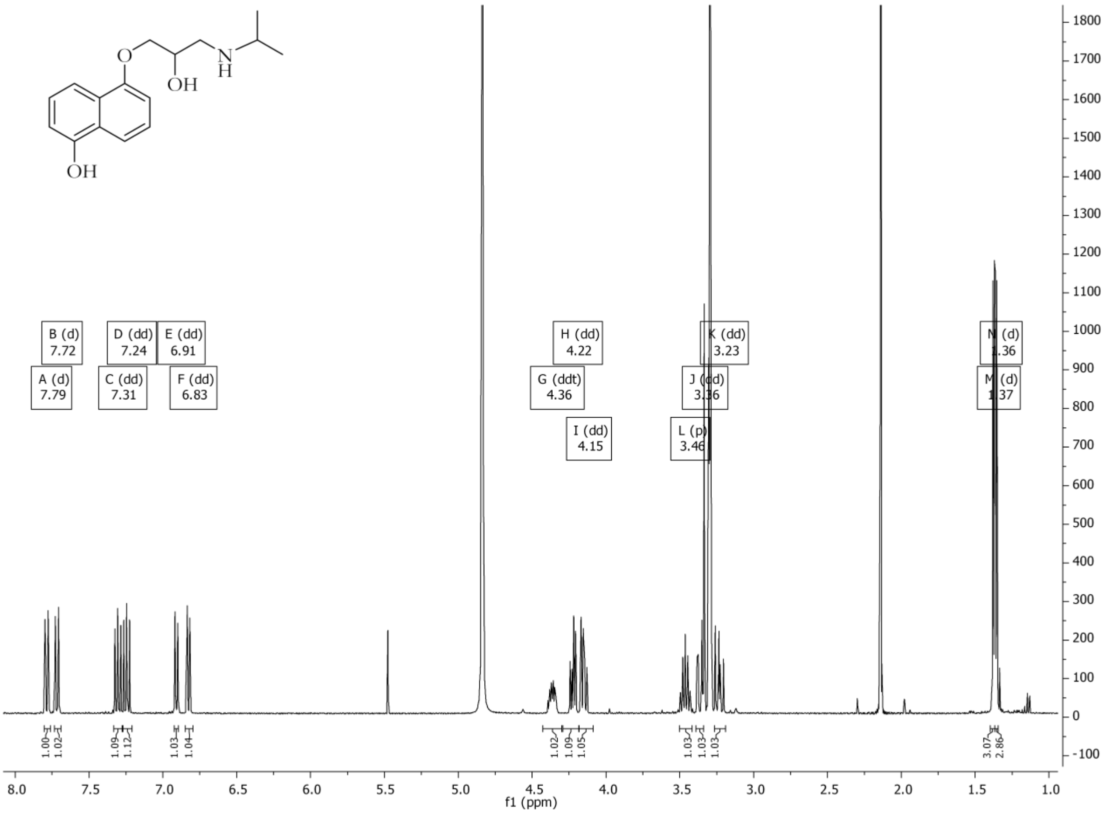

9.2. ^{1}H NMR and ^{13}C spectra for Chapter 2

Figure 9.2. ^{1}H NMR of dextrorphan received after product isolation.

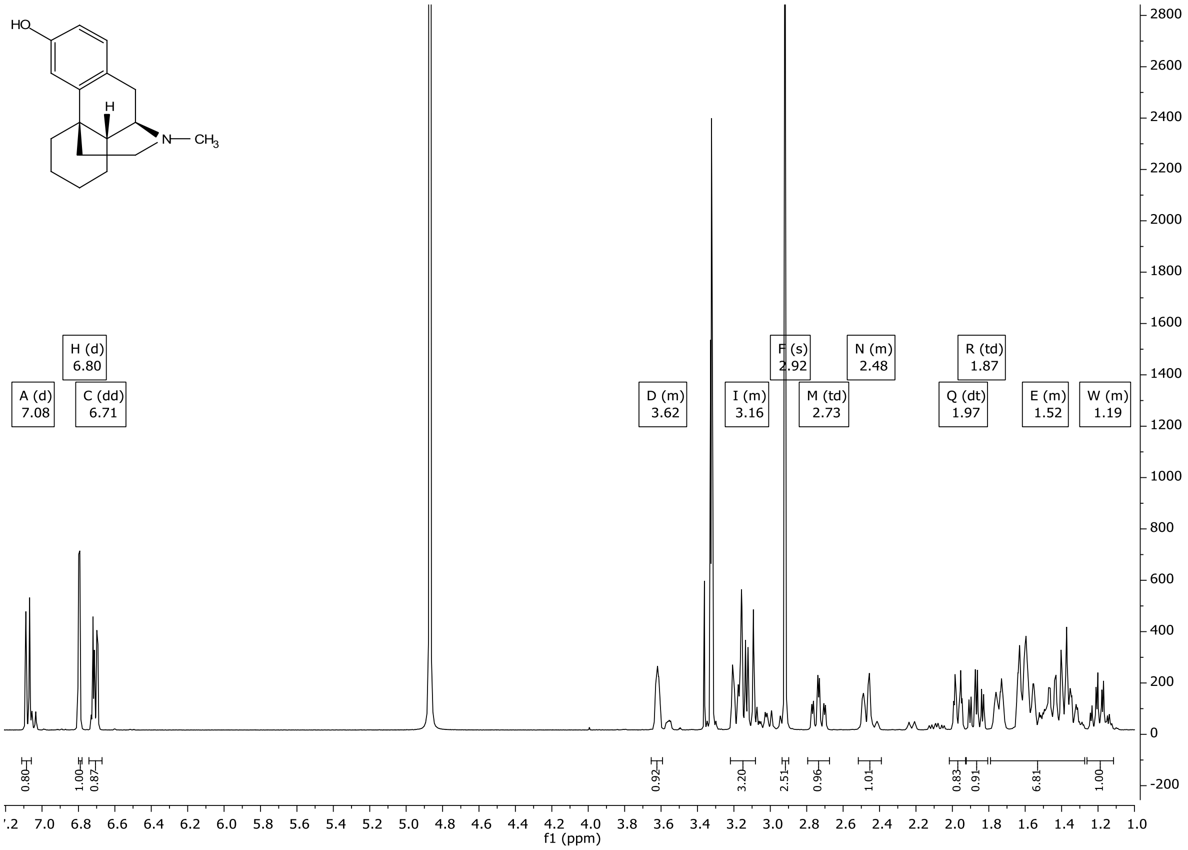

Figure 9.3. ^{13}C NMR of dextrorphan received after product isolation.

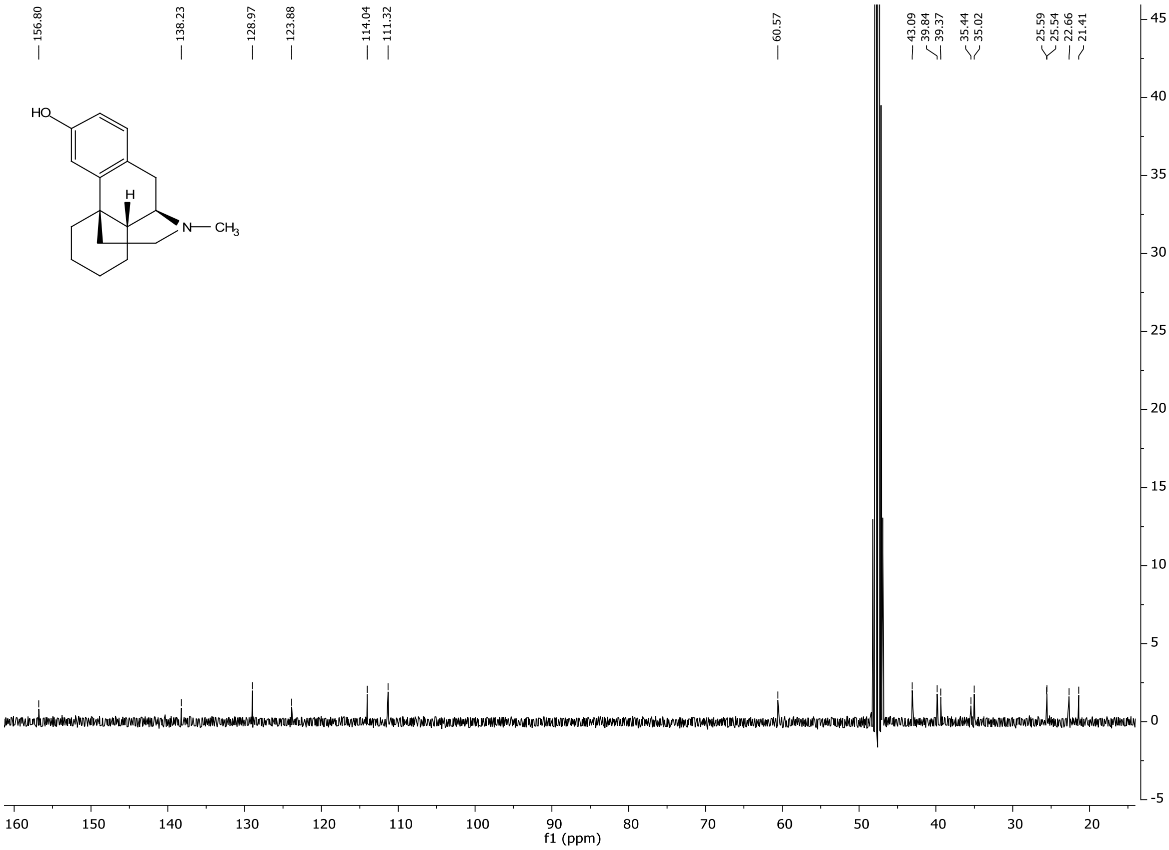

9.3. Publications and patent from the Doctoral Thesis

Gomez de Santos, P., Cañellas, M., Tieves, F., Younes, S.H.H., Molina-Espeja, P., Hofrichter, M., Hollmann, F., Guallar, V., Alcalde, M., 2018. Selective Synthesis of the Human Drug Metabolite 5´-Hydroxypropranolol by an Evolved Self-Sufficient Peroxygenase. *ACS Catal.* 8, 4789–4799.

Gomez de Santos, P., Cervantes, F.V., Tieves, F., Plou, F.J., Hollmann, F., Alcalde, M., 2019. Benchmarking of laboratory evolved unspecific peroxygenases for the synthesis of human drug metabolites. *Tetrahedron* 75, 1827–1831.

Gomez de Santos, P., Lázaro, S., Viña-González, J., Hoang, M.D., Sánchez-Moreno, I., Glieder, A., Hollmann, F., Alcalde, M., 2020. Evolved peroxygenase-aryl alcohol oxidase fusions for self-sufficient oxyfunctionalization reactions. *ACS Catal.* In press.

Molina-Espeja, P., Plou, F.J., Alcalde, M., **Gomez de Santos, P.**, 2016. Mutants of unspecific peroxygenase with high monooxygenase activity and uses thereof. Patent WO/2017/081355.

9.4. Other publications from the author

Hobisch, M., Holtmann, D., **Gomez de Santos, P.**, Alcalde, M., Hollmann, F., Kara, S., 2020. Recent developments in the use of peroxygenases – Exploring their high potential in selective oxyfunctionalisations. *Biotechnol. Adv.* 107615.

van Schie, M.M.C.H., Kaczmarek, A.T., Tieves, F., **Gomez de Santos, P.**, Paul, C.E., Arends, I.W.C.E., Alcalde, M., Schwarz, G., Hollmann, F., 2020. Selective Oxyfunctionalisation Reactions Driven by Sulfite Oxidase-Catalysed In Situ Generation of H2O2. *ChemCatChem* 12, 3186–3189.

Tieves, F., Willot, S.J.-P., van Schie, M.M.C.H., Rauch, M.C.R., Younes, S.H.H., Zhang, W., Dong, J., **Gomez de Santos, P.**, Robbins, J.M., Bommarius, B., Alcalde, M., Bommarius, A.S., Hollmann, F., 2019. Formate Oxidase (FOx) from Aspergillus oryzae: One Catalyst Enables Diverse H_2O_2-Dependent Biocatalytic Oxidation Reactions. *Angew. Chemie - Int. Ed.* 58, 7873–7877.

Ramirez-Escudero, M., Molina-Espeja, P., **Gomez de Santos, P.**, Hofrichter, M., Sanz-Aparicio, J., Alcalde, M., 2018. Structural Insights into the Substrate Promiscuity of a Laboratory-Evolved Peroxygenase. *ACS Chem. Biol.* 13, 3259–3268.

Gomez-Fernandez, B.J., Garcia-Ruiz, E., Martin-Diaz, J., **Gomez de Santos, P.**, Santos-Moriano, P., Plou, F.J., Ballesteros, A., Garcia, M., Rodriguez, M., Risso, V.A., Sanchez-Ruiz, J.M., Whitney, S.M., Alcalde, M., 2018. Directed -in vitro- Evolution of precambrian and extant rubiscos. *Sci. Rep.* 8.

Molina-Espeja, P., **Gomez de Santos, P.**, Alcalde, M., 2017. Directed Evolution of Unspecific Peroxygenase, in: Alcalde, M. (Ed.), Directed Enzyme Evolution: Advances and Applications. Springer International Publishing, Cham, pp. 127–143.

Mate, D.M., Gonzalez-Perez, D., Mateljak, I., **Gomez de Santos, P.**, Vicente, A.I., Alcalde, M., 2017. Chapter 8 The Pocket Manual of Directed Evolution Tips and Tricks, in: Biotechnology of Microbial Enzymes. pp. 185–213.

Martínez, V., **Gomez de Santos, P.**, García-Hidalgo, J., Hormigo, D., Prieto, M.A., Arroyo, M., de la Mata, I., 2015. Novel extracellular medium-chain-length polyhydroxyalkanoate depolymerase from Streptomyces exfoliatus K10 DSMZ 41693: a promising biocatalyst for the efficient degradation of natural and functionalized mcl-PHAs. *Appl. Microbiol. Biotechnol.* 99, 9605–9615.

Martínez, V., Hormigo, D., Del Cerro, C., **Gomez de Santos, P.**, García-Hidalgo, J., Arroyo, M., Prieto, A., García, J.L., de la Mata, I., 2014. Genome Sequence of Streptomyces exfoliatus DSMZ 41693, a Source of Poly(3-Hydroxyalkanoate)-Degrading Enzymes. *Genome Announc.* 2, e01272-13.